MINIATURIZED SINGLE PARTICLE DISSOLUTION TESTING

Sami Svanbäck
University of Helsinki
Faculty of Pharmacy
Division of Pharmaceutical Technology

September 2013

Contents

LIST OF ABBREVIATIONS

A	area
API	active pharmaceutical ingredient
BCS	biopharmaceutics classification system
C	concentration
C_s	equilibrium concentration
C_t	bulk concentration
D	diffusion coefficient
DMSO	dimethyl sulfoxide
disc-IDR	disc intrinsic dissolutin rate
f_1	difference factor
f_2	similarity factor
FaSSIF	fasted state simulated intestinal fluid
FDA	U.S. Food and Drug Administration
FeSSIF	fed state simulated intestinal fluid
GI	gastrointestinal
h	diffusion layer thickness
HPLC	high-performance liquid chromatography
HTS	high throughput screening
IDR	intrinsic dissolution rate
IR	immediate release
IVIVC	*in vitro* - *in vivo* correlation
IVIVR	*in vitro* - *in vivo* relationship
J	flux
j	intrinsic dissolution rate
MITT	mean intestinal transit time
MW	molecular weight
η	viscosity
NCE	new chemical entity
Ph.Eur.	European Pharmacopoeia

PK	pharmacokinetics
QbD	quality by design
QSPR	quantitative structure property relationship
SGF	simulated gastric fluid
SIF	simulated intestinal fluid
T	temperature
t	time
USP	United States Pharmacopoeia
UV	ultraviolet
V	volume
w	weight at time t
w_0	initial weight

1 INTRODUCTION

Most drugs today are developed to be used through the oral route of administration (Lipinski et al. 2001). Screening of physicochemical factors, affecting oral bioavailability, are thus of high importance in drug discovery and development. One of the most important of these physicochemical factors is the dissolution rate of a drug substance. The potential of mini-scale dissolution tests, for drug discovery and early development, lies in the opportunity of obtaining large amounts of quantitative data, from small amounts of substance. At the present, these early assessments are, however, performed through qualitative experiments, such as kinetic solubility assays (Sugano et al 2007). *In silico* computational tools are another largely used method for early qualitative characterization of new drug substances (Curatolo 1998). The reason why dissolution testing has not been used in a larger scale, for early quantitative physicochemical assessment, might be due to the lack of appropriate technological approaches for mini-scale dissolution testing (Gardner et al. 2004). The development of new small-scale dissolution techniques, therefore poses an interesting opportunity. While the general way of studying drug dissolution has been by the multipartuculate bulk approach, studying the single particles of these systems could give a deeper understanding of the core factors affecting the dissolution rate of drug substances (Marabi et al. 2008; de Villiers 1996). The aim of the present study was therefore, to develop a mini-scale dissolution method, for assessing the dissolution of single particles.

2 DISSOLUTION

A substance is regarded as dissolved when it has become molecularly dispersed in the solvent (Martin et al. 2011). In addition to a molecular monomer form, the dissolved substance can also exist in solution as a self-aggregated form, of two or more molecules,

and, in solutions including more substances, as complexes or included into micelles (Sugano et al. 2007). Nanosuspensions can also, sometimes, be regarded as solutions. The dissolution process, of a solid in a liquid, involves two steps. First a molecule is dissociated from the solid surface due to energetic interactions with solvent molecules, after which the dissociated molecule diffuses into the bulk solution. The rate of dissociation of a molecule from the solid surface depends on the strength of the intermolecular interactions of solvate and solvent molecules, respectively, and the strength of the intermolecular interactions between solute and solvent molecules (Martin et al. 2011). These interactions are for example van der Waals, dipole-dipole, ion-dipole interactions and, as often in the case of aqueous solutions, hydrogen-bonds. It is thus the strength of the affinities of molecules to each other, inside the different substances and between the substances, that determines the overall dissociation rate.

As the dissolution process is inherently a process of dissociation and diffusion, the dissolution rate is, accordingly, also determined by the accompanying rates of diffusion (Nernst 1904). The diffusional mass transfer process describes the random movement of molecules, the so called Brownian motion that results in a transportation of matter from one part of a system to another (Crank 1975). In 1855 Fick was able to derive the mathematical equation (Equation 1) describing this diffusional flux, by identifying the similarity of diffusion and heat conduction, the latter of which already had an equation established by Fourier in 1822 (Crank 1975; Fick 1855).

$$J = -DdC / dx \tag{1}$$

In this Fick's I law of diffusion, J symbolizes the rate of transfer per unit area, D is the diffusion coefficient and dC/dx expresses the one-directional change of concentration through the distance dx (Crank 1975; Hixson and Crowell 1931). The equation can subsequently be rewritten as,

$$dm / dt = - DAdC / dx \quad (2)$$

where *dm/dt* expresses the amount of diffusing solute per time through the area *A* and the rest of the symbols are as above (Hixson and Crowell 1931).

The diffusion coefficient *D* can be determined from experimental results. However, a theoretical diffusion coefficient for a spherical particle was also derived by Einstein in 1905,

$$D = \frac{k_B T}{6\pi \eta \ r} \quad (3)$$

where k_B is the Bolzmann constant, *T* is the temperature, η is the viscosity of the medium in which diffusion takes place and *r* is the hydrodynamic radius of the diffusing molecule (Einstein 1905; Higuchi 1967). This so called Stokes-Einstein relation is usable when the solvent molecules are of similar dimension with the solute molecules (Higuchi 1967).

2.1 Three physical models of dissolution

There are three physical models that are commonly used to model the dissolution of a pure solid substance in a homogeneous solvent (Higuchi 1967). These models are the diffusion layer model, the interfacial barrier model and Dankwerts' surface renewal model (Figure 1). The diffusion layer model assumes that the dissociation reaction at the interface of solute and solvent is much faster than the Brownian diffusion or convective rate of transport into the bulk solution (Wurster and Taylor 1965). Thus there exists a diffusion layer of thickness, *h* around the solid surface (Nernst 1904; Higuchi 1967). At the solid liquid interface saturation concentration is assumed and outside the diffusion layer the bulk concentration is assumed to be constant throughout. Thus, the concentration gradient inside

the diffusion layer becomes the rate limiting driving force of dissolution (Figure 1). This relationship was also derived by Noyes and Whitney in what has subsequently become the classical Noyes-Whitney equation (4) for expressing the dissolution rate,

$$dC / dt = k(C_S - C_t) \tag{4}$$

where k is a constant, dC/dt expresses the change in concentration with time, C_s is the equilibrium solubility and C_t is the concentration in the bulk solution at time t (Noyes and Whitney 1897).

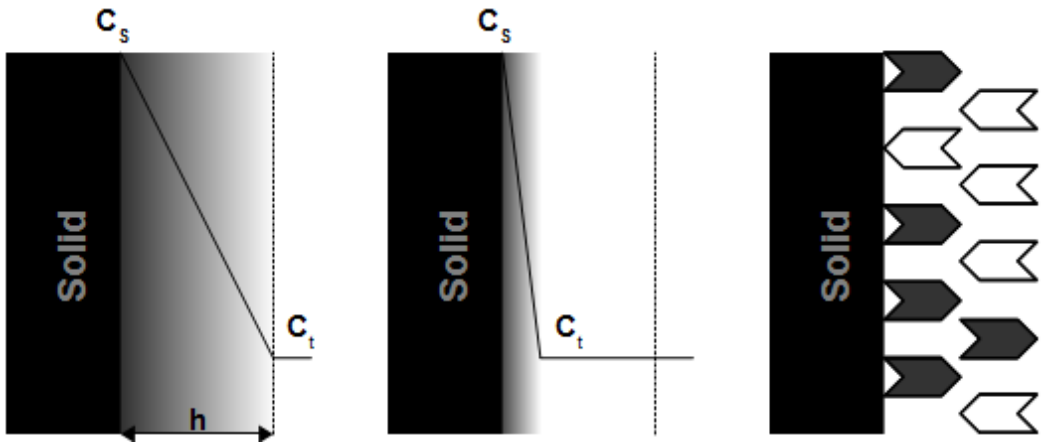

Figure 1. Illustrations of the concentration gradient change in the diffusion layer model (left), the interfacial barrier model (center), and the solvent packet transport of the Dankwerts' surface renewal model (right) (modified from Higuchi 1967).

The Noyes-Whitney equation was subsequently modified by Brünner and Tolloczko to include the surface area, A of the dissolving interface (Brünner and Tolloczko 1900),

$$dC / dt = kA(C_S - C_t) \tag{5}$$

and later with the aid of Fick's law of diffusion Brünner, while working for Nernst, was able to relate the constant, k with the diffusion rate constant, D to establish the Nernst-Brünner equation,

$$dC / dt = \frac{DA}{Vh}(C_S - C_t) \tag{6}$$

where A is the surface area of the dissolving substance or of the diffusion layer, h and V is the volume of the solvent (Nernst 1904, Brünner 1904). Although the diffusion layer model has been the most prominent model used to describe dissolution, it has been criticized throughout its existence (Wurster and Taylor 1965; Dokoumetzidis et al. 2008). The main point of criticism has been the assumption of the relatively instant formation of saturation concentration at the solid-liquid interface.

The interfacial barrier model, on the contrary, assumes that the activation energy of the interfacial transport step is high, and consequently that the reaction rate at the solid-liquid interface is much slower than the rate of transport into the bulk solvent (Wurster and Taylor 1965; Higuchi 1967). The interfacial reaction of dissociating solute molecules into the solvent thus becomes the rate limiting step (Figure 1). In this model saturation concentration at the solid-liquid interface may not be assumed, and it becomes much more difficult to derive a rate law (Higuchi 1967). The rate law can however be expressed as,

$$j = k_i(C_S - C_t) \tag{7}$$

where j is the dissolution rate per unit area, k_i is the effective interfacial transport rate and the other symbols are explained above.

The Dankwerts' surface renewal model takes another approach. It models packets of solvent that diffuse to the solid interface, absorb solute molecules and are subsequently replaced by new solvent packets (Figure 1) (Dankwerts 1951; Higuchi 1967). The rate limiting step in this model thus becomes the rate of solvent transport to the solid interface and the rate law can be expressed as,

$$j = S^{1/3}D^{1/3}(C_s - C_t) \tag{8}$$

where S is the mean rate of solvent transport *i.e.* surface renewal (Higuchi 1967).

2.2 Three single particle models of dissolution, and beyond

All of the above models assume dissolution from a constant surface area. Realizing that the reaction rate is directly proportional to the surface area available for reaction, Hixson and Crowell (1931) saw the need for a rate law incorporating this fact. Since the surface area is related to the weight, w of a particle, through volume and density, Hixson and Crowell started their derivation from the formula,

$$dw/dt = -KA(C_s - C_t) \tag{9}$$

where dw/dt expresses the change in weight of a particle with time. Substituting C_t with $(w_0\text{-}w)/V$ and C_s with w_s/V, where w_0 is the initial weight of the dissolving particle, w is the weight of the particle at time t and w_s is the weight needed for achieving saturation, gives,

$$V(dw/dt) = -KA(w_s - w_0 + w) \tag{10}$$

and ultimately the general solution, the Hixson Crowell cube root law is arrived at, following integration,

$$Kt = \frac{V}{a^2}\left(\sqrt{3}\tan^{-1}\frac{2\sqrt{3}a(b-x)}{3a^2+(2b-a)(2x-a)} + 1.1513\log\frac{(a+b)^2(a^2-ax+x^2)}{(a+x)^2(a^2-ab+b^2)}\right) \quad (11)$$

where $a = (w_s - w_0)^{1/3}$, $b = w_0^{1/3}$ and $x = w^{1/3}$. Thus, the "cube root law" name reflects the fact that the cube root of the weight at a specific time is the only variable, while all the other terms in the equation are constant.

In the special case where the concentration change is negligible due to the maintenance of sink conditions, the term $(C_s - C_t)$ can be assumed constant and is thus integrated into the Hixson-Crowell rate constant, K (Equation 13) (Hixson and Crowell 1931). Subsequently, the dissolution rate becomes dependent only on the surface area and Equation 11 is written as,

$$Kt = w_0^{1/3} - w^{1/3}, \quad (12)$$

$$K = \frac{\left(\frac{4\pi\rho}{3}\right)^{1/3} DC_S}{\rho h} \quad (13)$$

where ρ is the density of the particle and the rest of the symbols are as above (Wang and Flanagan 1999).

For the modeling of dissolution of single spherical particles, two other models are also used (Wang and Flanagan 1999). From the basic form,

$$w^x = w_0^x - k_x t \tag{14}$$

where k_x is a model specific rate constant, the three models are derived by substituting the exponent, x with ⅓, ½ or ⅔, the first one of these obviously being the Hixson-Crowell cube root law. The Hixson-Crowell cube root law, as all the previously mentioned equations, does not accurately model the dissolution rate for diminishing particles, since it assumes a constant diffusion layer thickness (Macheras and Dokoumetzidis 2000). As will be later discussed, the diffusion layer thickness does in fact change with particle size. The other two equations with square-root and two-thirds-root dependency on weight were derived by Niebergall et al. (1963) and Higuchi & Hiestand (1963) respectively. These two models do not either take into account the changing diffusion layer thickness, but they do model different phases of the single particle dissolution better than the Hixson-Crowell cube-root law (Wang and Flanagan 1999). While the Hixson-Crowell cube-root expression accurately models the dissolution of spherical particles, larger than the diffusion layer thickness, the square-root variation is more accurate for particles of the same size as the diffusion layer thickness. For particles smaller than the diffusion layer thickness the two-thirds-root dependency is the most appropriate.

One model that does take the diminishing diffusion layer into account was derived by Wang and Flanagan (2002),

$$t = \frac{\rho h}{DC_S}\left(r_0 - r - h\ln\left[\frac{h + r_0}{h + r}\right]\right) \tag{15}$$

where r_0 is the initial particle radius and r is the radius at time t (Wang and Flanagan 1999). The equation has been successful in modeling the dissolution of single particles over the whole size range (Wang and Flanagan 2002). Another model that has been successful in modeling dissolution rates over a wide range is the empirical Weibull function,

$$m = 1 - e^{\left(\frac{-(t-T_i)^b}{a}\right)} \tag{16}$$

where m is the accumulated fraction of drug dissolved at time t, T_i is the dissolution onset lag time, a is a time scale parameter and b expresses the dissolution curve shape parameter (Costa and Sousa Lobo 2001). The equation has however been criticized for its lack of a physical basis, and because of this general nature, it is not able to model dissolution kinetics other than descriptively. Adding to the equations mentioned above there exists several other formulas that describe the dissolution process. For the more complex dissolution processes connected to the diffusion in and from semi-solid and solid matrices the work done by T. Higuchi is most notable.

2.3 The intrinsic dissolution rate

The intrinsic dissolution rate (IDR) gives the dissolved amount of pure drug substance per surface area and time, and is determined by the mass transfer from the solid phase into the liquid, during constant temperature, pH, ionic strength and agitation (United States Pharmacopoeia (USP) 2001; Nicklasson and Magnusson 1985; Yu et al. 2004). To measure this propensity the effect of diffusion has to be eliminated through the maintenance of sink conditions, and the surface area of the dissolving solid is usually kept constant throughout the experiment. As a consequence of these fixations in the experiment setup, when the cumulative dissolved amount of substance per surface area (usually $mgcm^{-2}$) is plotted against time (usually in minutes), a straight line is acquired. The slope of this line gives the IDR. Usually only the data of the first 10% of the IDR test is used (USP 2001). The IDR, j can be expressed with the following equation,

$$j = \frac{VdC}{Adt} \tag{17}$$

with the symbols explained above (Yu et al. 2004). When assessing the IDR with a rotating disc Wood's apparatus, the IDR can be acquired by the semi-empirical Levich equation,

$$j = 0.62\left(\frac{D^{2/3}\omega^{1/2}}{\nu^{1/6}}\right)C_S \tag{18}$$

where ω *is* the angular velocity of the rotating disc and ν the kinematic viscosity of the solvent (Levich 1962). Because the initial dissolution rate is only limited by the mass transfer from solid to solvent, *i.e.* in many cases the solubility of a compound, the IDR can be used to predict the order of magnitude of equilibrium solubilities (Nicklasson and Magnusson 1985). Additionally, the data can be used to calculate the diffusion coefficient, a pH-dissolution rate profile, pKa, the activation energy of interfacial mass transfer and the relation between dissolution rate and solid form (Nicklasson and Magnusson 1985 ; Yu et al. 2004).

3 SOLUBILITY

In contrast to the kinetic nature of dissolution, solubility is an equilibrium event determined by the opposite kinetic rates of dissolution and crystallization. The equilibrium can thus be expressed with the aid of a similar rate law as the one used for chemical kinetics (Equation 19) (Dokoumetzidis et al. 2008).

$$a + nb \leftarrow \overset{k_1/k_{-1}}{\rightleftharpoons} \rightarrow c \tag{19}$$

In this rate law a molecule of the dissolving solute, *a* forms a solvent-solute complex, *c* with *n* solvent molecules, *b* driven by the rate constant k_1 (Figure 2). The inverse process of crystallization, where solute-solvent complexes dissociate and new solid surface is produced through recrystallization, is governed by the inverse rate constant k_{-1}. Equilibrium is consequently achieved when the opposing rates are equal. Since the kinetic energy of molecules is dependent on temperature, the rate constants, and thus the equilibrium solubility, are also temperature dependent (Bhattachar et al. 2006).

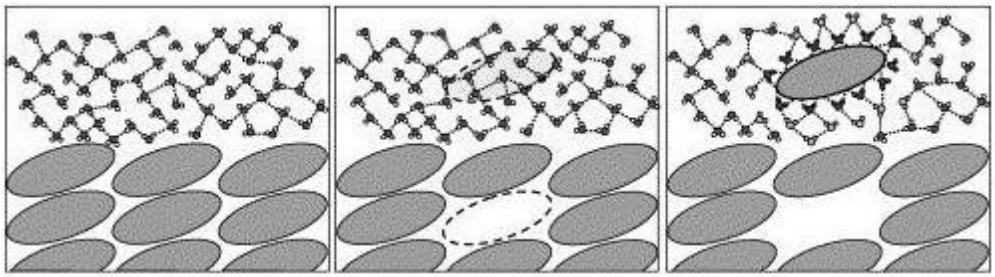

Figure 2. The interactions of solute and solvent molecules (left) result in the formation of new solute-solvent complexes (right) (from Bhattachar et al. 2006).

The term solubility generally refers to thermodynamic equilibrium solubility. Using Equation 19 thermodynamic solubility can be explained as the point, with constant volume, pressure and temperature, at which the rate of dissolution and recrystallization of the most stable crystal form are equal and, accordingly, the concentration of the solution keeps constant (Bhattachar et al. 2006; Sugano et al. 2007; Kerns et al. 2008). For this equilibrium to be determined an excess amount of solid has to be in contact with the solvent, and constant concentration has to be determined over long periods of time, usually several hours to days (Alsenz and Kansy 2007; Sugano et al. 2007).

Sufficient incubation time is important when measuring thermodynamic solubility, since all metastable physical forms will eventually recrystallize as the most stable crystal form, and thus the solid form with the lowest solubility (Bhattachar et al. 2006). When the incubation times are too short the measured solubility can, intentionally or not, be that of a metastable

physical form and is then called apparent solubility. Apparent solubility can also mean the result from experiments using shorter timescales (from a few, up to 24 hours), that are chosen on the basis of what is thought to be enough to reach equilibrium (Sugano et al. 2007). The solubility measurement in these experiments is done at the end of these time periods. This experimental setup is especially applicable in early drug discovery when faster, preliminary results are needed.

Another often used method to assess the solubility of a compound in early drug discovery is to measure the kinetic solubility (Sugano et al. 2007). The time scale of these tests ranges from minutes to hours, and is significantly shorter than equilibrium solubility incubation times. Kinetic solubility is often determined from pre-dissolved compounds in dimethyl sulfoxide (DMSO) stock solutions, making it in fact a measure of precipitation tendency. The reason why apparent solubility and kinetic solubility are not accurate measurements of equilibrium solubility, is the substantial risk of supersaturation in these measurements. The short incubation times might not be enough to settle at equilibrium, and the presence of a co-solvent, such as DMSO, can drive the concentration to supersaturation. This makes the results unreliable and incomparable with equilibrium solubility, since one cannot be sure if the solubility measured is the equilibrium solubility of the most stable crystal form, or in fact the higher apparent solubility of a metastable form (Bhattachar et al. 2006; Sugano et al. 2007).

A fourth form of solubility is the intrinsic solubility. This is the solubility of the unionized state of a compound and should not be confused with intrinsic dissolution rate (Sugano et al. 2007). For ionizable substances this solubility is thus measured at suitable pH, where the compound does not dissociate. The intrinsic equilibrium solubility, S_0 can be expressed by the Yalkowsky General Solubility Equation,

$$\log S_0 = 0.5 - \log K_{o/w} - 0.01(MP - 25) \quad (20)$$

where $logK_{o/w}$ is the logarithmic partition coefficient between octanol and water and *MP* is the melting point, *i.e.* the measure of the energy required to dissociate molecules in the crystal lattice (Jain and Yalkowsky 2001). This equation shows that the intrinsic solubility of a compound is dependent on the lipophilicity and crystal lattice energies of that compound.

4 FACTORS AFFECTING THE DISSOLUTION RATE AND SOLUBILITY IN AQUEOUS MEDIA – *IN VITRO* AND *IN VIVO*

While dissolution rate and solubility are tightly linked, and slow dissolution rate reflects low solubility when no chemical reaction accompanies the dissolution process, there are differences in the factors governing them (Florence and Attwood 2011). The equilibrium solubility and dissolution rate of a compound are determined by the physicochemical properties of the solute and solvent as well as the thermodynamic condition of the system (Martin et al. 2011). Dissolution rate is to a greater extent than solubility also governed by physical factors such as crystallinity, crystal form, particle size etc. These extrinsic factors do not change the equilibrium solubility but they can have an effect on the apparent solubility of a substance. Factors that affect the dissolution rate and solubility of a drug substance *in vivo* include physicochemical properties of the active pharmaceutical ingredient (API), excipients, formulation, and the gastrointestinal (GI) tract conditions (Dressman et al. 1998). Some of the factors (*e.g.* temperature, cosolvents and incubation time) have already been discussed, and below some further important factors are expanded upon.

4.1 Sink conditions

Dissolution under sink conditions refers to the dissolution under such circumstances where the concentration of dissolved compound does not affect the dissolution rate of undissolved compound (Mosharraf and Nystrom 1995). This is achieved by supplying sufficient amounts of fresh solvent to the solid interface by either removing dissolved solute from, or by using very large amounts of the dissolution medium. Different limits have been proposed for ensuring that sink conditions prevail. According to the USP sink conditions are achieved when the volume of dissolution medium is at least three times the volume needed for saturation concentration (USP 2001). Another proposed limit is that the concentration of dissolved substance does not exceed 10 % of saturation concentration, and yet another that the drug dissolves in less than 20-30% of available solvent (Mosharraf and Nystrom 1995; Amidon et al. 1995).

4.2 The effect of pH

For ionizable compounds pH plays a significant role on solubility and the dissolution rate through the extent of dissociation (Bhattachar et al. 2006). Since most pharmaceutical compounds are weak electrolytes, the pH of the solution and pK_a of the dissolving drug substance should always be assessed when determining solubility. The pH dependent solubility of monoprotic weak acids and bases can be expressed with modified Henderson-Hasselbalch equations, which for acids takes the form,

$$S_{pH} = S_0(1 + 10^{(pH - pKa)}) \tag{21}$$

and for bases is expressed as,

$$S_{pH} = S_0(1 + 10^{(pKa - pH)}) \tag{22}$$

where S_{pH} is the solubility at a certain *pH* and S_0 is the intrinsic solubility of the compound. The equations point out that increasing the pH of the solution where a basic compound is dissolving will lead to decreased solubility of the compound (Figure 3). Regarding acids the case is reversed. In the case of dissolving salts, the dissociation of salt into ionized drug and counterion is also an equilibrium phenomenon. This is a factor to be taken into consideration because of the common ion effect, where the solution has a concentration of ions alike the counterion, that will decrease the extent of dissociation and thus the dissolution rate and solubility. In the GI tract this effect is especially meaningful for hydrochloride salts.

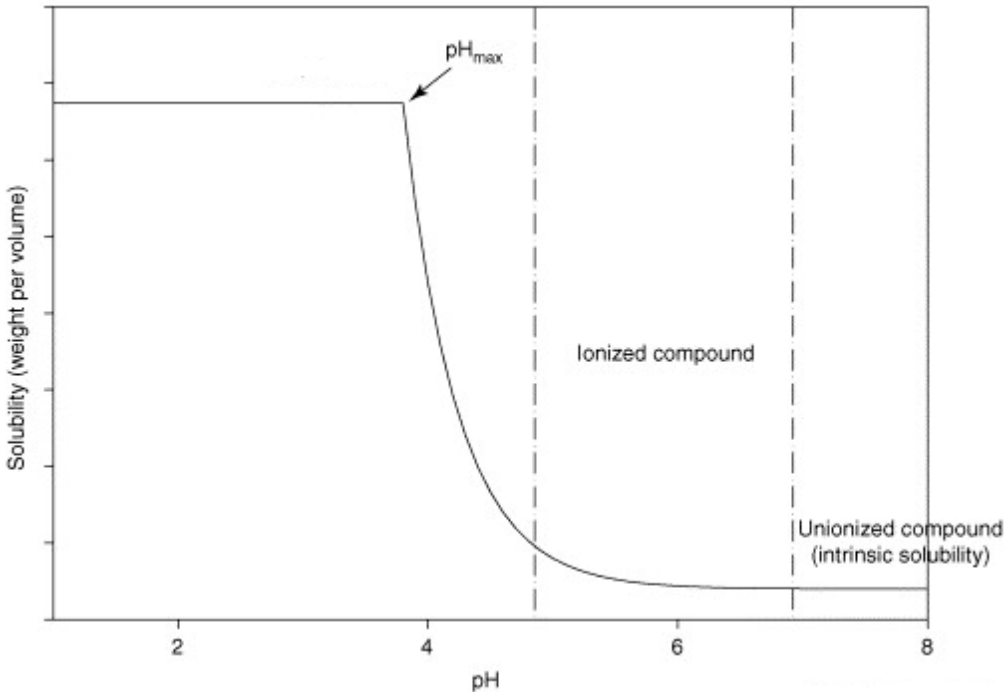

Figure 3. Dependency of the solubility on pH for a monoprotic base with pK_a 5. The maximum solubility is achieved just below pH = pK_a – 1(from Bhattachar et al. 2006).

4.3 Particle size, shape and agitation

Hydrodynamics and the intensity of agitation impact the dissolution rate through the effect of mixing (Hixson and Crowell 1931; Brünner and Tolloczko 1900). Mixing of the solution causes the stretching out of areas of high concentration, greatly increasing the contact area with regions of lower concentration and consequently leading to rapid equilibration of the concentration (Hixson and Crowell 1931). Additionally agitation affects the dissolution rate by decreasing the diffusion layer thickness, which is also affected by the particle shape and size of the dissolving substance (Wurster and Taylor 1965; Galli 2006). Irregular particle shapes have been shown to cause an increase in the diffusion layer thickness (Mosharraf and Nyström 1995). Thus, when studying irregular particles, a shape factor, which increases with increasing deviation from sphericity, is often considered in the calculations. Since dissolution rate is directly proportional to surface area of the dissolving compound, reducing the particle size is often the first approach for increasing the dissolution rate of poorly soluble compounds (Amidon et al. 1995; Wang and Flanagan 1999; Hörter and Dressman 2000). Effects of particle size on the dissolution rate have been predicted to be significant at particle sizes below 200 µm (Amidon et al. 1995; Wang and Flanagan 1999).

For particles above 50 µm it has been shown that the diffusional dissolution rate is inversely proportional to the particles diameter (Galli 2006). On the other hand, for particles below 50 µm the dissolution rates are higher than what the inverse proportionality would infer. This discrepancy is explained by the changing diffusion layer thickness. For particle sizes above 50 µm the diffusion layer thickness has been determined to bee constant at roughly 30 µm (Hintz and Johnson 1989). The diffusion layer thickness for particles below 50 µm however changes with, and is approximately equal to particle radius or diameter. As this shift occurs the dissolution rate becomes inversely proportional to the square of the particle diameter (Galli 2006).

Smaller particles, on the other hand, also have larger surface energies, due to the increased surface curvature of these particles (Wang and Flanagan 1999). This increases the probability of particle aggregation and agglomeration, which in turn decreases the effective surface area available for dissolution (Yu 1999). This phenomenon can be counteracted with surface active agents, which will improve the wettability of particles and decrease the cohesive forces that lead to aggregation and agglomeration (de Villiers 1996). When dissolving powders the mean effective surface area will accordingly be dependent on the particle size distribution and on the extent of aggregation and agglomeration of the particles. The dependency of dissolution rate on surface curvature can be derived from Fick's I law of diffusion and is expressed as follows,

$$j = DC_S\left(\frac{1}{h} + \frac{1}{r}\right) \tag{23}$$

where r is the radius of curvature, which for a spherical particle is equal to the radius (Wang and Flanagan 1999). The dependency of solubility on the particle size is given by the Ostwald-Freundlich equation,

$$\log\frac{S_r}{S_0} = \frac{2\gamma V}{2.303RTr} \tag{24}$$

where S_r is the solubility of a particle of radius, r, S_0 is the solubility of a relatively large particle, γ is the surface tension and V the molar volume of the small particle, R is the gas constant and T the temperature (Martin et al. 2011). The particle size effect on intrinsic solubility is however only seen for average particle sizes below 0.1 μm (Florence and Attwood 2011).

4.4 Solid state properties

Another property with great impact on solubility and dissolution rate is the solid state, *i.e.* different polymorphs, amorphous, (co-)crystal, solvate and salt forms of the drug (Huang and Tong 2004). Especially the dissolution rate and apparent solubility can be enhanced through chemical structure, salt and solid form modifications, and salt formation is considered to be one of the main routes to improved bioavailability (Huang and Tong 2004; Sugano et al. 2007). The effect on dissolution rate and solubility of different solid state modifications is explained by the different lattice energies of the different forms (Huang and Tong 2004). The apparent solubility is affected by these properties, since the higher energetic solid forms often induce supersaturation, which *in vivo* results in higher intestinal concentrations of drug substance and consequently in higher bioavailability (Takano et al. 2012). The time which the drug resides in the GI tract, *i.e.* the so called mean intestinal transit time (MITT) is also a factor to be taken into consideration, since the drug has to dissolve in this timeframe (one to three hours) in order to be absorbed (Dressman et al. 1998). It has accordingly been shown that if the drug does dissolve inside this timeframe and significant recrystallization does not occur, supersaturation, instead of solubility, can be used as the absorption predicting factor (Takano et al. 2012). The difference in solubility between different polymorphs and hydrate/anhydrate forms of the same drug substance have been found to generally differ twofold or less, while the difference in solubility between amorphous and crystalline material is more diverse and can show up to hundredfold differences (Huang and Tong 2004; Pudipeddi and Serajuddin 2005). The large difference in the solubility of amorphous and crystalline solids can be understood through the Yalkowsky General Solubility Equation (Equation 20), since the dissolution process of amorphous materials do not include the step of overcoming crystal lattice energies.

4.5 Gastrointestinal conditions

For ionizable compounds, pH changes along the intestinal tract will alter the solubility and dissolution rate during the transit (Amidon et al. 1995). Additionally the buffer capacity, ionic strength, and as mentioned before, the common ion effect impact the dissolution rate and solubility of these drugs (Kerns and Di 2004; Hörter and Dressman 2000). The possibility of decomposition, micelle formation and complexation with GI contents, *e.g.* other ions or bile salts can also lead to reduced activity of APIs (Amidon et al. 1995; Dressman et al. 1998; Avdeef 2007). Therefore, it is of particular importance to determine the site specific dissolution rate for drugs which demonstrate varying solubility, permeability and stability along the gastrointestinal tract (Amidon et al. 1995). For low solubility drugs the solubilization effect, which in the GI-tract is mediated by amphiphilic surfactants such as bile salts, lecithin and monooleins, is significant with up to 100-fold increases in solubility (Hörter and Dressman 2000). An additional factor is the viscosity of the GI contents, which affects the dissolution rate through the effect on diffusion.

The gastrointestinal environment for dissolution varies in pH, enzymes, surfactant, lipid and liquid content depending on the fasted or fed state, and also as a consequence of disease-induced changes (Amidon et al. 1995; McConnell et al. 2008). Additionally, the different states show variation in the cyclical motility of the intestines, intestinal transit times and gastric emptying, which in turn affect the hydrodynamics and time available for dissolution. In fact, during the course of transit of a drug in the intestines, all the factors of the extended Noyes-Whitney equation (Equation 4) may change, *i.e.* the surface area of the particles, the diffusion coefficient, solvent volume, the diffusion layer thickness, equilibrium solubility and concentration of dissolved substance (Table 1) (Macheras and Dokoumetzidis 2000). It can thus be seen why predicting drug absorption in this complex biological environment might impose difficulties (Amidon et al. 1995).

Table 1. The relationship between factors of the Noyes-Whitney equation and physicochemical and physiological parameters (adapted from Dressman et al. 1998)

Factors	Physicochemical parameters	Physiological parameters
Surface area (A)	particle size, wettability	surfactants in gastrointestinal fluids
Diffusion coefficient (D)	molecular size	viscosity of gastrointestinal fluids
Volume of solvent (V)		secretions and coadministered fluids
Diffusion layer thickness (h)	particle size	motility pattern, agitation and flow rate
Solubility (C_S)	logP, crystal structure, solubilization	pH, buffer capacity, bile, food components
Concentration of dissolved substance (C_t)		permeability

4.6 Formulation and experimental setup

While physicochemical properties of the API are the core underlying factors determining a products overall dissolution rate and solubility, formulation modifications can be used to affect these properties (Sugano et al. 2007; Tong et al. 2009). Especially the dissolution rate can be affected through formulation approaches. The formulation can however also negatively impact *in vivo* dissolution, such as in cases where the drug is not released fast enough, or at the proper site for absorption in the GI tract (Dressman et al. 1998).

In addition to properties of the solute and solvent, also the experimental setup and apparatus will impact the results, through the influence of the factors discussed above (Brünner and Tolloczko 1900). Sample preparation and analysis is also a factor to be taken into account. For example the capacity of the analytical method to distinguish between the analyzed substance and impurities, or the reliability of the calibration curve are to be

considered, since it has been shown that filters may act as nonspecific binders of the analyzable substance and that centrifugation can be insufficient in removing all suspended particles (Alsenz and Kansy 2007; Kerns et al. 2008). Especially in cases where an attempt to reflect *in vivo* conditions with the *in vitro* setup is made, the relevant factors are to be thoroughly assessed (Dressman et al. 1998). At the moment *in vitro* experimental setup and the pharmacopoeial apparatus for dissolution tests poorly reflect the *in vivo* conditions, and changes in both test equipment and media have been proposed (Hörter and Dressman 2000).

5 THE BIOPHARMACEUTICS CLASSIFICATION SYSTEM AND *IN VITRO – IN VIVO* CORRELATION

Oral absorption is controlled by three factors namely the dissolution rate, solubility and permeation of the intestinal membrane (Chen et al. 2006). The relation can be expressed by a membrane applied modification of Fick's I law,

$$J = PC \tag{25}$$

where J is the flux of drug substance through a point in the intestinal wall (mass/area/time), P is the permeability of the intestinal membrane and C the concentration of drug at the lumenal side of the intestine (Amidon et al. 1995). The lumenal concentration is of course a function of the dissolution rate. From this equation it follows that the driving force determining the flux of drug to the blood is the concentration gradient across the intestinal membrane (Lipinski et al. 2000). For high solubility compounds, when fast dissolution rate is assumed, the rate of absorption is limited only by intestinal permeability. If the drug dissolves faster than it is absorbed, solubility will be the limiting factor, and the maximum absorption rate, J^{max} can be expressed as,

$$J^{max} = PC_S \quad (26)$$

(Amidon et al. 1995, Chen et al. 2006).

In vitro – in vivo correlation (IVIVC) is defined by the USP as a correlation between a biological response and a physicochemical property of the same dosage form (USP 2001). In the case of bioavailability the biological parameter is the plasma drug concentration and the *in vitro* physicochemical property is the dissolution rate (Okumu et al. 2008). In order to establish IVIVC of dissolution rate, the dissolution medium used in *in vitro* studies should reproduce the *in vivo* gastro-intestinal conditions, with pH, surfactants, volume etc. as closely as possible (Amidon et al. 1995). Also physical factors such as particle size are important to be reflected in the actual *in vivo* case. Only in this way is it possible to assess the *in vivo* dissolution rate, and the limitations adhering to it, with sufficient accuracy (Dressman et al. 1998). Since the USP only provides a simulated gastric fluid (SGF, with or without pepsin) and a general simulated intestinal fluid (SIF, with or without pancreatin), other biorelevant dissolution media simulating fasted and fed states have been developed (USP 2001; Galia et al. 1998). These media, *i.e.* fasted state simulated intestinal fluid (FaSSIF) and fed state simulated intestinal fluid (FeSSIF) more closely mimic the fasted and fed state contents of the proximal small intestine, including physiologically relevant concentrations of bile salts (Galia et al. 1998). Therefore they are much more applicable to IVIVC studies, and have been shown to be able to predict *in vivo* data more accurately (Nicolaides et al. 1999).

Amidon and coworkers proposed in 1994 the Biopharmaceutics Classification System (BCS) in which drugs are divided into four categories, depending on their solubility and permeability (Table 2) (Amidon et al.1995). The classification has subsequently been adopted by regulatory agencies (*e.g.* the U.S. Food and Drug Administration (FDA) 2000).

According to the FDA guidance on biowaivers, a drug product is considered to have high solubility if the highest dose dissolves in 250 ml or less of aqueous media within physiologically relevant pH 1.0-7.5 (FDA 2000). Likewise a drug product is considered highly permeable if 90% or more of the administered dose is absorbed, and rapid dissolution is assumed when 85% or more of the dose is dissolved within 30 minutes, using USP Apparatus I with instructed biorelevant media. For certain compounds, as will be discussed, with dissolution rate limited absorption, the bioavailability of a new or existing drug products can be assessed with biowaivers, *i.e. in vitro* dissolution tests that substitute *in vivo* clinical tests.

Table 2. The Biopharmaceutics Classification System (adapted from Amidon et al. 1995)

BCS class I High solubility High permeability	BCS class II Low solubility High permeability
BCS class III High solubility High permeability	BCS class IV Low solubility Low permeability

BCS class I drugs have high solubility and high permeability making the drug absorption dissolution rate or, in cases where the drug dissolves very fast, gastric emptying rate limited (Amidon et al.1995). In the case where dissolution rate is slower than gastric emptying, saturation concentrations or maximum permeability are not reached and absorption is dissolution rate limited. Consequently an IVIVC of absorption with dissolution rate can be expected, and the biowaiver dissolution test for immediate release (IR) products of this class only have to prove rapid release from the dosage form in aqueous media (Dressman et

al. 1998).

BCS class II drugs have low solubility and high permeability (Amidon et al.1995). In this case maximum permeability is not reached at any point and thus all the drug that is dissolved in the GI tract is absorbed. Consequently the absorption rate will be highly dependent on the dissolution rate of the drug, except for very high doses where saturation of GI fluids occurs and solubility becomes the rate limiting factor (Dressman et al. 1998). Accordingly, a strong IVIVC can be expected if the *in vivo* GI conditions are adequately reflected *in vitro* (Amidon et al.1995; Dressman et al. 1998). BCS class III drugs have high solubility and low permeability (Amidon et al.1995). For this class the variation in drug absorption will be limited by the intestinal permeability, if the drug dissolves faster than the gastric emptying. Since the dissolution rate is not the absorption rate limiting factor, no or limited IVIVC is expected. However dissolution rate is relevant also for this class, since rapid dissolution increases the contact time with the intestinal wall, which consequently increases the possibility of absorption (Dressman et al. 1998). BCS class IV drugs have both low solubility and low permeability and show general poor bioavailability (Amidon et al.1995; Dressman et al. 1998). Since the dissolution rate is not alone the limiting factor, it is not possible to establish IVIVC based solely on the dissolution rate.

It can be seen from the above classification that dissolution rate and solubility play significant roles in the absorption and bioavailability of a drug product. Changing these factors also has a greater impact on the absorption than does changing the permeability (Lipinski et al. 2000). For a drug with low solubility and dissolution rate, increasing the permeability does not affect the absorption, since the amount of absorbable substance is not increased. Sub-par permeation, on the other hand, can be compensated by good solubility and dissolution rate, since a greater amount of compound is then available to be absorbed. The percentual distribution in the different BCS classes for new drug products between 1995 and 2002 where BCS class I 14%, BCS class II 12%, BCS class III 28% and BCS class IV 46% (Stegemann et al. 2007). If absorption of BCS class III drugs are taken to be

mainly permeation limited, it can be seen that for 72% of new products launched during this period, bioavailability was highly (BCS I & II) or partially (BCS III) dependent on dissolution rate and/or solubility. It can also be concluded that for BCS class I and II drugs with high permeability, sink conditions will prevail in the GI tract and the limiting factor will actually be the IDR of the substance.

It has been proposed that the IDR, rather than solubility, should be the basis of the biopharmaceutical classification of drugs, since the kinetic nature of intrinsic dissolution might correlate better with *in vivo* drug dissolution (Yu et al. 2004). Contrary to solubility the IDR is also dependent on wettability and diffusivity of the dissolving substance (Zakeri-Milani et al. 2009). Additional advantages of IDR studies over solubility studies are the lesser amounts of time and compound needed and the possibility of identifying solid form changes from acquired data (Yu et al. 2004). The suggested threshold for separating high and low solubility compounds is 1-2 $mgcm^{-2}min^{-1}$ (Zakeri-Milani et al. 2009). IDR measurements could additionally be very usable in API salt and solid form selection since the particle size does not affect the result (Sugano et al. 2007).

6 DISSOLUTION APPARATUS

The history of the compendial dissolution apparatus began in 1962 when the committee of the Pharmaceutical Manufacturers Association brought forth the idea of incorporating dissolution testing in the monographs of all solid dosage forms with less than 1% aqueous solubility (Cohen et al. 1990). Up until then, disintegration tests had been the general way for testing solid dosage forms, but the promotion of dissolution tests was based on the increased understanding of the relevance of dissolution phenomena for the bioavailability of drugs. In the beginning development was slow, but gradually the standardization and incorporation of dissolution tests advanced, culminating in the late 1980's when all

monographs for conventional dosage forms had been evaluated, and dissolution tests had been developed for the relevant compounds.

Today the United States and European Pharmacopoeias list four main apparatus for dissolution tests, all of which ought to be partially submerged in water baths of 37 ± 0.5 °C during the tests (European Pharmacopoeia (Ph.Eur.) 2013a; USP 2001). The first apparatus, generally called USP apparatus I or basket apparatus (Figure 4), was adopted by the USP in 1968 (Cohen et al. 1990). It consists of a transparent 1 liter, round bottomed dissolution vessel and a cylindrical stainless steel mesh basket connected to a rotating motor by a drive shaft (Ph.Eur. 2013a; USP 2001). During tests the basket, with sample, is rotated at constant speed, 25 ± 0.2 mm above the bottom of the vessel. USP apparatus II or paddle apparatus (Figure 4), together with USP apparatus I are the two most used apparatus for dissolution tests of solid dosage forms. The apparatus was adopted in 1978 and is identical with USP apparatus I, except that the basket is exchanged for a paddle, and the studied sample is kept at the bottom of the dissolution vessel during tests (Cohen et al. 1990; Ph.Eur. 2013a; USP 2001). Both USP apparatus I and USP apparatus II generally use 900 ml of dissolution medium for each test.

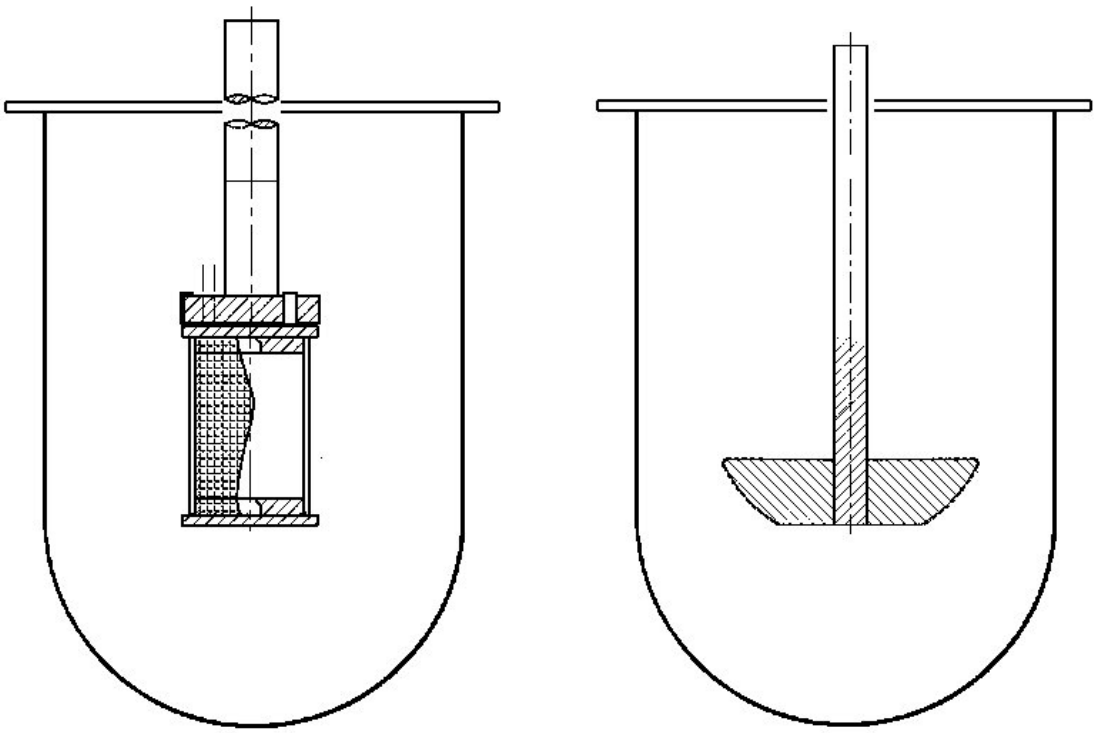

Figure 4. Schematic representation of the USP I basket apparatus (left) and the USP II paddle apparatus (right) (modified from Ph.Eur. 2013a).

The USP apparatus III or reciprocating cylinder is different entirely and is more rarely used (Ph.Eur. 2013a; USP 2001). It consists of outer and inner flat bottomed glass cylinders. The sample is put inside the inner glass cylinder, which is then sealed and vertically reciprocated, by a motor, inside the outer cylinder. The fourth apparatus is the flow-through cell or USP apparatus IV. It has a vertical setup, where the cell of inert transparent material has a cone-like lower part. The dissolution medium flows upward through the cone, which is usually filled with glass beads to allow a more even flow, and the sample is put inside the cell between the glass beads and an upper filter. The aim of the filter is to prevent undissolved particles from escaping. Standard flow-rates used are 4, 8, and 16 ml/min. Several non-compendial modifications of the flow-through cell also exist and it is a general denomination for dissolution methods that use pumps to provide a liquid flow across the sample. Sink conditions are maintained with open system set-ups, where fresh medium is

continuously provided to the sample surface. Recent flow-through measurements using biorelevant pH gradient changes, reflecting the GI tract passage of an oral dosage form, have been successful in assessing whole *in vitro* profiles and establish IVIVC (Okumu et al. 2008).

The intrinsic dissolution rate is traditionally measured by a modified USP apparatus II, with an additional pellet holder (Hulse et al. 2012). The apparatus is also called Wood's apparatus and the results disc intrinsic dissolution rates (disc-IDR). First a compacted pellet with a diameter of 0.1-1.0 cm is produced with a tablet press using a die and punch (USP 2001). The pellet, with a specific surface area exposed in the die is then mounted on the stirrer and rotated in the dissolution medium. Yu (2004) and coworkers showed in their studies that disc compression force, solvent volume and disc position do not have a notable effect on measured IDRs, as long as the compressed disc did not fall apart during the experiment. All these so called ”compendial” dissolution methods have become an established way to assess dissolution rates. However questions have been raised regarding their suitability in reflecting *in vivo* conditions (Dressman et al. 1998). For example, the hydrodynamics of the paddle and basket apparatus in relation to GI conditions have come under scrutiny. Other problems also exist, such as the settling of a disintegrated drug product at the bottom of a dissolution vessel, which can have a significant impact on the *in vitro* dissolution rate and thus not reflect *in vivo* conditions accurately (FDA 2000). Moreover, the flow rates of the small intestine range from 0-7 ml/min in the fasted and fed states, in light of which the USP flow-through apparatus flow rates of 8 or 16 ml/min can be considered high (Kerlin et al. 1982; Dressman et al. 1998). Additionally the one directional flow pattern that leads to non-equal dissolution from different faces of the compound, does not represent the mixing patterns of the intestines (Dressman et al. 1998).

7 DISSOLUTION TESTING IN DRUG DEVELOPMENT

After the introduction of dissolution testing of solid dosage forms in the 1960's, dissolution testing has become a widely used tool in many areas of the pharmaceutical development process. In drug development, dissolution assessment is used in the registration process, as a screen of API properties, guidance for formulation design, a way to assess time dependent drug release and as a quality-control and bioequivalence screening tool (Tong et al. 2009). Due to the large amount of new chemical entities (NCEs) being poorly soluble BCS class II or class IV compounds, the assessment of the dissolution rate of NCEs is gaining increased attention (Hulse et al. 2012). It can thus be seen that as the appreciation of the relevance of dissolution data grows and the analytical techniques evolve to accommodate to their broader usage, dissolution testing is being adopted ever earlier in the drug development pipeline (Figure 5).

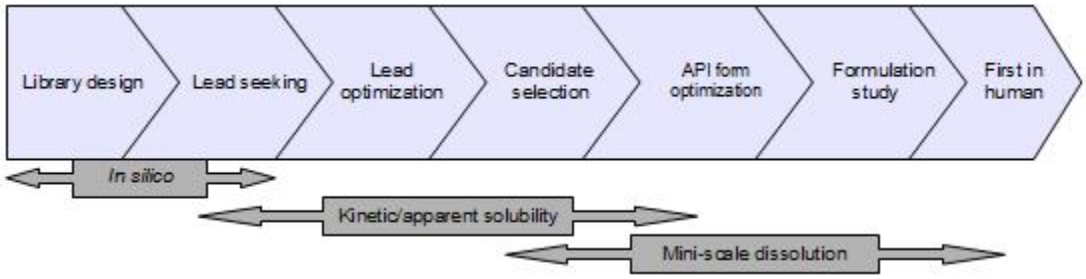

Figure 5. Current state of solubility and dissolution testing in drug discovery and early development (modified from Sugano et al. 2007)

7.1 Phase III

During phase III, *in vitro* dissolution testing is used to characterize drug-product performance (Tong et al. 2009). Dissolution testing, or surrogate tests established through the understanding of the critical parameters affecting the dissolution rate, may also be used to evaluate quality attributes and process parameters affecting product performance. These

product performance controls ensure that the process is kept inside the design space and, consequently, assures the products' clinical performance. The *in vitro* determination of similarity of dissolution profiles after formulation and process changes, is also to a large extent sufficient, even in certain cases when the product lacks IVIVC, to replace *in vivo* bioequivalence studies.

7.2 Phase II & I

During Phase II a finalized formulation is usually developed and the development effects on the dissolution rate should be continuously monitored (Tong et al. 2009). Through understanding of the critical factors affecting the dissolution of a specific product, surrogate tests, such as disintegration or API property characterization, can be developed to monitor product consistency. This is an example of the so called quality by design (QbD) approach in drug development, which is being increasingly applied in the pharmaceutical industry today. Bach release and batch-to-batch consistency in addition to product stability and IVIVC are the parameters being evaluated. During Phase I the emphasis of dissolution testing is on establishing an IVIVC or *in vitro - in vivo* relationship (IVIVR) for the primary formulation and biorelevant media of different pH are used to screen dissolution profiles, especially in cases where extended release formulations are attempted.

7.3 Early development

Dissolution profiles are currently assessed, and are in a central position in later drug discovery and early development, when screening for a compound’s most optimal salt-, polymorph- and (co-)crystal forms (Figure 5) (Curatolo 1998; Sugano et al. 2007). In this phase the amount of substance available is on the 100 mg scale (Sugano et al. 2007). In early development dissolution rate studies of API salt and solid forms are conducted in

order to establish the BCS classification, and to later enable the establishing of a quantitative structure property relationship (QSPR) between API properties and pharmacokinetic (PK) data (Tong et al. 2009). Early development dissolution screening is also used as an aid in primary formulation selection for animal toxicology studies and Phase I clinical studies. Additionally, adequate bioavailability has to be established in order to enable the determination of metabolic and pharmacological properties, side effects and the preliminary efficacy of a substance through *in vivo* tests.

8 DISSOLUTION TESTING IN DRUG DISCOVERY

In the beginning of the 1990's, high-throughput screening (HTS) of new drug compounds became widely used as an effective method for finding lead compounds with enhanced *in vitro* pharmacological potency (Kubinyi 1995). The advent of combinatorial chemistry also allowed an unprecedented amount of compounds to be automatically synthesized and to be available for discovery scientists. However, this departure from traditional screening methods unintendedly led to inferior physicochemical profiles of new compounds and poor solubility became an industry-wide problem (Curatolo 1998; Lipinski et al. 2000; Sugano et al. 2007). Simultaneously research and development (R&D) spending has continually increased in the pharmaceutical industry, while the rate of entry of new drug products to the marketplace has not grown accordingly (Table 3) (Venkatesh and Lipper 2000). The output of NCEs has actually decreased significantly and one of the reasons is that potent substances show, as a result of HTS and 'rational drug designing', higher molecular weight (MW >500 Da) and lipophilicity (logP >5) (Curatolo 1998; Lipinski et al. 2000; Gardner et al. 2004). As postulated by the Lipinski 'rule of 5', which states that the permeability and absorption of a compound is decreased if the compound expresses more than one of the following properties: over 5 H-bond donors, more than 10 H-bond acceptors, MW over 500 daltons (Da) or logP over 5, the higher MW and lipophilicity tend to decrease the

substances solubility and permeability, leading to increased development time and cost (Lipinski et al. 2000; Gardner et al. 2004). As stated by Curatolo (1998): ”An efficacious but non-absorbed agent is no better than a well-absorbed but inefficacious one”.

Table 3. Relationship between Pharmaceutical Industry R&D spending and NCE output (Venkatesh and Lipper 2000)

Output measure per company	1991-1995	1996-2000	Change
NCE output	12.3	7.2	-41%
R&D spending (billion US $)	5.9	8.5	+44 %

This problem has consequently been taken into consideration and modern candidate selection is becoming increasingly based on a more holistic consideration of potency, pharmacological, toxicological data and physical properties in addition to production suitability calculations (Figure 6) (Gardner et al. 2004; Sugano et al. 2007). Common physicochemical properties that are routinely profiled during discovery to assess the absorption potential of a NCE include solubility permeability, lipophilicity, pK_a, integrity and stability (Kerns 2001; Takano et al. 2012). All of these factors play an important role in subsequent decision making regarding developability, lead optimization, optimal formulation choice and risk assessment (Huang and Tong 2004). However, to be able to make accurate decisions the quality of the underlying data has to be sufficient. The lack of adequate technological approaches to assess these properties at an early stage has therefore imposed limitations (Gardner et al. 2004).

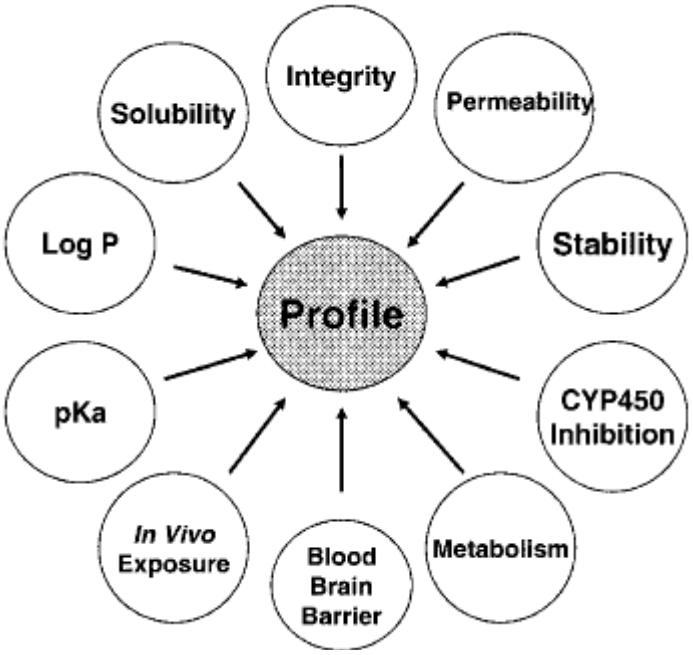

Figure 6. A more holistic view for drug candidate selection (Kerns 2001).

Poor solubility and dissolution rate can be, as previously discussed, improved through choosing an appropriate formulation (Lipinski et al. 2000). Advanced formulations can however result in increased risk, costs and delays and it has been estimated that a delay of entrance to the marketplace of a new important drug product can result in revenue losses of up to 1 million dollars per day (Kerns 2001). Therefore, the possibility of early assessment of drug solubility and dissolution rate in the discovery and development phases would be highly beneficial. This early characterization would allow modifications to be made to the API's chemical structure, which has been suggested to be the main way of correcting inadequate solubility of a compound and is only done during the discovery stage (Sugano et al. 2007). The problem of inadequate early physical characterization of a lead candidate is emphasized by the fact that these problems usually surface at a development stage, where optimization of other candidate properties are already at an advanced stage (Gardner et al. 2004). The possibility of early evaluation of physicochemical data would therefore narrow

the risk of downstream ADMET (absorption, distribution, metabolism, elimination, toxicity) problems and consequently reduce development delays (Kerns 2001).

The solid form of a compound has not necessarily been chosen at the discovery stage and variation in crystal forms are common (Kerns 2001; Sugano et al. 2007). The main challenge at these early stages is also to produce compounds of sufficient purity, and a degree of purity above 95% is regarded to be necessary in order to allow the acquisition of high quality data in line with non-miniaturized methods (Balbach and Korn 2004). However, the variation in crystal form does not necessarily impose a significant misinterpretation of the general solubility and dissolution profile, since it has been shown that the solubility ratios between pharmaceutical polymorphs are on the scale of twofold or less (Pudipeddi and Serajuddin 2004).

At these early stages dissolution methods are rare and solubility is the main factor being studied (Figure 5). Large amounts of compounds are also screened for qualitative physicochemical characteristics by *in silico* computational methods (Curatolo 1998). These widely used *in silico* modeling methods are used due to the lack of sufficient amounts (less than a few milligrams) of compounds for physical *in vitro* screening (Lipinski et al. 2000; Sugano et al. 2007). Computational methods are however based on theories and assumptions and are thus inherently lacking in accuracy (Sugano et al. 2007). Especially properties such as solubility and dissolution rate are difficult to predict, since the equations and assumptions related to these properties are built upon many other factors which are also difficult to predict, such as crystal lattice energies and pK_a. This, in combination with the uncertainty regarding the properties of NCEs can result in above 10-fold prediction errors. *In silico* models therefore need high quality input parameters from and validation through real experimental data.

HTS solubility methods commonly used in the industry today are based on the assessment of kinetic solubility (Kerns 2001). Common analytical techniques for the quantification of

solubility data include turbidimetric approaches where light scattering is used to measure dissolved or precipitated substance, UV plate readers, high-performance liquid chromatography (HPLC) and mass spectrometry coupled liquid chromatography (LC/MS). Kinetic solubility can however be significantly higher than equilibrium solubility due the presence of DMSO in the solution, the short incubation times and solid state effects (Kerns 2001; Sugano et al. 2007). Moreover, the act of predissolving in DMSO obviously masks the influence of crystal lattice energies and polymorphic forms, on solubility, and the data is not applicable for QSPR assessment (Huang and Tong 2004; Lipinski et al. 2000). The inherent problems in kinetic solubility measurements have led to a shift towards small-scale thermodynamic solubility studies, in order to produce early, higher quality solubility data for compound ranking and selection (Alsenz and Kansy 2007). However, as the incubation times needed for accurate assessment of thermodynamic solubility data, range from several hours to days, it is therefore not as applicable as the kinetic solubility assay for large-scale screening.

9 MINIATURIZATION OF DISSOLUTION METHODS

As has been made evident throughout this text, dissolution rate studies could have a significant advantage over solubility studies in drug discovery. First of all dissolution studies require substantially less time and substance for the single experiments. When carrying out equilibrium solubility measurements, an excess amount of solid substance has to be in contact with the saturated medium over long periods of time (Sugano et al. 2007). In cases when equilibrium is not immediately achieved after the first incubation, several more additions of substance may be required. However in dissolution studies, where saturation is not strived after, accurate data can be collected from the primary experiments, and from as small amounts of drug compound as the analytical method allows. Especially IDR data could be rapidly acquired since only data from the first 10% of the dissolution

curve is usually required (USP 2001). Regarding kinetic solubility studies, in which the timescale and compound consumption is reduced, the accuracy of the results is questionable and not directly interchangeable with equilibrium solubility (Sugano et al. 2007). Moreover, dissolution rates cannot be accurately predicted from equilibrium solubility, but the solubility can be predicted from dissolution rates and IDRs.

As has been previously discussed, the kinetic property of dissolution could reflect *in vivo* events more accurately, since the dissolution data includes both the initial wetting stage and the impact of diffusion. Additionally the dissolution rate incorporates the effect of particle size and physical, solid state properties into the data, none of which are reflected in solubility data. Chemical properties on the other hand are reflected in both dissolution rate and solubility data. Accordingly, early dissolution experiments would allow the screening of salt and solid form dependent dissolution rates, allowing early QSPR assessments. Furthermore, as has been shown, solubility can be exchanged for IDR data in determining the BCS classification (Yu et al. 2004). If IDR data could be collected at these early stages, this would mean that formulation and development scientists could have access to reliable primary biopharmaceutical classification from the very first batches of a NCE. This could greatly advance the initiation of their participation in the development process, and subsequently reduce development times. The possibility of using physiologically relevant conditions such as agitation, flow rates, pH and biorelevant media, in *i.e.* miniaturized flow-through apparatus, would also allow the acquisition of high quality *in vivo* relevant input parameters for early *in silico* modeling.

In spite of the considerable advantage of dissolution tests over solubility tests, regarding the amount and the accuracy of the data possible to collect from single experiments, mini-scale dissolution tests for drug discovery are few. The reason for this might be the lack of appropriate technological approaches for studying dissolution at a small scale (Gardner et al. 2004). The current aim of method development for physicochemical characterization is, however, in earlier characterization and further reduction of the amount of time, compound

and cost, and thus there lies a great potential in developing new small-scale dissolution methods (Alsenz and Kansy 2007). Especially miniaturized experiments for intrinsic dissolution could be suited for drug discovery and early development (Alsenz and Kansy 2007; Sugano et al. 2007). Also, the prospect of intellectually protecting polymorphic forms gives an additional incentive to develop higher throughput methods for characterizing dissolution profiles at the early stages (Alsenz and Kansy 2007).

Compendial dissolution apparatus require liquid volumes of 500 or 900 ml and API amounts from 100 to 700 mg and are therefore not applicable to drug discovery (Avdeef 2007). The small amounts of available compound to be used in these early experiments can also result in very low concentrations, preventing the quantification of dissolved substance, or at least leading to the use of additional analysis such as HPLC (Hulse et al. 2012). Obviously all additional and non-common analytical techniques will increase the workload and cost. During drug discovery, the aim is usually to downscale physicochemical characterization measurements to the 96-well plate size (Kerns 2001). However, most attempts for the miniaturization of dissolution tests have focused on the miniaturization of compendial apparatus for early development (Emmanuel et al. 2010). These so called ”mini-paddle” (Figure 7) and ”mini-basket” apparatus have the objective of producing similarity of compendial conditions, *e.g.* hydrodynamics, which is understandable since the aim is to produce results for primary formulations that will be in line with future ”normal scale” results.

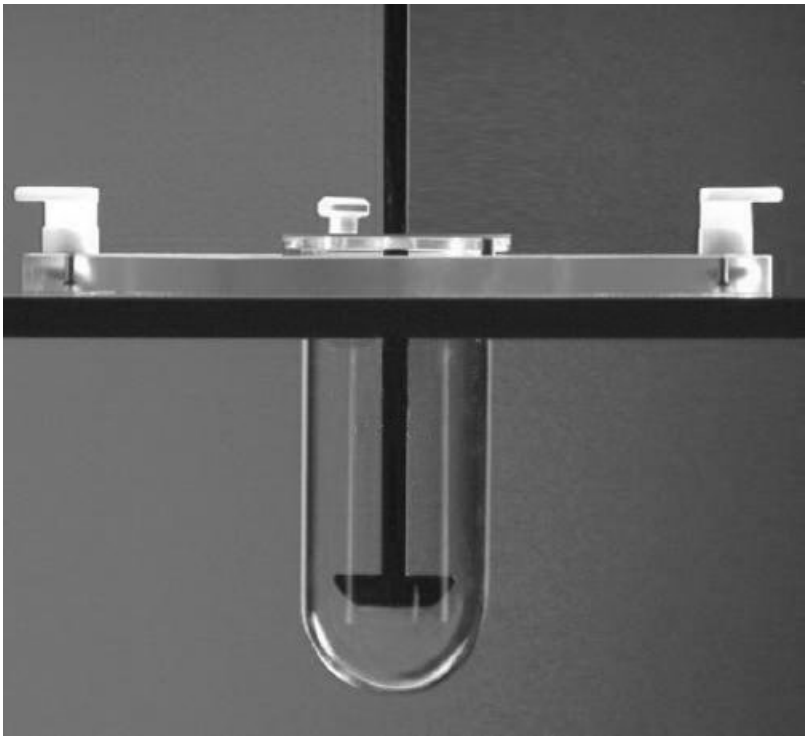

Figure 7. A mini-paddle apparatus with a 100 ml dissolution vessel (Christ 2009).

The miniaturized compendial methods are not however required for early characterization of NCE dissolution rates, and will certainly not be the best approach in developing new mini-scale dissolution tests. The aim of new small-scale tests is to produce as much high-quality data as possible, at sufficient throughput rates (Balbach and Korn 2004). Moreover, when developing new dissolution methods the accuracy, sensitivity, specificity and reproducibility of large scale equipment are to be maintained (Christ 2009). One approach through which it has been proven that it is possible to acquire high quality physicochemical data from small amounts of pure drug substance is the Aventis ”100 mg-approach” (Balbach and Korn 2004). The success of the approach is demonstrated by the fact that, since its introduction, physicochemical issues have not been the cause behind any candidate failure. For early screening of dissolution rates of different salt and polymorph forms, this approach uses a miniaturized flow through cell. The method requires approximately 1.5 mg of drug powder per sample and uses HPLC as analytical technique.

There are also some commercially available mini-scale dissolution tests that require only milliliter volumes and analyze the samples by *in situ* fiber-optic probes (Christ 2009). One example is the μdiss method, which uses 2 ml of dissolution media and 10-100 μg of compound per sample (Avdeef 2007). The method has been successful in predicting solubilities. A miniaturized IDR experiment was developed by Hulse et al. (2012). In their experiments, compressed discs of 3-10 mg of substance with a diameter of 2mm, were fixed at the bottom of a flow through apparatus and characterized by UV area imaging. A similarity was found with disc-IDR results from literature. IDRs comparable to results from standard disc-IDR measurements have also been obtained from powder samples as small as 0.06 mg using *in situ* fiber-optic UV analysis (Tsinman et al. 2009).

10 THE SINGLE PARTICLE APPROACH

The general way of studying dissolution rates, in both pharmaceutical and other sciences concerned with dissolution phenomena, have thus far been through the multiparticulate bulk approach (Marabi et al. 2008). However, one of the great disadvantages of this approach lies in the lack of understanding, and thus in the difficulty of modeling powder dissolution (Hulse et al. 2012). Important factors affecting the dissolution rate of solid substances such as particle size distributions, shape distributions and the degree of aggregation and agglomeration, as well as the time-dependent change in these, are difficult to measure accurately (Avdeef et al. 2009). Moreover, in the case of mini-scale powder dissolution methods, only rough estimations by *in silico* methods, requiring many assumptions, are possible. Thus, the single particle approach could be a more suitable approach.

While, according to Aristotle: ”the whole is greater than the sum of its parts”, it can nevertheless be argued that the whole is determined by its individual parts. This is also the

case with powders and powder dissolution, where the single particles composing the bulk powder are the main determinants of the overall bulk properties (de Villiers 1996). Studying dissolution on the single particle level will thus produce in depth understanding of individual particle dissolution kinetics and, consequently, important information about the dissolution kinetics of pure substances (Marabi et al. 2008). By analyzing dissolution with the single particle approach, the cohesive interactions between particles can be ignored and the particle shape and size may be exactly observed. The single particle approach thus minimizes the assumptions regarding the factors influencing the dissolution rate, and the data can therefore be regarded as more accurate. Additionally, knowing the exact particle size and shape allows a direct correlation between these factors and the dissolution or intrinsic dissolution rate. This in turn allows the extrapolation of the acquired data to any particle shape(distributions), size(distributions) or effective surface areas.

Thus far the single particle approach has been implemented only in a few cases, mainly in chemical engineering as compiled by Marabi et al. (2008), but lately also in the food (Börjesson et al. 2013) and pharmaceutical sciences (Prasad et al. 2002; Raghavad et al. 2002; Østergaard et al. 2011). Prasad et al. (2002) investigated the dissolution rate from different faces of fixed single paracetamol crystals with optical microscopy. They found that different faces showed variation in surface topography and also significant differences in the dissolution rates. The varying dissolution rates of the different faces lead to anisotropic dissolution of the crystals. Additionally they found that edges and corners had a preferential dissolution, leading to the rounding off of these areas. Similar results have also been reported for single crystals of α-lactose monohydrate by an almost identical test (Raghavan et al. 2002). Østergaard (2011) and coworkers studied the dissolution of single lidocaine crystals in a stagnant liquid. The crystals were mounted into holes drilled in the dissolution cell and analyzed by UV area imaging. They found that it was possible to apply this analytical method to dissolution studies of single particles. Their results also showed a decrease in dissolution rate for smaller crystals, which was assumed to be caused by the smaller surface area.

The spherical form of particles is a general assumption when modeling powder dissolution since the geometry is simple and easy to model (Marabi et al. 2008). The sphere is also the geometrical form with the lowest surface area per volume ratio, and thus with the lowest surface energy. It is therefore expected that the spherical shape is the most geometrically stable and, accordingly, the shape which will dissolve most isotropically. One of the early studies with single spherical particles was conducted by Parrot et al. in 1955. They studied the dissolution rate of single 1.27 cm compressed spheres of pure drug substances in 2000 ml volumes of agitated liquid. The dissolution rate was calculated from radius and weight measurements, as well as by titration. They concluded that the spherical particle shape was maintained throughout the experiment and that dissolution rates calculated based on the radius did not significantly differ from chemical analysis results. They also found that the dissolution rate was practically independent of density and directly proportional to weight and surface area.

Marabi et al. (2008) studied the dissolution of single spherical sucrose particles in stagnant liquids. Through image analysis of micrographs they were able to measure the dissolution rates of the single spheres. They also used a mathematical shrinking sphere model to derive a dissolution rate constant and to correlate this rate constant with the viscosity of the different dissolution media. Additionally they also found that the particle retained the spherical shape throughout the experiment. Börjesson et al. (2013) also used optical microscopy to measure the dissolution rates of single sodium caseinate powder particles, in a custom made flow through cell. They fixed the spray dried powder particles by squeezing them between two glass slides and assumed a cylindrical shape in their calculations. In their density measurements they observed a large difference in intraparticle porosity, which was assumed to cause the difference in dissolution rates between particles. They also found a similarity between particle and time averaged, surface specific dissolution rates of the particles and disc-IDR measurements.

11 OPTICAL MICROSCOPY AS ANALYTICAL TECHNIQUE

It can be concluded based on the literature, that in the few single particle dissolution studies that have been made, optical microscopy has been the most used analytical method (Prasad et al. 2002; Raghavad et al. 2002; Marabi et al. 2008; Börjesson et al. 2013). This is a novel application for optical microscopy as an analytical technique, which has been enabled by recent advances in computing, imaging technologies and image analysis software (Almeida-Prieto et al. 2006). The fast development in digital imaging has also made digital microscopy a viable analytical tool for the acquisition of high quality morphological particle data.

Optical light microscopy is generally used to study particles in the size range of 3 μm – 150 μm, with the theoretical minimum resolution being 0.2 μm (Allen 1997). However, the smaller the analyzed particle, the greater the ring of diffracted light around the particle will be, with respect to the particle size. Accordingly the overestimation of particle size increases with decreasing particle size, and it becomes significant at particle sizes below 3 μm. Because of this effect, 0,8 μm is considered to be a realistic threshold for particle size analysis. Another limitation of the optical microscope is the shallow depth of focus. This means that areas of large particles, or of multiparticulate samples with a large difference in particle size, cannot be brought into focus in the same image. In the case of single particles, the shallow depth of focus means that the particle either has to stay or be fixed at a specific distance from the lens.

Despite these limitations, the advantages of studying dissolution through physical analysis, instead of chemical analysis, are many. Common chemical analysis techniques such as UV-spectrometry and HPLC need chemical calibration in order to identify the dissolved substance. Particle size analysis of micrographs, on the other hand, does not require any chemical calibration and is therefore highly applicable to the analysis of NCEs, for which compound properties are relatively unknown and the available amounts scarce.

Additionally, the visual area analysis of a dissolving particle provides more accurate data than *in situ* analytical techniques that measure the concentration at a certain point in the medium. This is because the concentration will be unevenly distributed throughout the dissolution medium, with areas of higher and lower concentration, and the positioning of the analytical probe will therefore be a source of error. Furthermore, image analysis does not require any liquid sample collecting or preparation, both of which are possible additional sources of error, and therefore have to be validated. Moreover, the more preparation steps that are needed between sample collection and the final analysis, the higher the risk of sample loss. The accuracy and discriminatory capabilities of chemical analysis methods are also greatly reduced when using more complex dissolution media *i.e.* biorelevant media, making it difficult to distinguish the analyzed substance from other dissolved substances or impurities. Lastly, the simplicity of digital image acquisition and computational image analysis makes this a fast analytical technique, highly applicable for automation and real-time data analysis.

11.1 Image analysis

A digital image is composed of multiple squares called picture elements or pixels (Sandler 2011). In order to analyze and process the images, they are usually converted into grayscale (monochrome) images (Sandler 2011; Allen 1997). The pixels of monochrome images are represented by a numerical value between 0 and 255. This value determines the grayscale shade, depending on the brightness and hue of the individual pixels, where 0 represents a black pixel and 255 a white pixel (Allen 1997). To enable the analysis of particle properties the monochromatic image is further processed, by *i.e.* removing background noise and converting the monochromatic image into a black and white image, through thresholding. Thresholding means choosing a threshold value on the grayscale, below which all numerical values get the value 0 (black) and all numerical values above the threshold get the value 255 (white). Thus a black and white binary image is produced. This action, where

the particle to be analyzed is distinguished from the background, is also called segmentation (Carlton 2011).

If the binary particle is incompletely segmented, due to the inadequate quality of the primary digital image, the binary image can be further optimized (Carlton 2011). Examples of this optimization include smoothing of particle edges and filling holes inside the edges. In order to analyze the particles they obviously also have to be separated from each other, a problem avoided when studying single particles (Allen 1997). Processing the images can however only maximize the amount of possible data to be collected, but cannot add any new information that did not exist in the original picture. Therefore, the most important factor that determines the quality of the image analysis data is the initial quality of the digital picture.

Microscopical imaging is usually performed only from one angle, which means that the orientation of the analyzed particle, at the moment of capturing an image, determines the two-dimensional projection of the particle (Allen 1997, Stainforth and Aulton 2007). Symmetrical objects such as spheres show the same two-dimensional projection in all directions and it is therefore not important from which angle the particle is observed. However, when analyzing the particle size of asymmetrical particles *i.e.* fibers, it has to be taken into account that they have a preferential orientation at which they will tend to settle on a surface (Stainforth and Aulton 2007). In order to simplify the analysis of asymmetrical particles an equivalent diameter conversion is usually applied. The conversion is based on the assumption that the calculated particle volume belongs to a sphere of equal volume. This equivalent sphere volume can for example be calculated using the diameter of the two-dimensional projected surface area of the studied particle, a so called projected area diameter. It can also be obtained based on other measurements of the analyzed particle, *i.e.* maximum and minimum perimeter diameters or circumference.

12 AIMS OF THE STUDY

There were five major aims in the present study:

- To study the dissolution of single particles, through image analysis data obtained by optical digital microscopy;
- To investigate and verify the applicability of optical microscopy as an analytical technique for drug dissolution testing, by correlating the image analysis data with UV-spectrophotometric chemical data;
- To design and build a flow-through apparatus in which it would be possible to conduct dissolution studies of freely moving single particles;
- To compare the acquired single particle dissolution rate data with the Hixson-Crowell cube root law;
- To assess the possibility of obtaining intrinsic dissolution rate data, based on single particle surface areas and dissolution rate data.

13 METHOD DEVELOPMENT

In order to study the dissolution of single particles of pure drug substances by optical digital microscopy, two different experimental setups, one semi-static and one dynamic, where developed. In order to validate the applicability of optical microscopy for dissolution testing, liquid samples from the same systems of single dissolving pellets were also to be collected and analyzed by UV-spectroscopy. When developing the methods, the limitations of the analytical technique and the aim of maximizing the quality of the data meant that certain issues had to be taken into consideration. These were the following:

- Due to the limited depth of focus of optical microscopes, the particle had to be maintained at a fixed distance from the microscope lens;
- The magnification had to be fixed and maximized in order to enable the use of the same scale calibration for all images, and to achieve the greatest resolution;
- The particle had to be sufficiently distinguished from the background and stay within the limits of the image area, throughout an experiment.

13.1 The semi-static setup

The limiting requirements where easily met with the semi-static setup, and after trying different dissolution vessels a 24-well plate well was chosen (Figure 8). One well could hold 3 ml of dissolution medium, which was sufficient to allow adequate dissolution times for the studied substances, ranging from one to a few hours. The flat bottom of the well plates also allowed the particle to settle there for imaging, taking care of the focus issue. By inverting the microscope (DigiMicro 2.0 Scale, dnt Drahtlose Nachrichtentechnik Entwicklungs- und Vertriebs GmbH, Dietzenbach, Germany) and imaging the particle through the transparent bottom of the 24-well plate, it was possible to use the maximum resolution and a fixed magnification. The well plate had to be shaken before every sampling time, in order to even out the concentration in the well before collecting liquid samples. It was found that shaking the well plate approximately 30 seconds before sample collection allowed a suitable time-frame for the particle to settle at the bottom, and to move it into the image area of the microscope. Sample sizes of 1 ml where found to be appropriate for UV-analysis, since the UV-spectrophotometer was able to analyze samples of 2.5-3 ml. The minimum 2.5-fold dilution of all samples meant that smaller than 1 ml samples became too diluted to analyze, and larger samples disturbed the dissolution system too much. Larger than 1 ml samples also significantly increased the risk of sucking the sample pellet into the pipette. It was also found, through testing different backdrops, that a non-reflecting dark surface produced the highest contrast between the white drug pellets

and the background.

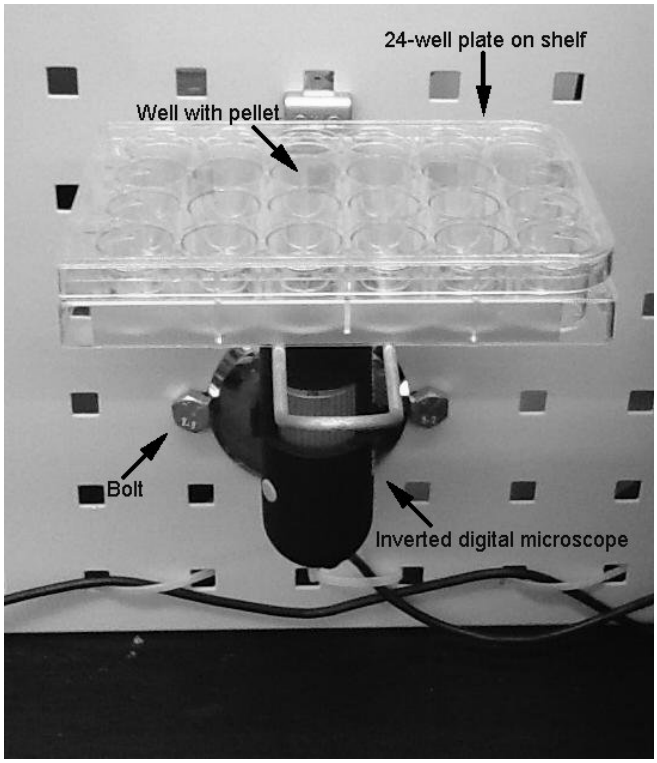

Figure 8. The semi-static single particle dissolution setup.

13.2 Einstein's teacup

Developing a dynamic setup proved to be more challenging. In previous small-scale single-particle experimental setups, where optical microscopy has been used, the particles have either been analyzed under static conditions (Marabi et al.2008) and/or they have been fixed by gluing or squeezing (Prasad et al. 2002; Raghavan et al. 2002; Börjesson et al. 2013). The aim of the present study was however to develop a flow-through system where it would be possible to analyze a single, freely moving particle, which would allow certain advantages. Firstly, the gluing and fixing of small particles could be a laborious and time-consuming step. Additionally, by gluing or squeezing parts of the surface will become covered, making it more difficult to calculate exact effective surface areas. The act of

squeezing should also theoretically increase the lattice energies of the particles by increasing the intraparticle tension, which in turn would have an effect on the dissolution rate of the particles. Furthermore, a freely moving particle would reflect the *in vivo* conditions of particles in the GI tract more closely than a fixed particle. The free movement would also allow a more even agitation on, and flow across the particles, leading to more isotropic dissolution. Finally, a freely moving particle would not be allowed to settle in its preferential orientation, and would therefore show different area projections at different time-points, enabling a three-dimensional (3D) assessment of the particle shape.

After unsuccessfully attempting a few microfluidics based flow-through systems, another method based on the tea leaf paradox was tried. The ”tea leaf paradox” is a common name for a phenomenon explained by Einstein (1926) in his paper on the meandering of rivers, *i.e.* the tendency of streams to move in serpentine patterns, as a consequence of uneven erosion of opposite river banks. To explain this phenomenon he used the analogy of a flat-bottomed teacup (Figure 9). When stirring the teacup, with tea and fragments of tealeaves in it, a centrifugal force is induced in the liquid. This centrifugal force is however not evenly distributed inside the teacup, due to the frictional force opposing the circular movement at the sides and bottom of the cup. At the bottom, the centrifugal force is especially diminished due to the interfacial friction that restrains the outward movement of liquid molecules. As a consequence of this uneven flow, the centrifugal force will be greatest at the surface, leading to a strong outward flow. Thus, the primary circular flow around the teacup will be accompanied by a secondary circular flow, going outwards and downwards at the top and sides respectively and inwards and upwards at the bottom and center respectively. The combination of these two circular flows will produce a vortex flow-pattern in the teacup, causing the tealeaves to collect in the middle of the bottom (Figure 9). This phenomenon has been applied in one previous study, where it succeeded in trapping erythrocytes from small-volume blood samples (Yeo et al. 2006; Arifin et al. 2007). The stirring motion in the study was achieved by an airflow at the surface of the liquid, produced by the ionic wind from a small electrode.

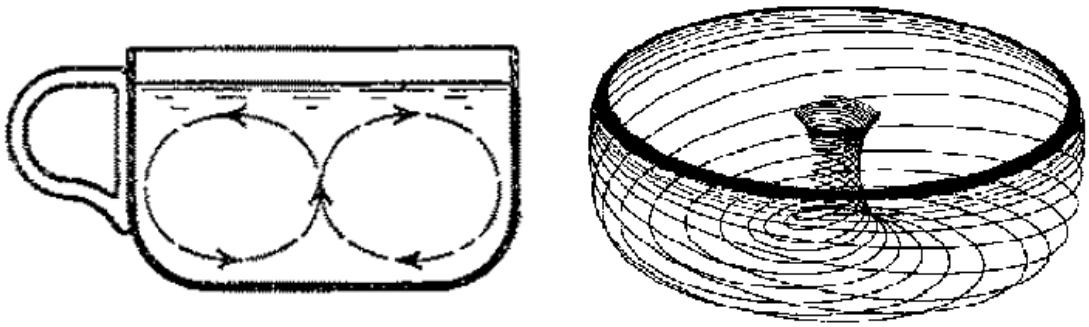

Figure 9. Eistein's teacup with secondary circular flow patterns (left), and the three-dimensional vortex flow caused by the primary and secondary flows in the stirred cup (right) (Einstein 1926; modified from Arifin et al. 2007).

13.3 The initial apparatus and challenges

The stirring method used by Yeo et al. (2006) might not be suitable for drug dissolution studies, since the charge of the ionic wind might interact with drug substances, many of which are weak electrolytes. However, by using the liquid flow to produce the vortex pattern, a flow-through method based on the tea leaf paradox could be achieved. An initial apparatus was subsequently built to assess the feasibility of the chosen method in trapping single particles. The apparatus consisted of a glass microscope slide, two syringe needles, an Eppendorf tube, a rubber eraser, tubing, a syringe and a piston pump (Watson-Marlow 503U, Smith & Nephew, Falmouth, Cornwall, England) (Figure 10). The Eppendorf tube was modified by cutting off the rounded bottom and making a hole through the wall at the lower part the tube. A larger hole was also prepared through the tube cap, in which the hub of a needle was fitted from the inside, and glued tight. Into this hub, from which the shaft had been removed, the outflow-needle was inserted from the outside. Another hole was drilled through the flat rubber eraser into which the halved tube was tightly pressed, whereafter the eraser was glued onto the microscope slide, so that the lower rim of the tube pressed towards the slide. Finally, the inflow-needle was pushed through the eraser into the

prepared hole in the tube wall and positioned as closely as possible to the inner wall. The function of the eraser was thus to act as an insulator, and to hold the inflow-needle in place.

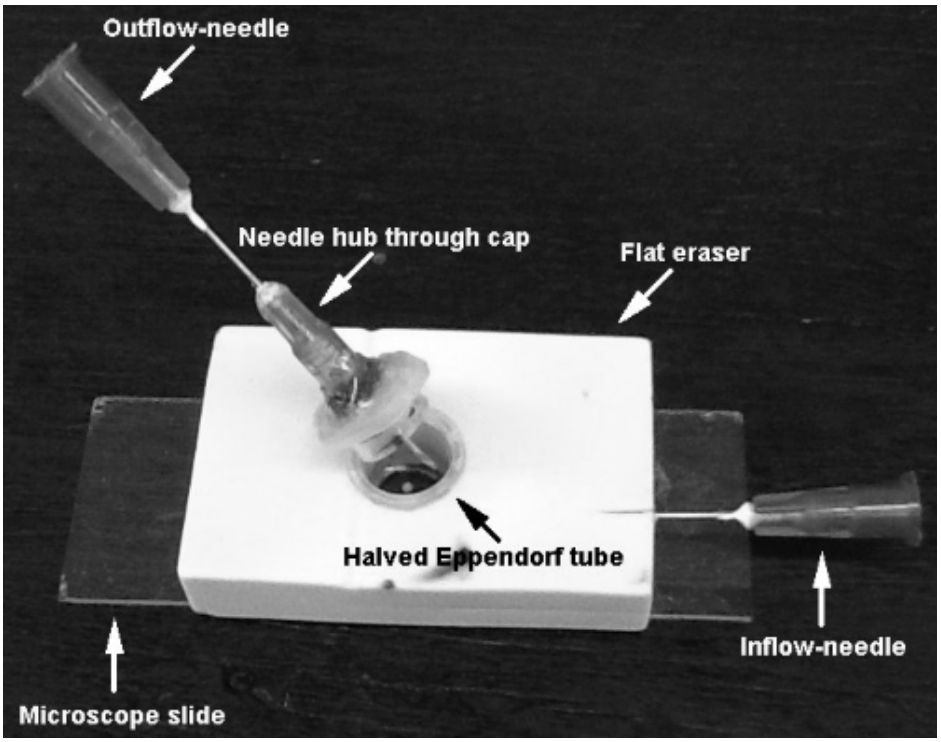

Figure 10. The first working modified Einstein teacup prototype.

Image data was collected in the same way as in the semi-static setup, by imaging through the transparent bottom, which in this case was the microscope slide. When studying single particles in the dissolution chamber, the cap of the Eppendorf tube was closed, leaving the needle in the cap as the only route for liquid outflow. The inflow-needle was connected to the syringe in the piston pump by tubing. Because of the positioning of the inflow-needle opening close to the wall of the tube, the incoming flow was forced into circular motion, by continuous contact with the wall. Thus the apparatus was able to produce a vortex flow in the dissolution chamber, trapping the particle at the bottom, in a sufficiently small area to enable imaging.

Several limitations and problems also occurred. The piston pump could only accommodate

a syringe with the maximum volume of 50 ml**,** which added an unfavorable step of syringe changing to the process. One major issue was also the leaking of the dissolution vessel, caused by the high pressure buildup inside the dissolution chamber. This pressure, caused by the continuous inflow of fresh dissolution media, was used to force the liquid inside the chamber out through the outflow-needle. The seal between the outflow-needle hub and the tube cap was however not tight enough to withstand the force. Another initial problem was the forming of air bubbles on the particle surface and on the bottom of the dissolution chamber (Figure 11). The bubbles on the bottom prevented the rotation of the particle by adhering to it, which in turn caused uneven dissolution of the particle, leading to a significant change in particle shape. Additionally, the bubbles prevented an accurate and rapid assessment of the particle surface area. The formation of bubbles was initially thought to be caused by intraparticle air pockets, which would have been revealed as the particle dissolved. It was however later realized that the bubbles were formed on the surface of the particles by dissolved air in the water. The problem was consequently solved by degassing the water by boiling.

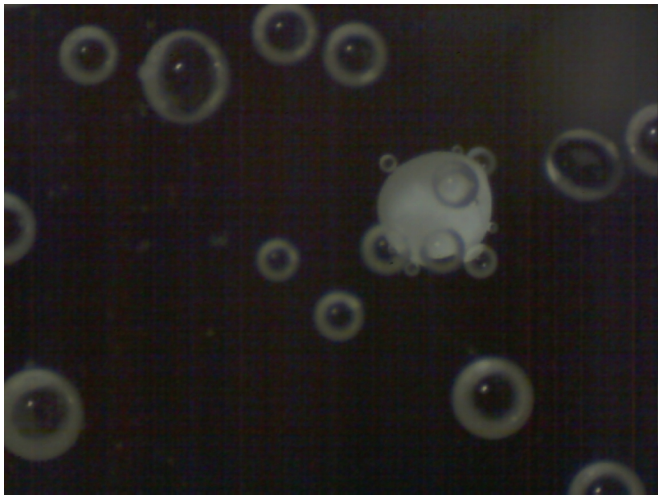

Figure 11. Formation of air bubbles initially prevented an accurate assessment of the particle size.

The rotating particles also caused challenges for surface area measurement, since the rapid movement initially resulted in blurred images (Figure 12). This issue was solved by using stroboscopic lighting, produced by a light emitting diode (LED) in a darkened room. The flashing was produced by attaching the LED to a pulse generator (TGP110 10MHz Pulse Generator, Thurlby Thander Instruments LTD, Huntingdon, Cambridgeshire, England) coupled power supply (AL370S Stabilized DC Power Supply, Alpha Elettronica, Parma, Italy). The fast flashes of light where shorter than the exposure time of an image, and therefore produced still pictures of the rotating particle. The stroboscopic lighting however caused an additional problem of a dark segment in the images (Figure 12). This moving segment was probably caused by the rapid change in lighting during the exposure time of an image. It was not possible to remove this occurrence, but it was possible to control the width and the speed at which the segment moved across the screen, by adjusting the flashing frequency. There was however a limit in the rotational speeds, up to which the stroboscopic effect worked. At higher angular velocities of the rotating particles, the images again became blurred. Therefore there existed a narrow optimal region for the flow-rate, below which the particle did not rotate, and above which the images became blurred. It was also observed that the problem was magnified at higher resolutions, wherefore the highest resolutions were not usable at this initial stage. Additionally the LED had an optimal intensity at approximately 10V, below which the particle was not sufficiently illuminated, and above which the background became too bright.

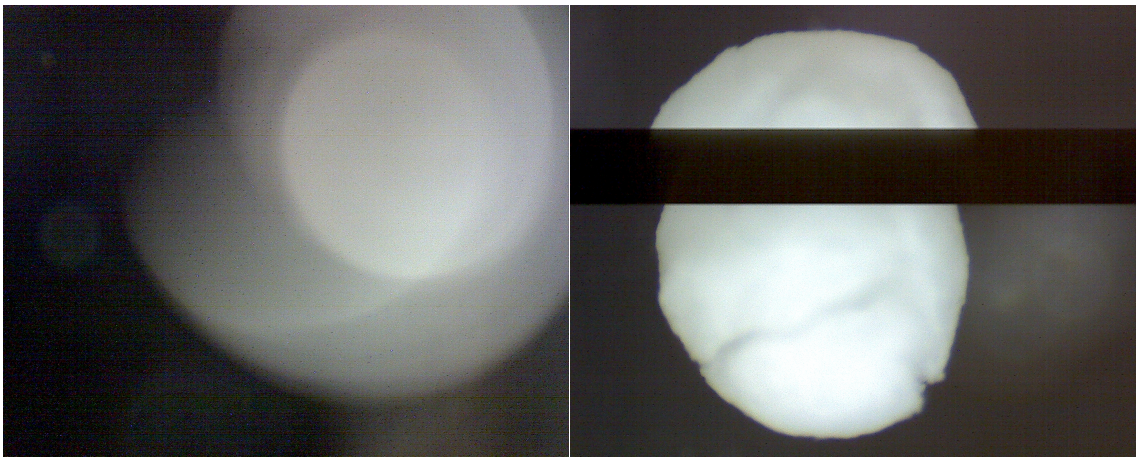

Figure 12. The rotating particles initially caused blurred images (left). The problem was fixed using a stroboscopic LED, however, this produced another problem of a moving dark segment in the images (right).

13.4 The experimental apparatus

After verifying the functionality of the modified Einstein teacup named flow-through apparatus, and identifying the critical issues and parameters, further optimization was carried out. The initial apparatus was miniaturized to the 96-well plate size, which is the norm for drug discovery physicochemical screening methods (Kerns 2001). To produce an inlet to a well for the vortex producing needle, a narrow groove, that barely punctuated the bottom corner of the well to be used, was cut along the bottom of the 96-well plate. Into this groove the inflow-needle was fitted and adjusted, so that the final positioning of the opening of needle was as close as possible to the bottom corner of the well (Figure 13). The needle stayed well fixed inside the tight groove, but was additionally fixed by gluing. It was found that the most effective flow pattern was produced when the incoming liquid was allowed to initially flow tangentially to the wall. On the contrary, if the inflow-needle was pushed inward, so that the flow was more towards the wall, the flow pattern got disturbed. The outflow-needle was prepared by bending the last centimeter of the shaft in a 90° angle. This needle was then fixed to the well plate by a strong holder clip, in a manner that positioned the bent end of the needle vertically in the center of the chamber (Figure 13).

This was the positioning found to produce the most centered and even flow pattern.

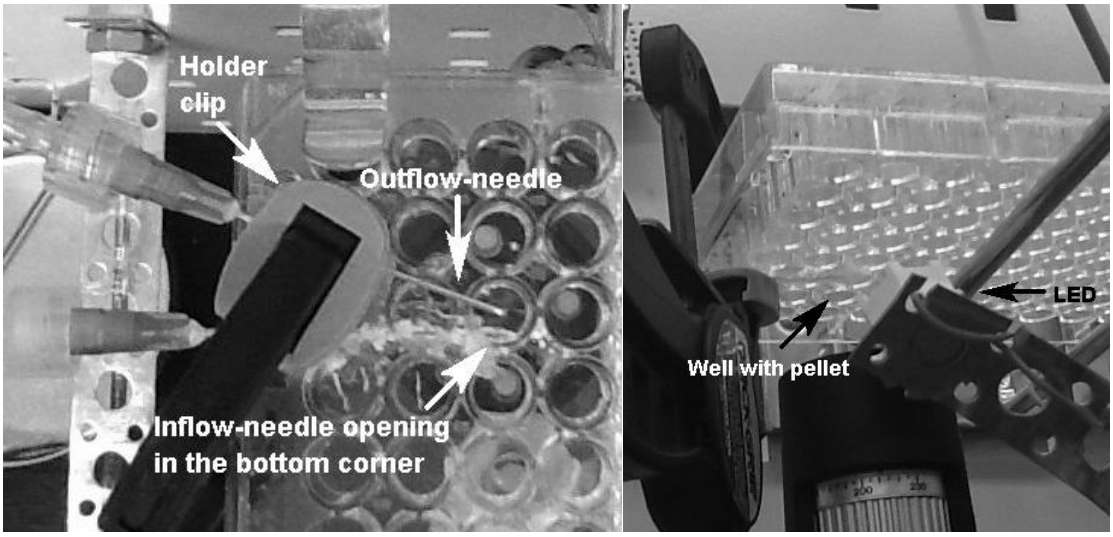

Figure 13. The 96-well plate modified Einstein teacup flow-through system, pictured from above (left) and below (right).

The piston pump was exchanged for a peristaltic pump for the new setup, in order to avoid the problematic changing of syringes during the experiments (Figure 14). Additionally, the connecting of the tubing was changed so that both inflow and outflow were regulated by the same peristaltic pump, with the same flow rate (Figure 15). As a consequence of this, the medium was removed from the dissolution chamber at the same rate as fresh medium was pumped in. This eliminated the problem of pressure buildup, avoiding the leakage issue and allowing an open system without the need for a closing cap. It was found that a 25 rpm setting on the pump produced a flow rate of 5 ± 0.05 ml/min (n=3), which was suitable for rotating the particle, image acquisition and liquid sample collection. Because all the collected medium was from the dissolution chamber, this meant that sample volumes of 5, 10 and 25 milliliters corresponded to dissolution times of 1, 2 and 5 minutes. This in turn made sample collection easy and reproducible, since timekeeping was not needed and the occasional air that was sucked into the outflow tube did not affect the results. It was also found that stroboscopic lighting from below produced the best images, and that the

maximum resolution could be used by optimizing the microscope settings. Additionally it was observed that approximately every fifth picture was of desired quality and the maximum image capturing rate of 6 images/min was therefore used for the microscope. To make the setups more robust and repeatable both the semi-static and dynamic apparatus where fixed onto a wall. In the semi-static setup the microscope was bolted to the wall, and a shelf was mounted for the 24-well plate, which allowed the replacing of the well plate at the same distance, after every shaking step (Figure8). In the dynamic setup both the microscope and the 96-well plate where fixed to the wall. Hence, the magnification and positioning where maintained throughout an experiment and also between experiments.

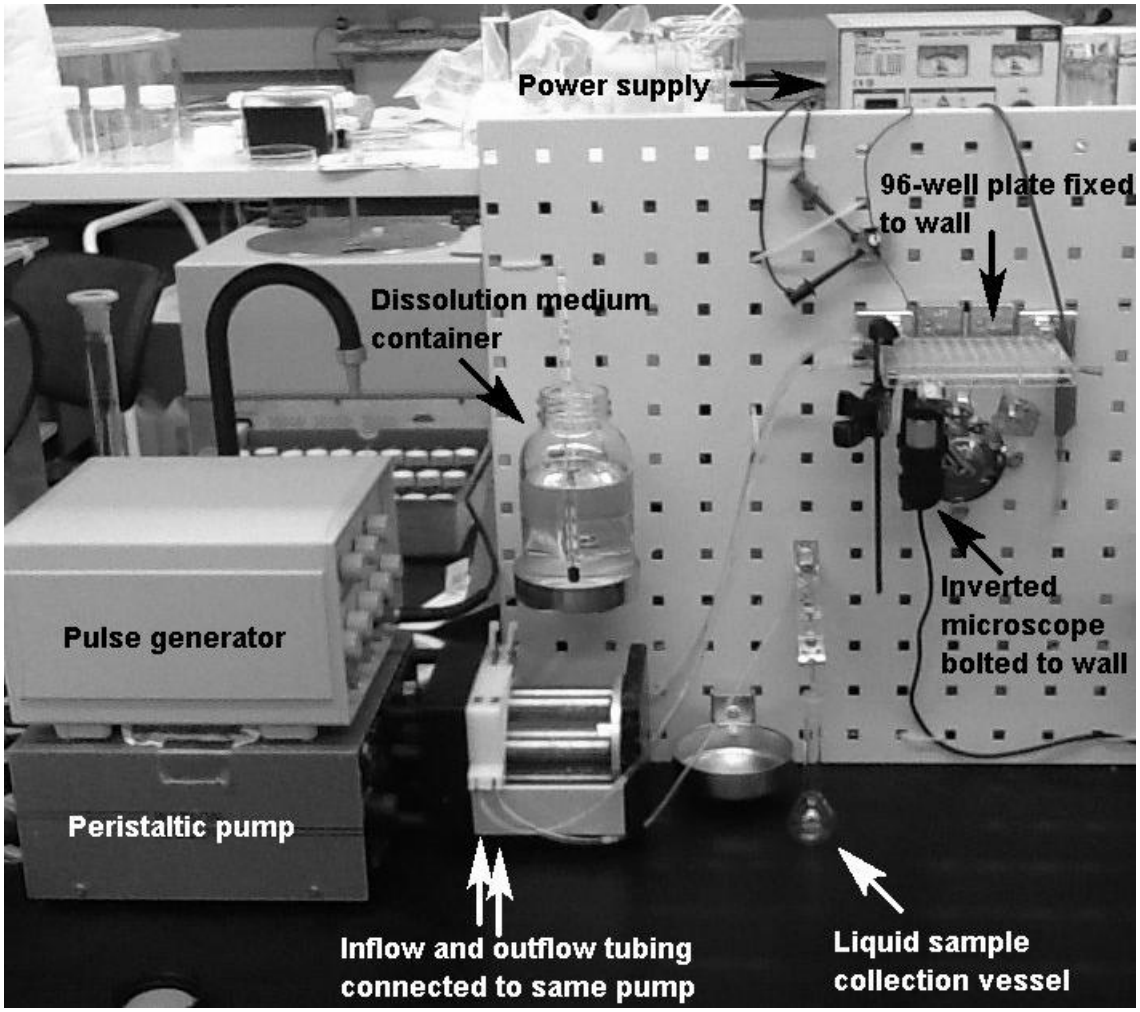

Figure 14. The modified Einstein teacup flow-through setup.

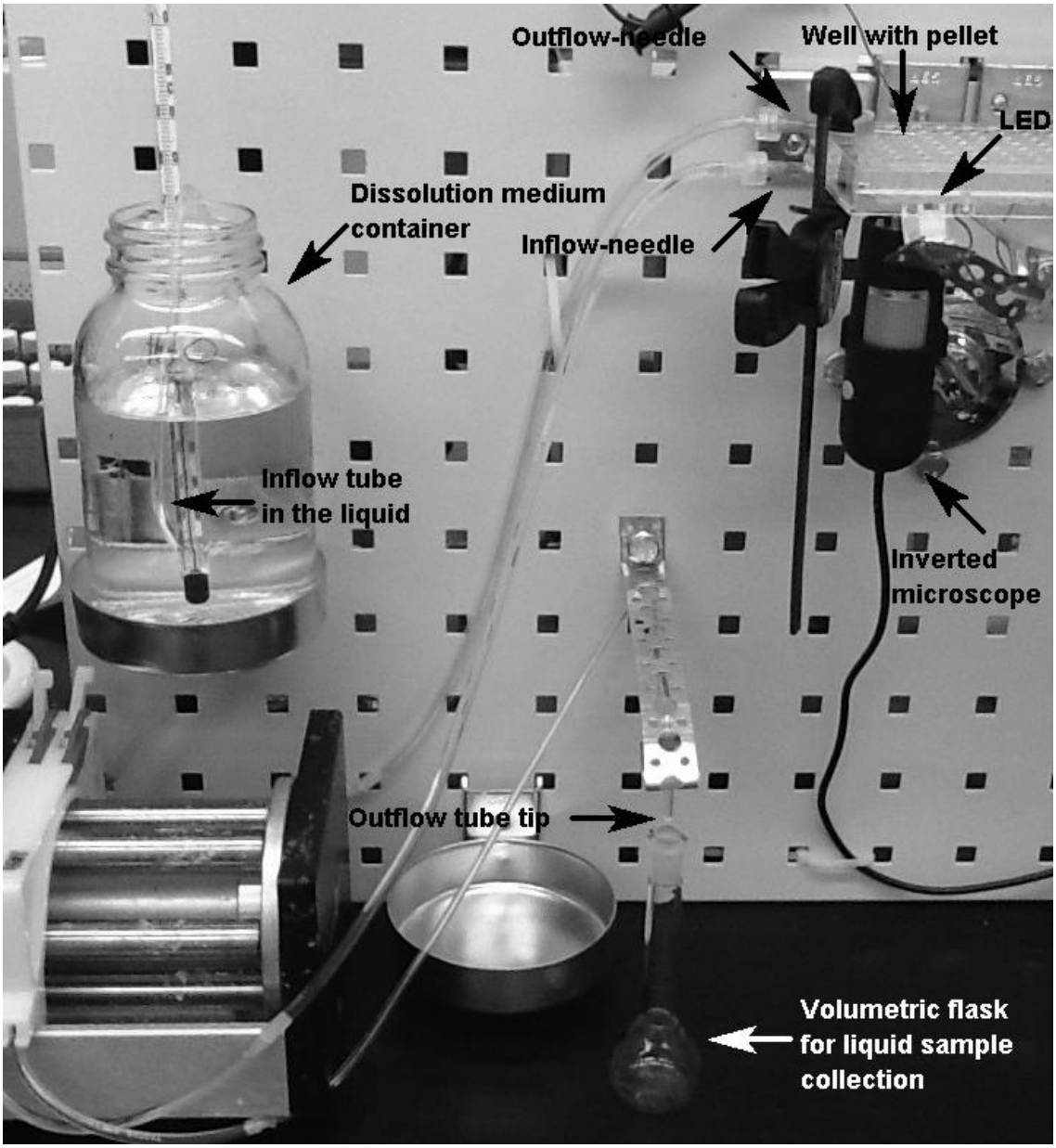

Figure 15. Close-up of the modified Einstein teacup setup.

14 MATERIALS AND METHODS

14.1 Materials

Pure substance pellets of the initial weight range 0.20-0.85 mg where used in the single particle dissolution studies. The pellets where produced from micronized powders of anhydrous theophylline (theophylline anhydrous, BASF, Ludwigshafen, Germany) and acetylsalicylic acid (ASA) (acetylsalicylic acid, Orion Pharma, Espoo, Finland) (Table 4), using a miniaturized spheronization method recently developed at the Division of Pharmaceutical Technology, Faculty of Pharmacy, University of Helsinki (D'Hollander 2013). Pellets of other substances of higher and lower solubilities where also attempted, but the higher solubility pellets where too friable and the lower solubility pellets dissolved too slowly in water to produce feasible experiment times. However, despite both studied substances having similar qualitative solubilities, the differences in dissolution behavior between these two substances produces an interesting case to be studied.

Table 4. Physicochemical properties of theophylline and acetylsalicylic acid

Physicochemical property	Theophylline	Acetylsalicylic acid
Solubility according to Ph.Eur 7.8 (2013b)	Slightly soluble (1-10 mg/ml)	Slightly soluble (1-10 mg/ml)
Water solubility* (mg/ml; 25°C)	7.36	4.60
Melting point* (°C)	273	135
pK_a*	8.81	3.49
logP*	-0.02	1.19

*ChemIDPlus Advanced 2013

14.2 Methods

All experiments where done in triplicate, *i.e.* three semi-static and dynamic experiments for both theophylline and ASA pellets, respectively, in order to get statistical reference groups, with which the individual single particle dissolution data could be compared. This would allow the assessment of the repeatability and accuracy of the methods. The experiments are henceforth referred to as AS1,AS2,AS3 and TS1,TS2,TS3 for the three semi-static ASA and theophylline experiments, respectively, and AD1,AD2,AD3 and TD1,TD2,TD3 for the three dynamic ASA and theophylline experiments, respectively. Image data was acquired using a digital optical microscope (DigiMicro 2.0 Scale, dnt Drahtlose Nachrichtentechnik Entwicklungs- und Vertriebs GmbH, Dietzenbach, Germany) under optimal setup conditions, determined during the method development, and listed in chapter 11. The microscope was connected to a computer via the PC USB port and controlled with the accompanying software (MicroCapture V2.0, dnt Drahtlose Nachrichtentechnik Entwicklungs- und Vertriebs GmbH, Dietzenbach, Germany). The software enabled either manual or timer-controlled image capturing, which were used in the semi-static and the dynamic methods respectively. All pellets where weighed using an analytical balance with an accuracy of 0.01 mg (DeltaRange AX105, Mettler-Toledo GmbH, Greifensee, Switzerland). The accuracy of the scale was affirmed by weighing ten pellets three times each and one pellet ten times. It was found that the standard deviation for both weighings was 0.01 mg.

As discussed in chapter 2, there are a multitude of factors that affect the dissolution rates of solids in liquids. However, all these factors, apart from the density of the pellets, would have equally affected the results from physical and chemical analysis. Therefore, because the main aim of the present study was to correlate image analysis and absorbance data, from the same systems of a dissolving pellet, the factors are not of relevance for the results. The density issue will be discussed in upcoming chapters. Liquid sample collection and solvent replacement in the semi-static experiments, as well as all UV-sample pipetting, was

performed using the same Finnpipette (Finnpipette® 4027, Thermo Fisher Scientific Inc., Waltham, Massachusetts, USA). Because of the small sample sizes, the relative impact of any deviations in volume would have been pronounced. Therefore, only one pipette was used, in order to avoid calibration related sources of error. The necessity of filtrating was investigated by analyzing samples from three different time-points of a theophylline and ASA single particle dissolution assay, with and without filtrating (Table 5). It was found that the difference in absorbance was randomly higher for either filtrated or non-filtrated samples, and that the calculated concentration difference was on average below 1%. Filtration was therefore determined as not being necessary in this case. The dissolution medium in all experiments was degassed distilled water. The degassing was carried out by boiling the water for 5 minutes. Immediately after boiling the liquid was filled into containers and tightly sealed with a screw lid. The hot containers where then left overnight to allow the temperature to stabilize. All tests where performed at ambient temperature, and the temperature of the medium was recorded at the beginning, middle and end of every experiment. Finally, the liquid samples where analyzed with a UV-spectrophotometer (UV-1600PC Spectrophotometer, VWR International, Leuven, Belgium) and image analysis performed, as discussed in chapter 14.2.4.

Table 5. UV-spectrophotometric data of filtered and non-filtered samples, and the difference in absorbance units (AU) and in percental concentration. The difference in absorbance units was randomly larger or smaller, and the difference in concentration on average below 1 %. Filtration was therefore determined not to be necessary in this case

Theophylline	Non-filtrated (AU)	Filtrated (AU)	Difference in absorbance units	Difference in concentration (%)
1	0.8357	0.8360	-0.0003	0.04
2	0.7774	0.7762	0.0012	0.16
3	0.8864	0.8876	-0.0012	0.14
ASA				
1	0.2627	0.2642	-0.0015	0.67
2	0.1692	0.1685	0.0007	0.54
3	0.1167	0.1180	-0.0013	1.68

14.2.1 The semi-static method

Before beginning a semi-static experiment, an image was taken of the weighed pellet in a cleaned and dried well of the 24-well plate. The experiment was then initiated by adding 3 ml of dissolution medium to the well. The following sampling time-points were at 2, 5 and 10 minutes, and after this every 5 or 10 minutes depending on the initial weight of the particle. When approaching the end of the experiments in which 10 minute intervals were used, sample collecting was again shifted to every 5 minutes, increasing the frequency of data points. This was necessary since the data obtained from the dissolution process became increasingly inaccurate towards the final stages. Between two sampling-points the well plate was kept untouched upon the custom mounted shelf, with the lid on. Thirty seconds before each sample collection, the contents of the dissolution vessel were agitated by turning the well plate upside down three times with a frequency of one turn per second, thus producing a more uniform concentration for pipetting.

After each shaking step, the pellet was allowed to settle at the bottom of the well. The well plate was then placed on the shelf, so that the whole particle was visible in the image, and an image was subsequently captured at approximately the predetermined time-point. Following this a 1 ml medium sample was pipetted and put into a small test tube. Immediately after emptying the sample into the test tube, the tip of the Finnpipette was changed and an equal volume of dissolution medium added into the well to replace the removed sample. The time was recorded for both image capturing and liquid sample collecting. This process was continued until the particle size had decreased, so that it no longer could be detected with the microscope. Immediately following an experiment the liquid samples where analyzed with the UV-spectrophotometer, which had an accuracy optimum in the range of 0.5 – 1 absorbance units (AU). Since the liquid samples where dilute, the additional mandatory dilution was always started from the smallest volume, *i.e.* 1.5 milliliters of added water. The dilution of subsequent samples with 1.5 milliliters was continued until the absorbance value approached the value of 1, after which the diluent volume was increased upwards in a stepwise manner. When again approaching the value of 0.5 AU, towards the end-point samples, diluent volumes where decreased downwards. Thus the absorbance value was always kept inside the optimal limits, except for the cases where the minimum dilution of 1.5 ml produced absorbance values below 0.5.

14.2.2 The modified Einstein teacup method

The 96-well plate modified Einstein teacup dissolution chamber was washed between every experiment by pumping 200 ml of degassed distilled water through the system. In this way any residues from previous experiments were removed. Before initiating a single pellet dissolution test, all liquid had to be removed from the tubing, in order to allow the measuring of accurate volumes from the dissolution chamber. The emptying of the tubing was achieved by pumping air at maximum speed through the system, with an inversed flow direction. The inversed flow at high speed also created a very strong spray of water from

the outflow needle towards the bottom of the cup, as well as a strong suction out from the well through the inflow needle at the bottom. This caused an effective final washing of the dissolution chamber. When all liquid had been removed from the system, the flow was inversed back to normal, and dissolution medium pumped into the inflow tube until it reached the inflow-needle hub.

The experiments where initiated by turning on the stroboscopic lighting and the timer on the image capturing software, using the maximum timer rate of 6 images/minute. During the experiments the room was darkened, leaving the flashing LED as the only source of illumination. After these preparations a drug pellet was put into the dissolution chamber, whilst simultaneously turning on the peristaltic pump. The liquid inflow began immediately, since the medium had been prepumped into the inflow tube. By starting the image acquisition before turning on the liquid flow, it was possible to determine the exact starting-point of an experiment from the first image in which liquid was observed. Dissolution medium samples from the outflow tube were collected in 5 and 10 ml scaled test tubes and 25 milliliter volumetric flasks. The collection time-points were 1 (5ml), 3 (10 ml) and 5 (10 ml) minutes and after this every 5 (25 ml) minutes until the end of an experiment. Because the samples where already very dilute, and the amounts sufficient to fill the UV-spectrophotometer cuvette, no additional dilution was needed.

14.2.3 Calibration curves and UV-spectrophotometry

Calibration curves for theophylline and ASA were produced by first scanning the UV spectra for a standard sample, from 200-500 nm, with 0.1 nm intervals. It was found that theophylline had an absorption maximum at 203.2 nm and ASA at 200.0 nm. These wavelengths where subsequently used in quantitations. Samples ranging over a ten-fold difference in concentration, 1 μg/ml – 13 μg/ml (n=10) for theophylline and 3 μg/ml – 40 μg/ml (n=6) for ASA, where analyzed and the calibration curves plotted. A first degree

polynomial fit was then made to the absorbance (y) against concentration (x) plotted data, producing the equations y = 146.2x + 0.03 (R^2=0.999) for theophylline, and y = 41.5x + 0.12 (R^2=0.997) for ASA. These equations where used to convert absorbance values of the samples into concentrations. Between every sample the cuvette was washed, with the same medium as used in the assay, and wiped on the outside with a clean cloth, whereafter the cleanliness was visually inspected. The same dissolution medium was also used for possible dilutions and for blanking before each set.

14.2.4 Image processing and analysis

Image analysis was similar for both the semi-static and dynamic methods and is therefore discussed commonly in this section. Before the first experiments of both methods an image was taken of a micrometer graticule for subsequent calibration of the scaling. The graticule was imaged again before every semi-static experiment in order to ensure the constancy of the calibration. Because the dynamic apparatus was fixed to the wall throughout the experimental phase, any tampering with the equipment would have caused disturbances in the experimental setup. This hindered the verification of the calibration scale between experiments. Consequently the fixed magnification was controlled before every experiment, and the calibration assumed to be constant in all subsequent analyses. Because of the large amount and generally suboptimal quality of the dynamic method images, all acquired images could not be used for analysis. Since the dynamic experiments lasted between 30 and 85 minutes, it was decided that one image, of representative quality, every one or two minutes would be appropriate, both in regard of the workload of the processing and the sufficiency of data points. In order to get a better representation of the average projected surface area, an attempt was also made, whenever possible, to select images close in time to each other in which significant variations of the projected surface area was observed.

After the images had been selected, they were processed and subsequently analyzed using the public domain ImageJ software (ImageJ 1.46r, U.S. National Institutes of Health, Bethesda, Maryland, USA). The images from the semi-static setup were generally of good quality and therefore easily segmented, without the need for any substantial removal of background noise (Figure 16). After binary conversion the images were analyzed using the built in particle size analysis tool of the software. Besides calculating the equivalent sphere surface area, the analysis data also contained several other parameters such as different diameters, the aspect ratio, circularity and roundness of the particle.

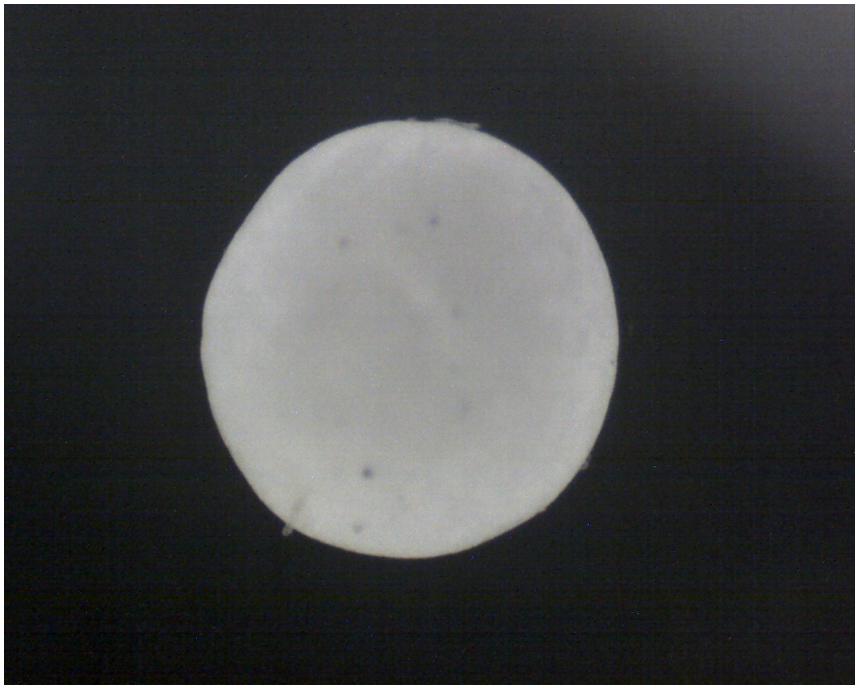

Figure 16. A typical single particle image from the semi-static method.

Images from the dynamic experiments however required more elaborate processing (Figure 17). The first step was typically to enhance the contrast of the image in order to better distinguish the edges of the pellet. This was done before conversion to monochrome, since the particle edges where better distinguished in color images. After the contrast enhancement, background noise had to be removed manually in cases where parts of the

background where of the same brightness as darker parts of the pellet. This was done to allow a successful segmentation of the image by thresholding. If areas of the background in contact with brighter parts of the pellet would have had the same brightness as the darker areas of the pellet, both the background and the darker areas of the pellet would have been removed during segmentation. After thresholding, the images where made monochrome and converted into black and white. The binary images where then further processed with the 'close' command, which smoothed the edges of the particles in areas where the segmentation had been incomplete. Also the 'fill holes' technique was applied to fill white areas inside of the black particles edges. Finally, the images where analyzed as in the semi-static case.

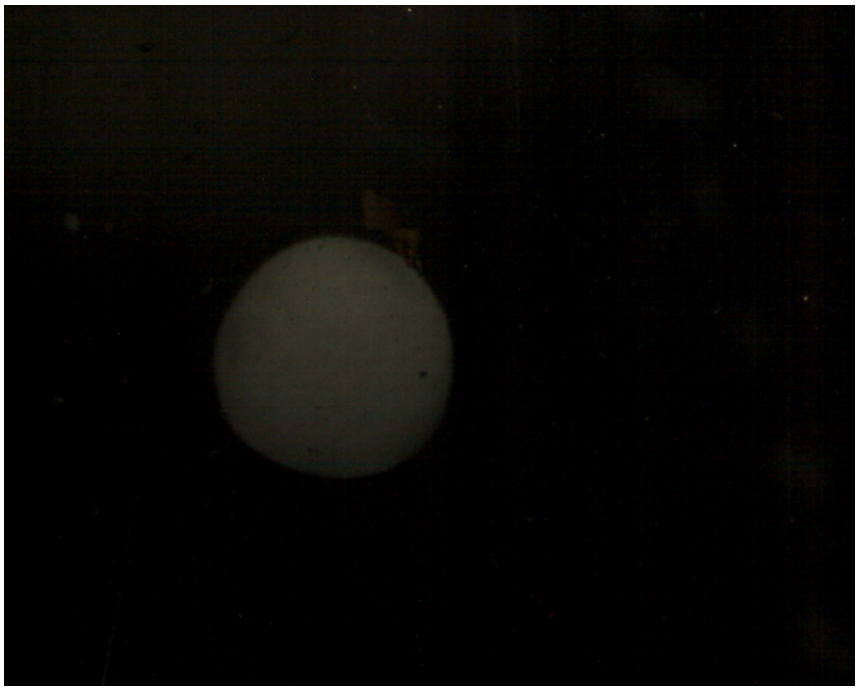

Figure 17. Typical single particle image from the Einstein teacup method.

14.2.5 Correlating physical and chemical data

To compare image analysis and absorbance data, it was found that the weight of the particles had to be normalized. This was due to the fact that the measured initial weights of the particles where not always equal to the weights predicted from UV-spectrophotometric data, which caused deviations of the dissolution profiles in these assays. Since, due to the limitations of the analytical equipment, it was not possible to observe the end of the single particle dissolution profiles, by either microscopy or UV-spectrophotometry, the endpoint and total cumulative amount dissolved had to be calculated. To normalize the weight, a second degree polynomial fit was performed to the decreasing curve of surface area per time. The extrapolated endpoint from this second degree fitting was used as the end point of an experiment. This value was then inserted in the third degree polynomial fit of the absorbance data dissolution curve, and thus the total amount of mass dissolved was acquired. This value was used to normalize both the image analysis and absorbance dissolution curves, as percent released per time. The initial pellet surface area was also extrapolated from the second degree fitting of the surface area per time plot. This was necessary since the initial surface area projection of a dry pellet before the start of an experiment was found to be constantly smaller than the first projections after the start of an experiment. This occurrence was also observed by Marabi et al. (2008) and Börjesson et al. (2013), who explained the occurrence with a swelling of the particle after coming into contact with the dissolution medium. The apparent increase in size could, however, also be a consequence of the different optical properties of air and the denser dissolution medium.

When comparing two dissolution profiles the FDA advocates the use of a similarity factor, f_2,

$$f_2 = 50 * \log\left[\left(1 + \left(\frac{1}{n}\right)\sum_{t=1}^{n}\left(R_t - T_t\right)^2\right)^{-0.5} * 100\right] \quad (27)$$

where n is the number of samples, R_t is the percental dissolved amount of the reference curve at time, t and T_t is the percental dissolved amount of the test curve, at the same time-point (FDA 2000, Costa and Sousa Lobo 2001). The equation calculates the logarithmically converted sum-squared error of the two curves, over all data points, and gets a value between 0 and 100 depending on the similarity. Two curves are regarded as similar for f_2 values over 50, which indicates an average of less than 10% difference in the dissolution curves (FDA 2000). Another factor that correlates the dissolution curves over all time-points is the difference factor, f_1,

$$f_1 = \left[\frac{\left(\sum_{t=1}^{n} \left| R_t - T_t \right| \right)}{\left(\sum_{t=1}^{n} R_t \right)} \right] * 100 \qquad (28)$$

which calculates the percental difference between two curves over all data points, with a value below 15 considered as proving equivalency. Since the images and liquid samples where not collected at the same time-points, third degree polynomial fits where used to calculate the similarity and difference factors.

The similarity and difference factors can be calculated from data sets of more than four data points (FDA 2000). The values are however also susceptible to the number of sampling points, with a higher n value leading to better correlation. Therefore it is suggested that no more than one sample, past the point where 85% of the initial mass has dissolved should be used. In the present study it was however important to compare the dissolution curves over the whole range from 0 – 100%. Since the values where calculated from the third degree fittings, it was decided that ten data points would be enough to allow accurate assessment of the f_2 and f_1 values, and few enough not to cause an improvement of the data. Thus the final time-point of an experiment was chosen as the tenth data point, and the other nine data

points where calculated so that the difference between each data point was equal. The data from chemical analysis was used as reference in all calculations. To visualize the collective data of the three pellets from an experiment setup, plots normalized both with regard to mass dissolved and time, were also needed. The normalized time values were calculated as percental differences from the final time-point.

14.2.6 Evaluating the relationship of the obtained single particle data with the Hixson-Crowell cube root model and the calculation of intrinsic dissolution rates

The relationship between the data of the single dissolving particles, and dissolution following the Hixson-Crowell cube root law (Equation 12), was investigated by plotting $w_0^{1/3} - w^{1/3}$ against time. Of the three single particle dissolution models (modifications of Equation 14) the Hixson-Crowell cube root law is the model best suited to describe the dissolution rate in the size range of the pellets used in the present study. This is because it has been shown that the Hixson-Crowell cube root law is the most accurate of the three equations, in modeling the dissolution of spherical particles larger than their diffusion layer thickness (Wang and Flanagan 1999). The pellets used in the present study are significantly larger than their diffusion layer thicknesses, throughout the major part of the experiments. The IDRs where calculated by plotting the cumulative amount dissolved, against the average surface area up to that time-point. The surface area was derived from the second degree curve fit, and the average value was received by dividing the time-point with two and inserting this value into the fitting. Only data from image analysis was used in these calculations, since it was the primary objective of this study to demonstrate the usability of this particular data.

15 RESULTS AND DISCUSSION

15.1 Validation of image analysis data

Validation of optical microscopy as analytical technique, by comparison to conventional analytical techniques, has not been performed in the previous single particle dissolution studies (*e.g.* Prasad et al. 2002; Raghavan et al. 2002; Marabi et al. 2008; Börjesson et al. 2013). There can therefore have been no certainty of the accuracy of the obtained image analysis data. In the present study the validation was, however, performed. There were two assumptions involved in the analysis of the dissolution data of the single particles. Firstly, the density was assumed to be evenly distributed throughout the particles. This assumption is discussed in relation to individual experiment data in the following chapters. Secondly, isotropic dissolution, where the pellets keep their spherical shape throughout the dissolution process, was assumed. The sphericity can be assessed by analyzing the change in aspect ratios of the pellets (Table 6). It can be seen from this data that the average aspect ratios of the particles ranged between 1.09 and 1.22, with small standard deviations. This indicates the retaining of a spheroidal shape throughout the experiments, for all particles, which is in line with results from other single particle assays where spherical particles have been used (Parrott et al. 1955, Marabi et al. 2008).

Table 6. Initial weight, aspect ratios and the change (+/0/-) in the aspect ratios during single particle experiments. A general tendency for increased and decreased aspect ratios for the static (T/ASX) and dynamic (T/ADX) experiments, respectively, can be observed

Experiment	Initial weight (mg)	Initial aspect ratio	Average aspect ratio with standard deviation	Change
TS1	0.45	1.09	1.11 ± 0.06	+
TS2	0.85	1.17	1.22 ± 0.07	+
TS3	0.27	1.08	1.19 ± 0.06	+
AS1	0.20	1.11	1.19 ± 0.07	-
AS2	0.41	1.09	1.09 ± 0.05	0
AS3	0.66	1.10	1.10 ± 0.05	0
TD1	0.24	1.18	1.13 ± 0.06	-
TD2	0.62	1.14	1.11 ± 0.06	-
TD3	0.26	1.14	1.13 ± 0.10	-
AD1	0.71	1.12	1.11 ± 0.06	-
AD2	0.75	1.11	1.18 ± 0.09	+
AD3	0.29	1.20	1.22 ± 0.11	+

A general trend of slightly increasing aspect ratio, from the initial value, can be observed for the semi-static experiments. Especially the two smallest particles, TS3 and AS1, showed an increase from the initial aspect ratio. This could be due to the buildup of uneven concentration gradients around the stagnant particles. As was shown by Østergaard et al. (2011), the concentration around a dissolving single particle, in a stagnant liquid, is always highest towards the bottom. This would cause different concentration gradients ($C_S - C_t$) around the single pellets which would lead, according to the Noyes-Whitney equation (Equation 4), to varying dissolution rates from different parts of the pellet surface. Additionally Østergaard (2011) and coworkers showed that density gradients in the liquid led to uneven convection around the particles, which would further have enhanced the anisotropic dissolution. The general trend in the dynamic experiments is on the other hand a constant or decreased aspect ratio, from the initial values, and no dependency on initial

particle weight can be observed. It thus seems that the modified Einstein teacup method with a constant flow and sink conditions around the rotating particle, was able to produce a more isotropic dissolution with a tendency towards higher sphericity for the dissolving pellets.

15.1.1 The semi-static method

The semi-static system was exposed to varying conditions throughout an experiment. In the beginning sink conditions would have prevailed and, for a short time, the dissolution rate would have been intrinsic dissolution rate driven. However, the lack of agitation between sampling-points, very quickly would have established a growing diffusion layer around the dissolving particle, as shown by Østergaard et al. (2011). The dissolution rate would then have been diffusion limited, following Fick's I law of diffusion (Equation 1). When the contents were mixed, the diffusion layer would have decreased and consequently the driving force ($C_S - C_t$) of the Noyes-Whitney equation (Equation 4) would have increased (Hixson and Crowell 1931). The concentration gradient ($C_S - C_t$) would have been further increased by removing of sample, and subsequent replacement with fresh solvent, leading to even higher dissolution rates. After sampling, this cycle would have been repeated, starting with a buildup of a diffusion layer in the stagnant liquid.

The purpose of the semi-static method was, however, only to establish a correlation of dissolution rate data from image analysis and UV-spectrophotometry. To this end the semi-static method was very suitable. Due to the static conditions during the capturing of an image, the image quality was good and the images easily processed (Figure 16). The stagnant medium also allowed the sometimes uneven particles to settle in their preferential position, leading to constant overestimation of the particle volume. Since the overestimation was constant, it did not notably affect the results. This is because the mass dissolved from an overestimated volume was calculated based on the density of the initial

overestimated volume. The data of the individual particles used in the semi-static method are represented in Table 7. It can be seen that the correlation data of the ASA pellets are very good, with an average (± standard deviation) R^2 value of 0.988 ± 0.013 and an average similarity factor (f_2) of 76 ± 27. Henceforth, average values are reported as mean ± standard deviation. The similarity (f_2) and difference (f_1) factors are even better, around 90 and 2 respectively, for two out of three ASA single particle experiments, demonstrating almost identical curves, as can be seen in Figure 18.

Table 7. Correlation of physical and chemical analysis data from the semi-static single pellet experiments of acetylsalicylic acid (ASX) ant theophylline (TSX), as well as physical factors affecting the results. Average values are presented with standard deviation in the relevant cases. The similarity factors (f_2) and difference (f_1) factors indicate the very high similarity of physical and chemical analysis data

Expeiment	R^2	f_2	f_1	Weighed mass (mg)	Predicted mass (mg)	Density (mg/mm^2)
AS1	0.974	45	15	0.20	0.15	0.67
AS2	0.993	89	2	0.41	0.42	0.64
AS3	0.998	94	1	0.66	0.67	0.62
Average	0.988 ± 0.013	76 ± 27	6 ± 8	0.42	0.41	0.64 ± 0.03
TS1	0.980	81	3	0.45	0.40	0.66
TS2	1.000	96	1	0.85	0.83	0.67
TS3	0.996	96	1	0.27	0.25	0.67
Average	0.992 ± 0.011	91 ± 9	2 ± 1	0.54	0.49	0.67 ± 0.01

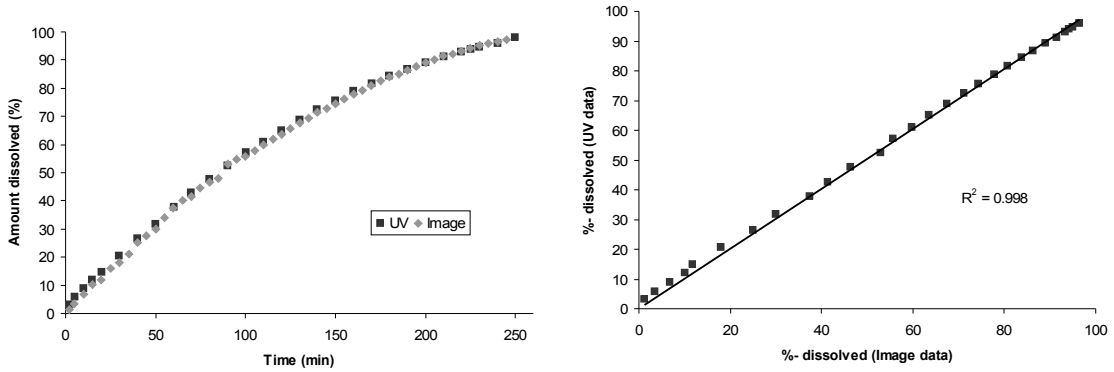

Figure 18. Dissolution curves of physical (Image) and chemical (UV) analysis data from a semi-static acetylsalicylic acid single pellet experiment (AS3) (left) and the correlation curve of the data sets (R^2=0.998) (right).

The higher deviation in the ASA1 experiment was a result of a deviating chemical analysis curve for this sample. This can be clearly seen in Figure 19 where the one deviating UV dissolution curve shows a continuously higher dissolution rate, when compared to the collective data. The same is also visualized in Figure 20, where the standard deviation of the weight and time normalized UV dissolution curve is significantly higher that that of the image analysis dissolution curve. There are two possible causes for the deviating AS1 data. First, it can be seen that the pellet had a larger than average difference in weighed and predicted mass, which could cause a erroneous normalization of the percentual mass dissolved for the absorbance data (Table **7**). The other cause of error might be the inaccuracy of the UV-spectrophotometer. Since the AS1 pellet mass was the smallest of the three, it consequently produced the most diluted samples, of which 10/18 had absorbance values below the optimum of 0.5 AU. The four last data points of experiment AS2, that show a clear deviation from the previous data points, were an anomaly that could not be explained. However, the data points are equally observed in both image analysis and absorbance data, which means that it was not caused by an error in either analytical technique. The significant deviation from the prior rate profile could have been caused by the mixing. If there was a significantly porous and friable area in the pellet, the agitation could have caused it to disintegrate and thus rapidly dissolve. As discussed by Yu et al.

(2004), the disintegration of the studied solid would cause an increase in the dissolution rate.

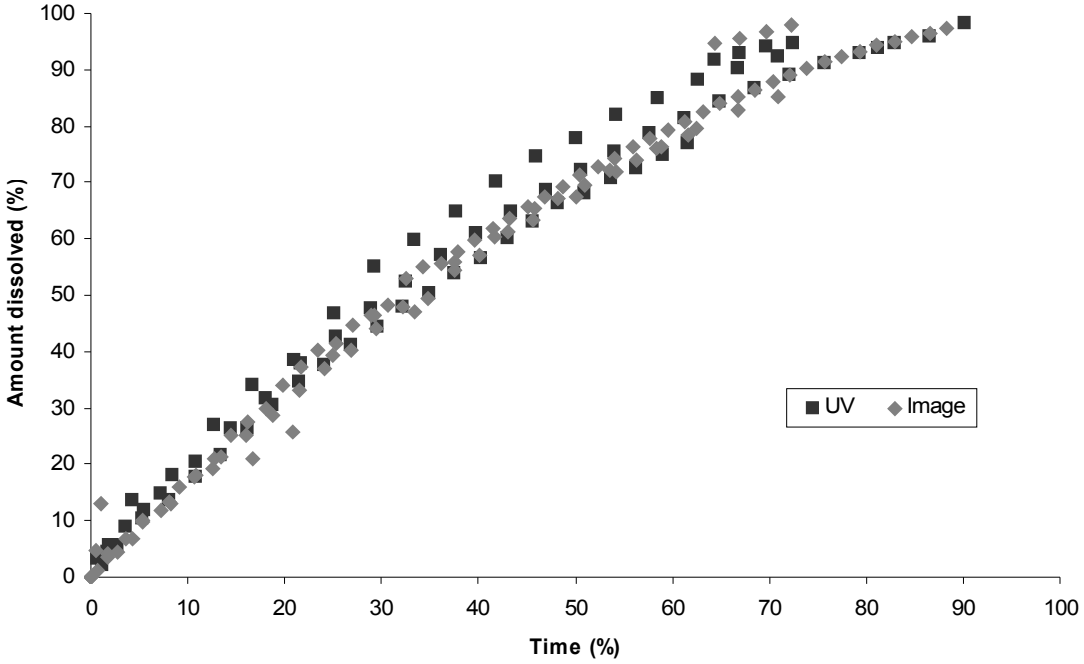

Figure 19. Collective acetylsalicylic acid single pellet dissolution curves of all three semi-static experiments, from UV-spectrophotometric (UV) and image analysis (Image) data. The constantly deviating absorbance curve of sample AS1 is observed.

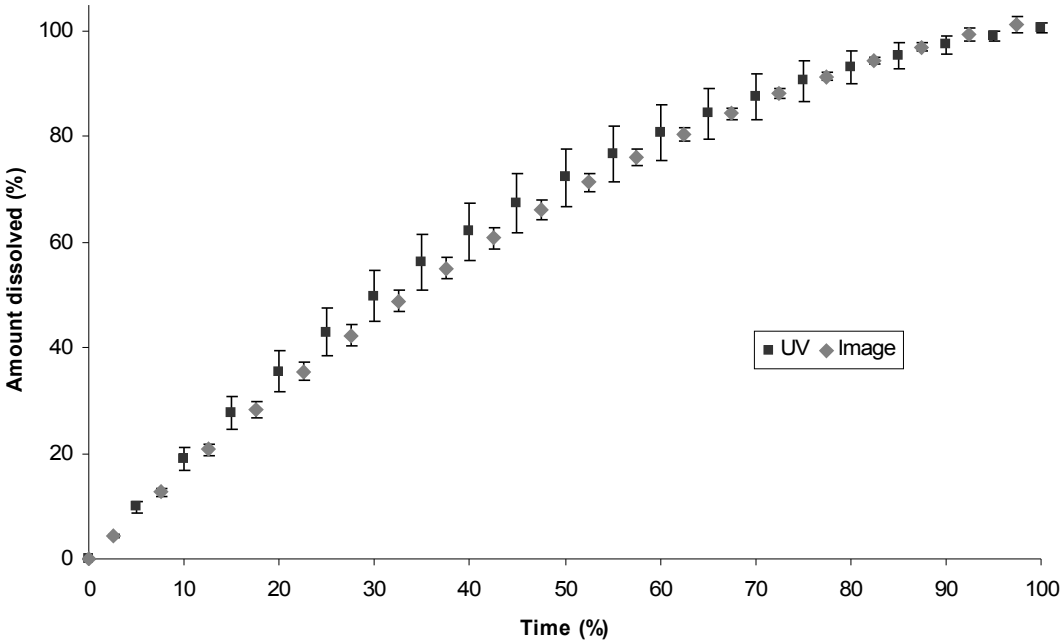

Figure 20. Average (n=3) acetylsalicylic acid dissolution curves from UV-spectrophotometric (UV) and image analysis (Image) data from the semi-static method, with standard deviation. A clearly higher standard deviation, caused by one deviating curve, of the absorbance data can be observed.

Physical and chemical data from the theophylline single particle experiments did not seem to correlate very well at first. However the R^2 value was very high for all experiments and it was found that the dissolution curves varied by a constant value over all time-points (Table 7). As shown by D'Hollander (2013) in her masters thesis, developing the miniaturized pelletization method, the anhydrous theophylline pellets recrystallized as theophylline monohydrate after the wetting process. Since the calibration curve for theophylline was produced from theophylline anhydrate powder, a correction factor of 1.0999, which is the ratio of the MW's of theophylline anhydrate/theophylline monohydrate, was used to correct the UV-absorbance data. This resulted in significantly higher correlations. The theophylline pellets all produced similar results, with average f_2 and f_1 values of 91 ± 9 and 2 ± 1 respectively (Table 7). This shows a very high similarity between the physical and chemical data, as depicted in Figure 21, with an average 2 ± 1% difference over all data points.

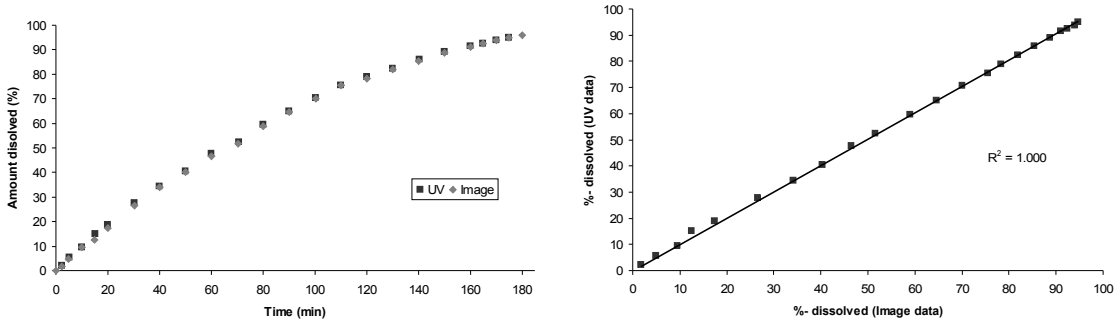

Figure 21. Dissolution curves of physical (Image) and chemical (UV) analysis data from a semi-static theophylline single pellet experiment (TS2) (left) and the correlation curve of the data sets (R^2=1.000)(right).

There was again one experiment that produced slightly lower correlation. This TS1 sample showed the greatest variation in measured and predicted particle weight, as was the case with the AS1 pellet. The data from experiment TS1 could have been predicted to be the most accurate of the three theophylline pellets, since it had the lowest aspect ratio (1.09 ± 0.07) and the highest roundness (0.92 ± 0.05) throughout the experiment. A possible difference in density could therefore be the cause of this result. Parrot and coworkers (1955) concluded that the dissolution rate was independent of the density of the particles. Similar results where shown by Yu et al. (2004) who found that the dissolution rate, when using the rotating disc method, was not notably affected by the compression force applied when producing the studied sample. However, both of these studies used compressed samples, and it can therefore be assumed that the density of their samples would have been significantly higher, and more evenly distributed, than what is the case with non-compressed pellets.

As shown by Börjesson et al. (2013) the intraparticle porosity of spherical particles can be significant. They assumed that this unevenly distributed density was the cause for the varying dissolution rates, for single dissolving particles. Since, in the present study, the

density of a pellet was assumed to be constant throughout the whole pellet, particle size analysis of the dissolution from a lower density area would cause an erroneously high interpretation of the mass dissolved. However, the weight normalized TS1 dissolution curve from image analysis data showed a slightly lower dissolution rate than absorbance data, and it is therefore assumed that the weight of the TS1 pellet was the primary cause of error. The strong correlation of the overall, weight and time normalized data, can be seen in Figure 22 and the slightly higher standard deviation of average (n=3) dissolution rate data from image analysis can be seen in Figure 23. The deviation in image analysis data can be explained by the fact that the particles where not perfectly spherical, and a misinterpretation of the particle size was therefore possible. As discussed, intraparticle density variations might be another source of error as well as the image processing. Despite of these possible sources of inaccuracy, the overall data shows surprisingly little variation.

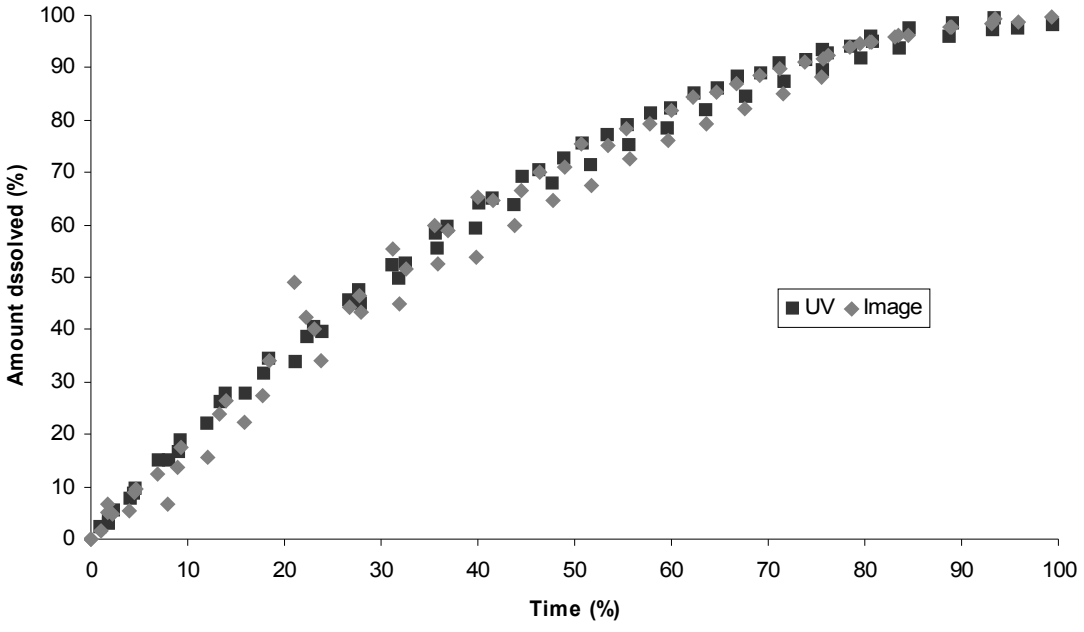

Figure 22. Collective theophylline single pellet dissolution curves of all three semi-static experiments, from UV-spectrophotometric (UV) and image analysis (Image) data. A very high similarity can be seen.

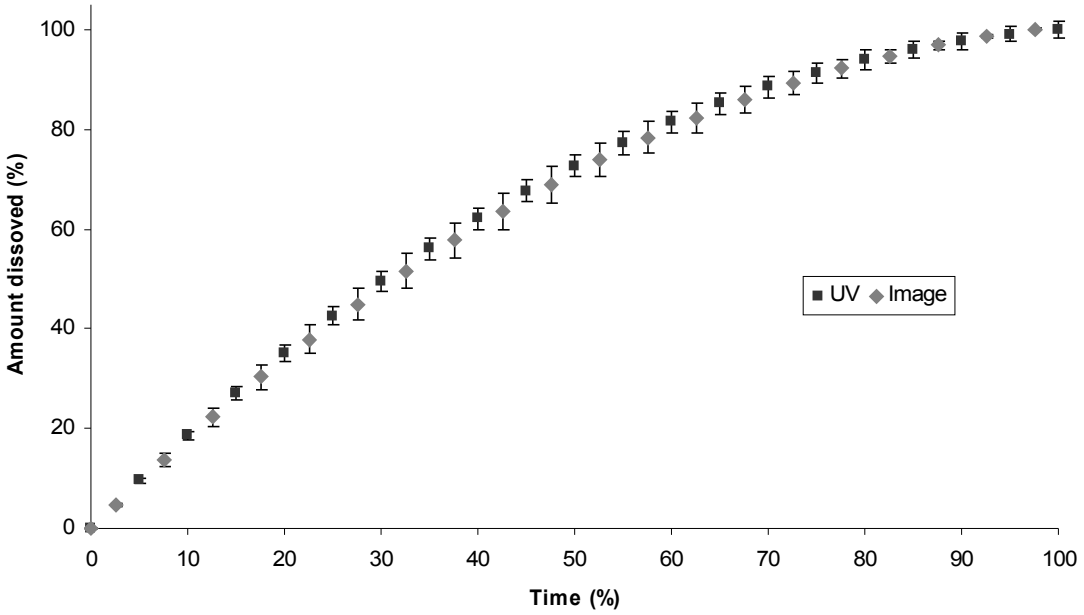

Figure 23. Average (n=3) theophylline dissolution curves from UV-spectrophotometric (UV) and image analysis (Image) data from the semi-static method, with standard deviation. A slightly higher standard deviation of the image analysis data can be observed.

From the semi-static data it can concluded that a very high correlation of physical data from image analysis and chemical data from UV-spectrophotometry is achieved. Most of the dissolution curves are practically identical and where discrepancies are observed, these can, mostly, be explained by lacking accuracy of the analytical apparatus used and not so much by the image analysis method. It can also be seen that where accurate measurements of particle mass and chemical data are achieved, the single experiments actually give a better correlation than the average data.

15.1.2 The modified Einstein teacup method

The novel 96-well plate modified Einstein teacup succeeded in trapping the single freely moving particles in a sufficiently small area to allow their microscopic imaging. The flow-through setup is assumed to have been sufficient to produce constant sink conditions, since 5 ml of fresh liquid was pumped through the 300 µl well every minute (Mosharraf and Nyström 1995). This would have made the dissolution rate solubility and intrinsic dissolution rate driven throughout the experiments, in accordance with the Noyes-Whitney equation (Equation 4). The sink conditions where also a prerequisite for the Hixson-Crowell cube root law correlation and the IDR calculations, which are discussed in the following chapters (Hixson and Crowell 1931; USP 2001). The correlation results of physical and chemical data from the dynamic method are not as high as for the semi-static method. This was expected since the dynamic method contained several more variables and, therefore, possible sources of error. It can be seen in Figure 24 that limited image analysis data was received during the first minutes of the experiments. This was due to the fact that the initially large rotating pellets tended not to be fully visible in the imaging area, which prevented the calculation of the projected surface area. The problem disappeared with decreasing particle size, since the smaller pellets remained for longer periods completely inside the imaging area. Also other challenges such as the not as good image quality, and the consequently increased processing, caused more variability in the image analysis data from the dynamic experiments.

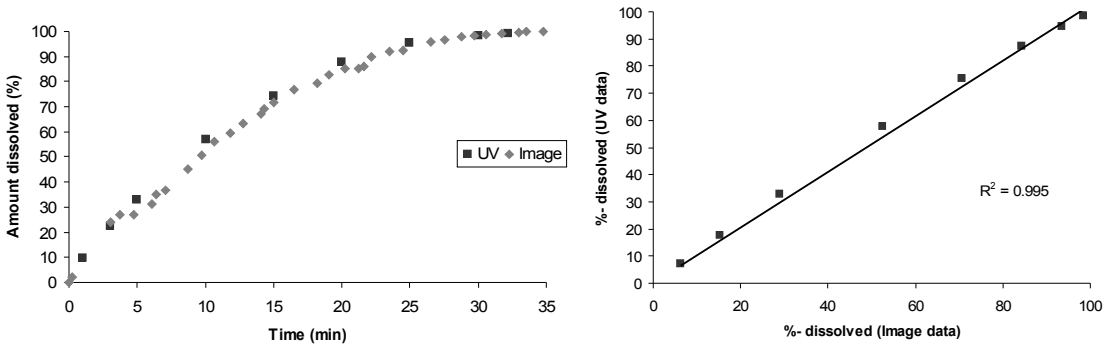

Figure 24. Dissolution curves of physical (Image) and chemical (UV) analysis data from a modified Einstein teacup theophylline single pellet experiment (TD1) (left) and the correlation curve of the data sets (R^2=0.995) (right).

The rotating pellets showed quite different area projections in successive images, which led to a sometimes strong oscillation in the calculated amount dissolved. The variability, however, evened out over time, and gave a good representation of the average 3D particle size. Because only one image every one or two minutes was used, the data could possibly have been more accurate if more data points could have been analyzed. The acquisition of more data points is, however, easily achieved using more sophisticated equipment, with which it would be possible to analyze image data more frequently and with better accuracy. While the dissolution curves might seem to be similar to those of the semi-static method, this is an illusion caused by the decreasing effective surface area of the single pellets (Equation 17). If the surface would have been kept constant throughout the experiments, the dissolution curves would have followed zero-order kinetics and produced straight lines (Yu et al. 2004).

Despite the many possible sources of error, the correlation is very high as seen in Table 8. For the theophylline pellets, the average f_2 value of 69 ± 12 is clearly above the value of 50, which according to the FDA is required to indicate similarity of two curves (FDA 2000). The average difference factor of 6 ± 4 also clearly demonstrates the similarity of the curves. From the weight and time normalized data in Figures 25 and 26 it can be notated that the

absorbance data produces a continuously faster dissolution rate, compared to image analysis data. Since this was not the case in the semi-static method nor in the dynamic ASA results, it can be speculated that the reason lies in the correction factor. Even if the pellets where not of purely monohydrate form in the semi-static method, the static conditions would have allowed possible anhydrous substance on the surface of the pellet to convert into monohydrate form (*e.g.* Aaltonen et al. 2006). However, the flow agitation and the sink conditions inside the modified Einstein teacup could have been sufficient to remove any dissolved anhydrous form from the surface of the pellet, thus preventing it from recrystallizing as monohydrate (Hulse et al. 2012). In this case the dissolution rate would have been a combination of the dissolution rates of both theophylline monohydrate and anhydrous, and the correction factor would consequently have been too high. This is, however, only speculation and the actual case could be investigated by monitoring the solid state with e.g. *in situ* Raman spectrophotometry (Aaltonen et al. 2006). The anomalous TD2 sample was again the sample with greatest difference in measured and predicted weight. The R^2 value of 0.998 however signals a high correlation between the curve shapes, which can indicate a constant deviation over all data points, and could therefore be explained by an erroneous correction factor. It can be seen from the standard deviations in Figure 26 that no significant difference in variability between the image analysis data and the absorbance data exists.

Table 8. Correlation of physical and chemical analysis data from the modified Einstein teacup single pellet experiments of theophylline (TDX) and acetylsalicylic acid (ADX), as well as physical factors affecting the results. Average values are presented with standard deviation in the relevant cases. The similarity factors (f_2) and difference (f_1) factors show the high similarity of physical and chemical analysis data

Expeiment	R^2	f_2	f_1	Weighed mass (mg)	Predicted mass (mg)	Density (mg/mm^2)
TD1	0.995	72	4	0.24	0.24	0.70
TD2	0.998	55	11	0.62	0.58	0.84
TD3	0.994	79	3	0.26	0.24	0.74
Average	0.996 ± 0.002	69 ± 12	6 ± 4	0.37	0.35	0.76 ± 0.07
AD1	0.995	73	4	0.71	0.70	0.76
AD2	0.999	84	2	0.75	0.81	0.77
AD3	0.998	71	4	0.29	0.33	0.92
Average	0.997 ± 0.002	76 ± 7	3 ± 1	0.58	0.61	0.82 ± 0.09

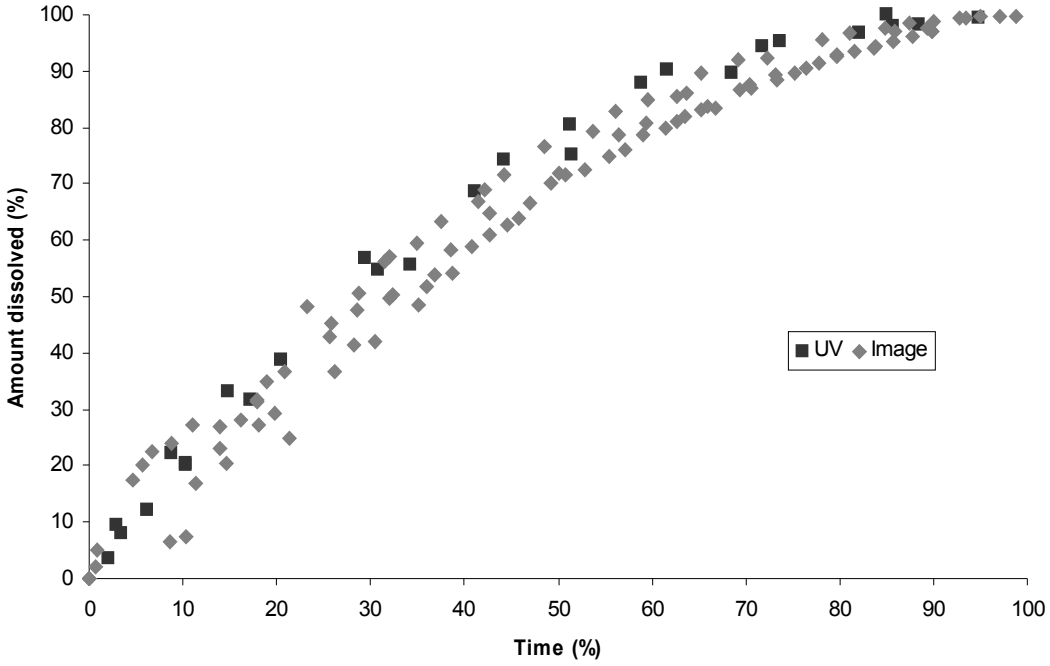

Figure 25. Collective theophylline single pellet dissolution curves of all three semi-static experiments, from UV-spectrophotometric (UV) and image analysis (Image) data. The absorbance data is constantly higher that respective image analysis data.

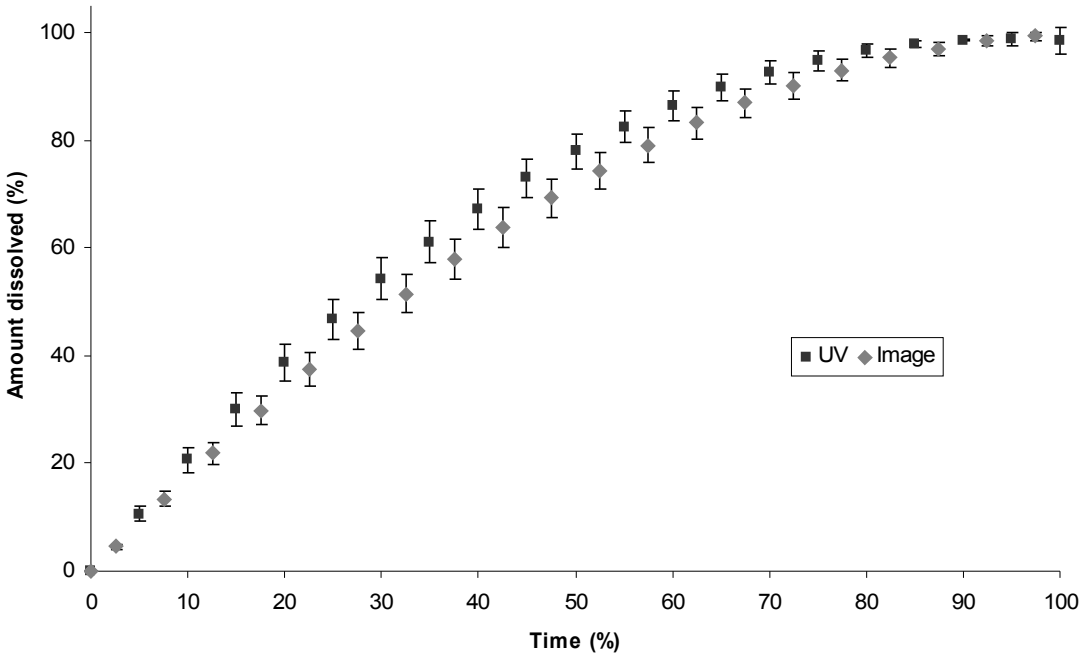

Figure 26. Average (n=3) theophylline dissolution curves from UV-spectrophotometric (UV) and image analysis (Image) data from the modified Einstein teacup method, with standard deviation. No difference in standard deviation is observed but the constantly higher values of the absorbance data can be seen.

The modified Einstein teacup dissolution data of ASA shows a very good correlation for all three experiments (Table 8). The average f_2 and f_1 values of 76 ±7 and 3 ±1 respectively, demonstrate the high similarity of the dissolution profiles. This is visualized in both the data from a single experiment (Figure 27) and in the combined data (Figure 28). Two out of three experiments ended at approximately 80% of the total time, and thus the deviation towards the end of the image analysis data dissolution curve in Figure 29**,** is due to the weakness of the third degree polynomial fit and not of the experimental data. A clear increase in the standard deviation of the absorbance data can however be seen before the 80% time-point, which indicates the loss of accuracy of the UV-spectrophotometer at lower concentrations.

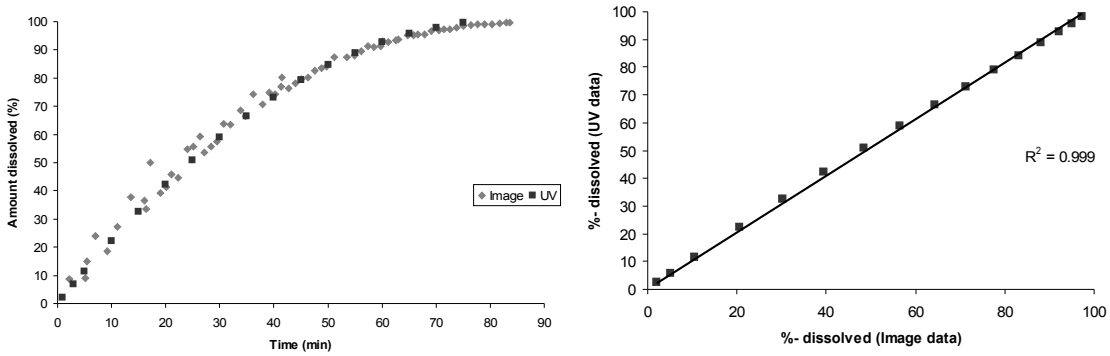

Figure 27. Dissolution curves of physical (Image) and chemical (UV) analysis data from a modified Einstein teacup acetylsalicylic single pellet experiment (AD2) (left) and the correlation curve of the data sets (R^2=0.999)(right).

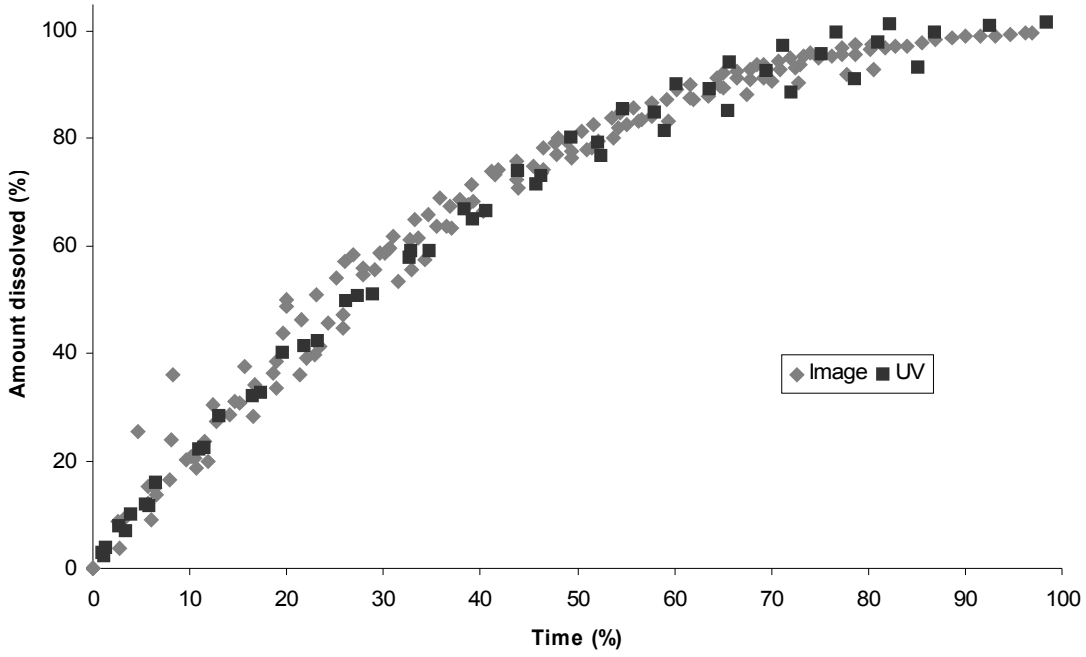

Figure 28. Collective acetylsalicylic acid single pellet dissolution curves of all three semi-static experiments, from UV-spectrophotometric (UV) and image analysis (Image) data. Higher variations in absorbance data is observed towards the end, while image analysis data shows decreasing variation.

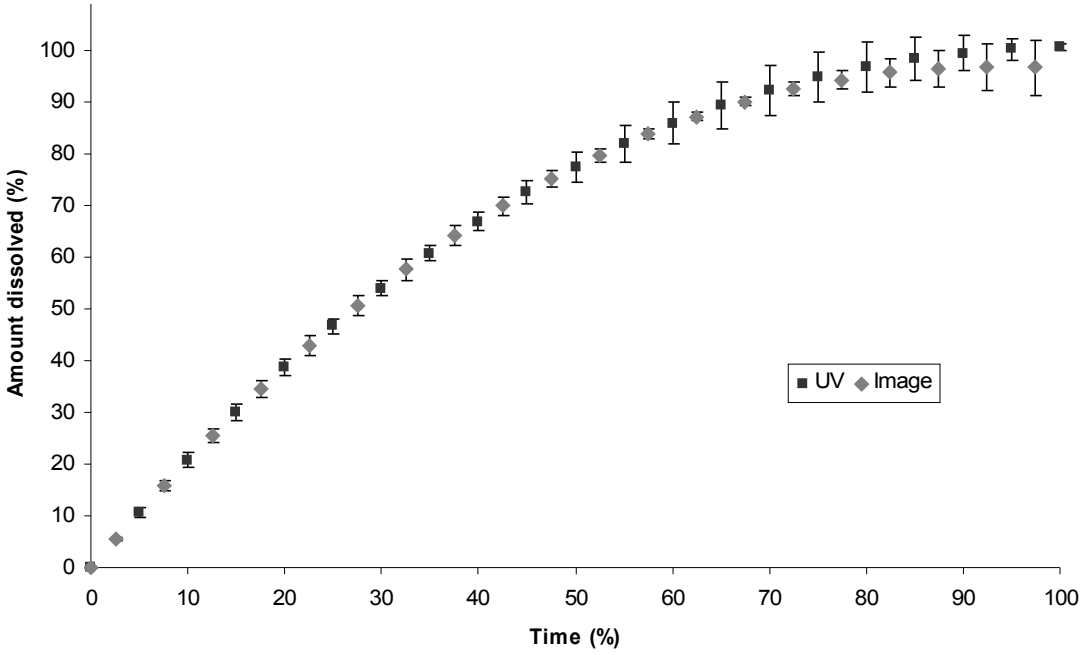

Figure 29. Average (n=3) acetylsalicylic acid dissolution curves from UV-spectrophotometric (UV) and image analysis (Image) data from the modified Einstein teacup method, with standard deviation. The increasing standard deviation of the absorbance data is clearly observed, while all data past 80% on the Time axis are unreliable due to the weakness of the curve fit.

As in the case of the semi-static results, it can be observed from both theophylline and ASA dynamic dissolution data that the single experiments often produce equal or higher correlation, between physical and chemical data, than the average data. It can also be observed from Figures 25 and 28 that the general trend for the image analysis data of the dissolving particles is towards smaller variation as the particle size decreases. This is not the case for the chemical analysis data, where a sometimes large increase in variation is observed as the samples become more dilute and the chemical analysis approaches its limits. The smaller variation of the image analysis data is, however, not always reflected in the values calculated by intrapolation based on regression analysis, as can be seen in Figure 29. It can also be concluded that, as in the case of the semi-static data, the deviating results can be assumed to be caused by factors unrelated to the analytical accuracy of particle size

analysis. The one common factor of all deviating results was the higher difference in measured and predicted weight of the particle. This problem can easily be overcome using a more accurate scale. Also the limitations of the current dynamic setup, with regard to the number of data points and the image quality, are easily corrected using more sophisticated equipment.

15.2 Using the Hixson-Crowell cube root law to explain the obtained dissolution rate data

It was expected that a linear correlation of the obtained data with the Hixson-Crowell cube root law, would be achieved up until the time-point where the particle diameter decreased below 200 μm. This was because it has been theorized that the dissolution rate will start to notably increase below this particle size (Wang and Flanagan 1999). A significant increase would also be expected for particles below 50 μm, when the diffusion layer thickness would start to decrease (Hintz and Johnson 1989). The threshold diameter of 200 μm was however only crossed in two experiments, TD1 and TD3. In experiment TD3 the four last data points start to deviate from the relatively linear tendency of the previous data points. However, only the two last data points are below 200 μm and are calculated from images of suboptimal quality, which means that the uncertainty regarding the accuracy of the data has to be taken into account. Therefore, no generalization can be derived from this data. Experiment TD1 (Figure 30) had five data-points below 200 μm, which means that a general tendency can be better investigated with this data. No significant increase towards the end of the curve can be seen in the TD1 dissolution profile, but a continuous increase can on the other hand be observed from the curved shape. This continuous increase can also be observed from the Hixson-Crowell rate constant (Equation 13) of sample TD1 (Figure 31).

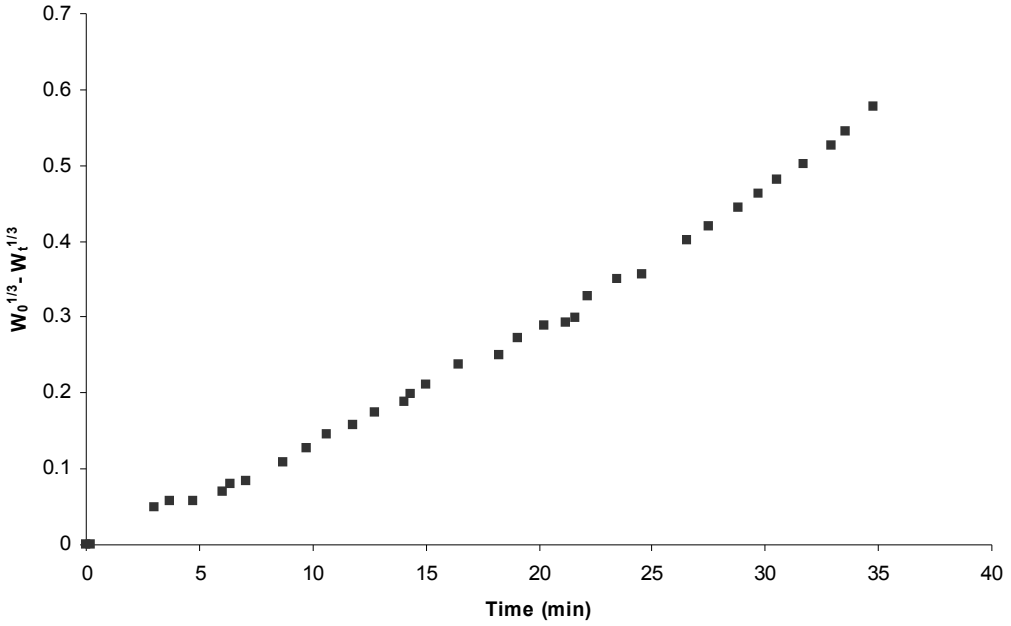

Figure 30. Hixson-Crowell cube root law correlation curve for dissolution data from single particle theophylline experiment TD1. Non-linear correlation can be observed.

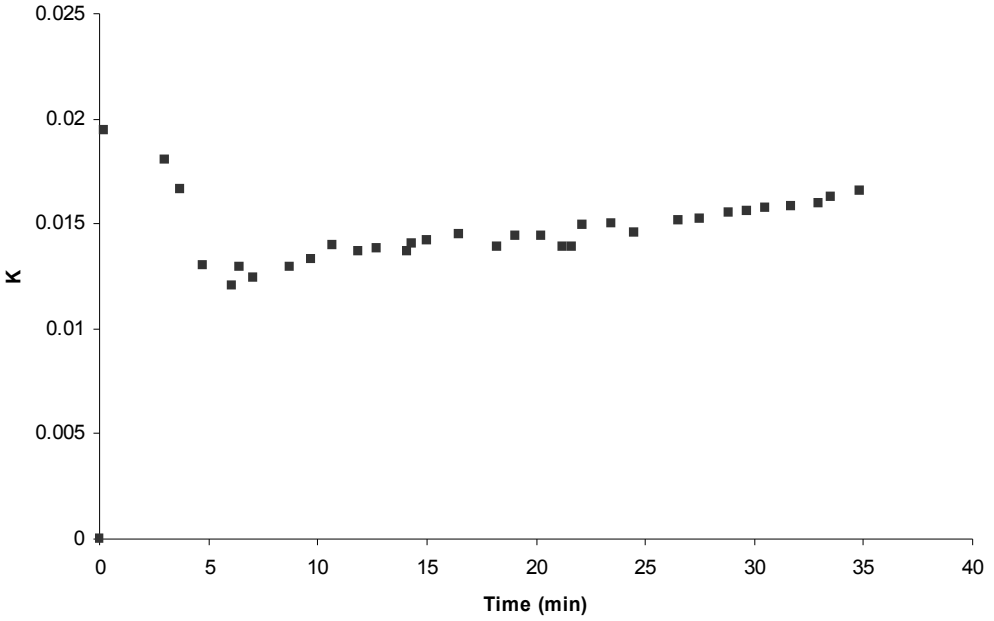

Figure 31. The change of the Hixson-Crowell rate constant, K with time for single particle theophylline experiment TD1. A general increase can be seen.

The data from all ASA experiments however showed a high linear correlation with the Hixson-Crowell cube root law, of which one example is the correlation curve of the AD1 experiment in Figure 32. When trying both first and second degree fits to the Hixson-Crowell cube root law correlation data of all ASA and theophylline experiments, the difference in dependency is demonstrated (Table 9). It can be seen that while all the theophylline dissolution profiles show a clear increase in the R^2 value when moving to a higher order polynomial fit, no or minimal change is observed for the ASA data. This constantly increasing dissolution rate of the theophylline pellets could indicate a continuous decrease of the diffusion layer thickness, which the Hixson-Crowell cube root law is not capable of modeling (Macheras and Dokoumetzidis 2000). According to the Nernst-Brünner equation (Equation 5) a constant decrease of the diffusion layer thickness, *h*, would lead to a constant increase in the dissolution rate.

However, the dissolution behavior of theophylline is very complex, due to the possible anhyrdate/monohydrate polymorph transformations (Lehto et al. 2008). As was shown by Aaltonen et al (2006), the phase transformation from anhydrate to monohydrate, in aqueous media, begins immediately after liquid immersion in a flow-through cell. They also showed that as the proportion of the monohydrate form increased, the dissolution rate accordingly decreased. This is in accordance with Equation 20, since the more stable monohydrate form will decrease the solubility, and thus the dissolution rate (Huang and Tong 2004). However, Hulse et al. (2012) who also studied the dissolution of anhydrous theophylline in a flow-through cell, did not observe any conversion into monohydrate form. They speculated that the differing results of solid phase transformations, from different studies, might be due to different hydrodynamics of the experiments. Neither of these cases, *i.e.* conversion to monohydrate or stable anhydrate, can however explain the constantly increasing dissolution rate of the present study. There is thus some additional factor involved that causes the dissolution rate to increase faster than what would be expected from the decreasing surface area of the Hixson-Crowell cube root model (Hixson and Crowell 1931).

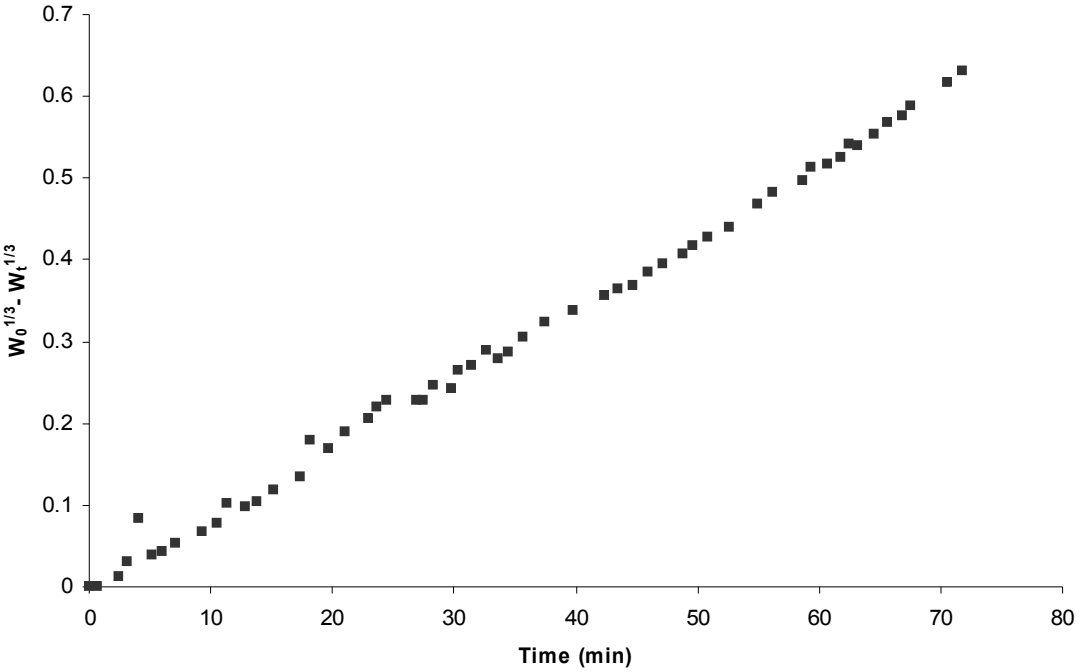

Figure 32. Hixson-Crowell cube root law correlation curve for dissolution data from acetylsalicylic acid experiment AD1. A linear correlation is observed.

Table 9. R^2 values for first and second degree fits to correlation curves of the Hixson-Crowell cube root law and single particle theophylline (TDX) and acetylsalicylic acid (ASX) dissolution data. A clear increased correlation is observed for theophylline pellets with a higher degree fit, whilst no or minimal increase is observed for acetylsalicylic acid pellets

Fit	TD1	TD2	TD3	AD1	AD2	AD3
First degree	0.985	0.984	0.956	0.996	0.993	0.985
Second degree	0.996	0.994	0.985	0.996	0.996	0.987

15.3 The intrinsic dissolution rate of single particles

When assessing the IDR of a substance, the exact surface area, from which dissolution takes place, has to be known. In the miniaturized IDR setup developed by Hulse et al.

(2012), where compressed discs of 3-10 mg of substance with a diameter of 2mm were characterized by UV area imaging, a similarity was found with disc-IDR results from literature. The similarity was however not further specified. Tsinman et al. (2009) were able to produce IDRs, comparable to results from standard disc-IDR measurements, from powder samples as small as 0.06 mg. The surface area of this multiparticulate sample would, however, have been significantly higher than that of a single particle. In single particle dissolution studies, a constant monitoring of the dissolving particle surface area has to be performed in order to assess the IDR. This is not possible when using only chemical analysis, such as UV area imaging. Parrott et al. (1955) assessed the dissolution from a single spherical particle of the initial radius of 1.27 cm, and calculated the mass dissolved per time and radius, not surface area. This large particle will not, however, have been very representative of real drug particles of bulk powders. Börjesson et al. (2013) assumed a cylindrical shape of their fixed pellets, and calculated IDRs for the single dissolving cylinders, based on a theoretical mass transport coefficient. The mass transport coefficient was calculated through simulation of the flow profile in the flow-through cell. They where able to show some similarity of, particle and time averaged, IDR data with disk-IDRs from literature. Due to the fact that they were not able to calculate the IDR for individual particles, their result cannot be regarded as single particle IDR.

In the present study, the intrinsic dissolution rate from single particle image analysis data produced clearly consistent results (Table 10). It is the first time that the IDR has been calculated from an individual experiment of a single three-dimensional surface. It is also the first time that the IDR has been calculated from a single particle of a drug substance, and from a single drug particle of *in vivo* relevant size. The average IDRs for theophylline and ASA single pellets where 2.81 ± 0.22 $mgcm^{-2}min^{-1}$ and 1.76 ± 0.07 $mgcm^{-2}min^{-1}$ respectively. The results are not directly in line with IDRs from literature, in which IDR results of 0.9 $mgcm^{-2}min^{-1}$ (pH 6.8, 37°C) for both theophylline and ASA have been reported (Peltonen et al. 2003; Peltonen et al. 2004). The single particle IDRs are, however, clearly reflected in the dissolution times of the theophylline and ASA experiments, where

the increase in experiment duration is approximately twice the decrease in IDR (Table 10). There is also a clear correlation between the ratio of the solubilities (Table 4) and the ratio of the IDRs for theophylline vs. ASA, both of which are 1.6. Also the consistency of the data as shown in Figures 33 and 34 cannot be ignored.

Table 10. The intrinsic dissolution rates of single pellets of theophylline (TDX) and acetylsalicylic acid (ASX), and the duration of the experiments. Mean values are presented with standard deviation. It can be seen that the increase in the duration of the experiments is approximately twice the decrease in IDR

	TD1	TD2	TD3	Average	AD1	AD2	AD3	Aveage
IDR ($mgcm^{-2}min^{-1}$)	2.85	2.58	3.01	2.81 ± 0.22	1.79	1.80	1.68	1.76 ± 0.07
Duration (min)	34	49	29	37	91	86	82	86

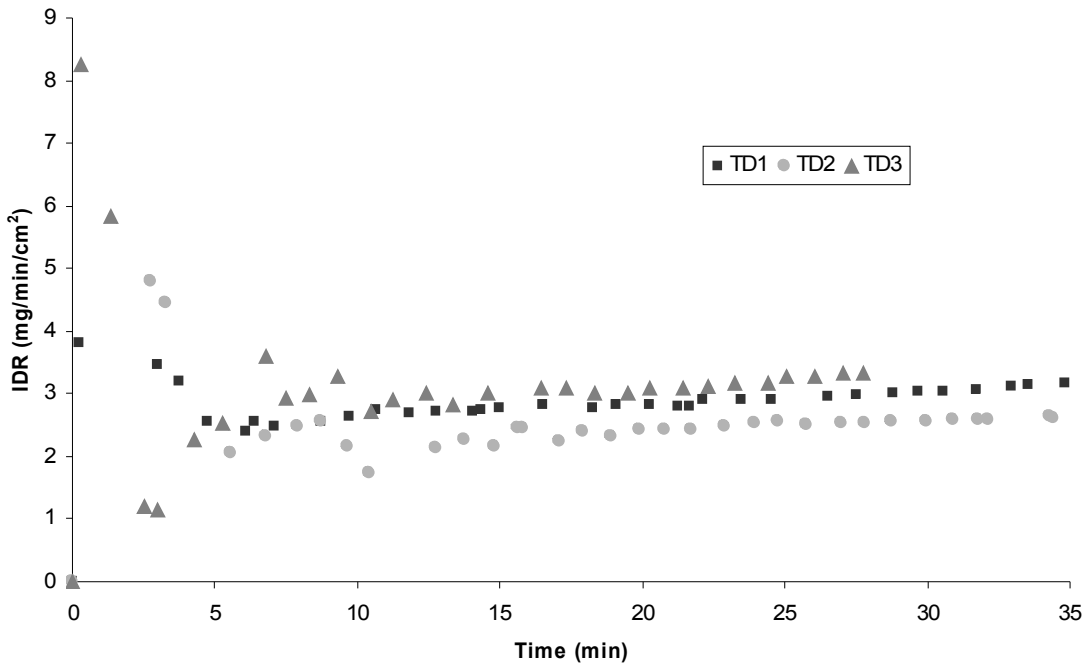

Figure 33. The change in the intrinsic dissolution rates of theophylline single pellets (TDX) with time. The individual pellet results are clearly consistent and a slight tendency for increased rates can be observed, after the initial onset lag time.

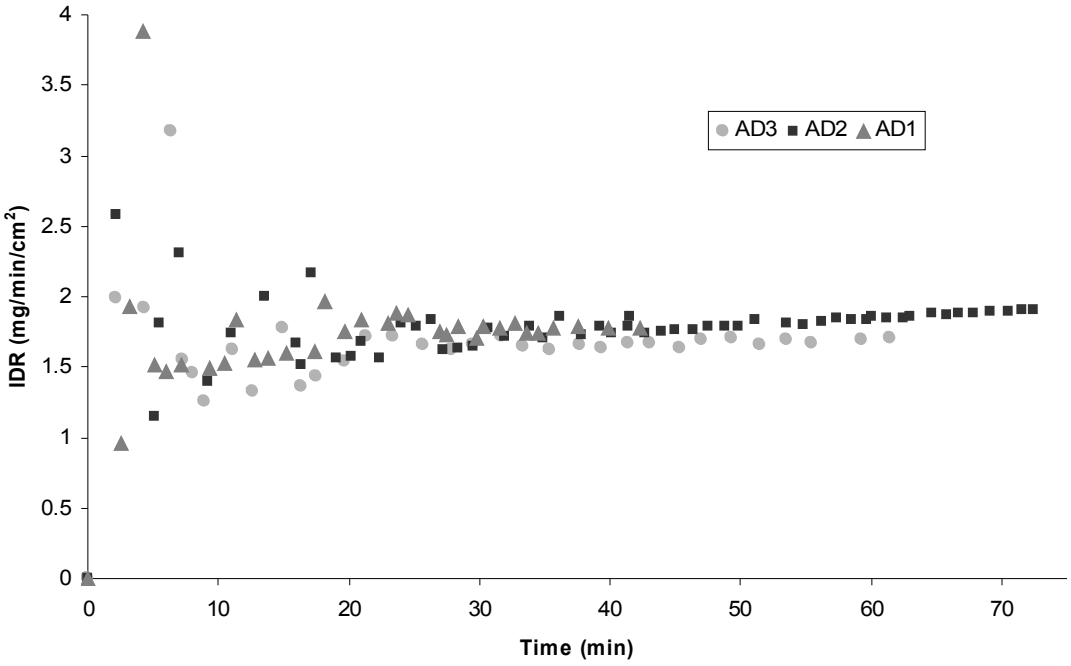

Figure 34. The change in the intrinsic dissolution rates of acetylsalicylic acid (ADX) single pellets with time. As with the theophylline pellets, the individual pellet results are clearly consistent and a slight tendency for increased rates can be observed, after the initial onset lag time.

The deviation from literature IDR data cannot be explained by differences in dissolution media. Since the dissolution medium used in the present study was degassed distilled water, the pH was close to 7. Additionally the average temperatures of the dissolution media where 23 ± 0.4°C and 23 ± 0.7°C for the three theophylline and ASA experiments, respectively. The slight difference in pH is not enough to explain the differences, and in the case of theophylline, with a pKa of 8.81 (Table 4), the higher pH of the present study should have produced slower dissolution rates, in accordance with Equation 22. The lower temperature should also, in accordance with Equations 3 and 6, have resulted in lower IDRs. One possible explanation can however be the particle size. It can be seen in Figures 33 and 34 that there is a tendency, for both theophylline and ASA pellets, towards increased IDRs with decreasing particle size. For a large compressed tablet the IDR could therefore

very well decrease to the levels presented in literature. Another possible explanation is the difference in hydrodynamics, of the modified Einstein teacup and other methods, which have been shown to produce differing intrinsic dissolution rates for different liquid flow dynamics (Lehto et al. 2008, Hulse et al. 2012). This effect is also derived from the Levich equation (Equation 18), where the angular velocity of the rotating disc is directly proportional to the disc-IDR. The initial high variability which can be seen in the IDR data in Figures 33 and 34, could imply a lag time of wetting and diffusion layer buildup. It could also be caused by the swelling and consequent disintegration of the particle surface, when coming into contact with the dissolution medium (Marabi et al. 2008; Börjesson et al. 2013). It can be seen when following a data set from the beginning, that the data seems to oscillate in a kind of pulsating motion between high and low IDRs. It is therefore possible that the pulsating profile is due to some kind of dynamic diffusion layer buildup. To the knowledge of the author, only already formed diffusion layers and the decrease in these, with decreasing particle size, has been investigated (*e.g.* Hintz and Johnson 1989; Mosharraf and Nyström 1995; Galli 2006).

An interesting occurrence was also observed when comparing the IDRs to the Hixson-Crowell rate constants of the respective experiments (Figures 35 and 36). It was found that the IDR values, over all data points of all six dynamic experiments, where on average 212 ±16 (n=252) times larger than the respective Hixson-Crowell rate constant values. This means that the cumulative amount dissolved per average surface area (Equation 17), at a specific time, is directly proportional, by a constant of around 200, to the difference of the cube roots of the initial weight and the weight of the particle at that specific time (Equation 13). It is not immediately apparent why this would be the case, however, the weight of a spherical particle relates directly to the surface area of that particle, trough volume and density. The same equivalent sphere surface area, that was used fore IDR calculations was also used to calculate the mass of a pellet. To the knowledge of the author, this relationship has not been previously assessed, and could be further investigated. Since the high solubility IDR threshold for biopharmaceutics classification is 1-2 $mgcm^{-2}min^{-1}$, both

theophylline and ASA are placed in the correct BCS classes of BCS class I and BCS class III respectively (Lindenberg et al. 2004; Zakeri-Milani et al. 2009). It has been previously shown that the BCS classification can be done based on the disc-IDRs of drug substances (Yu et al. 2004; Zakeri-Milani et al. 2009). This is, however, the first time it has been demonstrated that the BCS classification can be determined from a single drug particle.

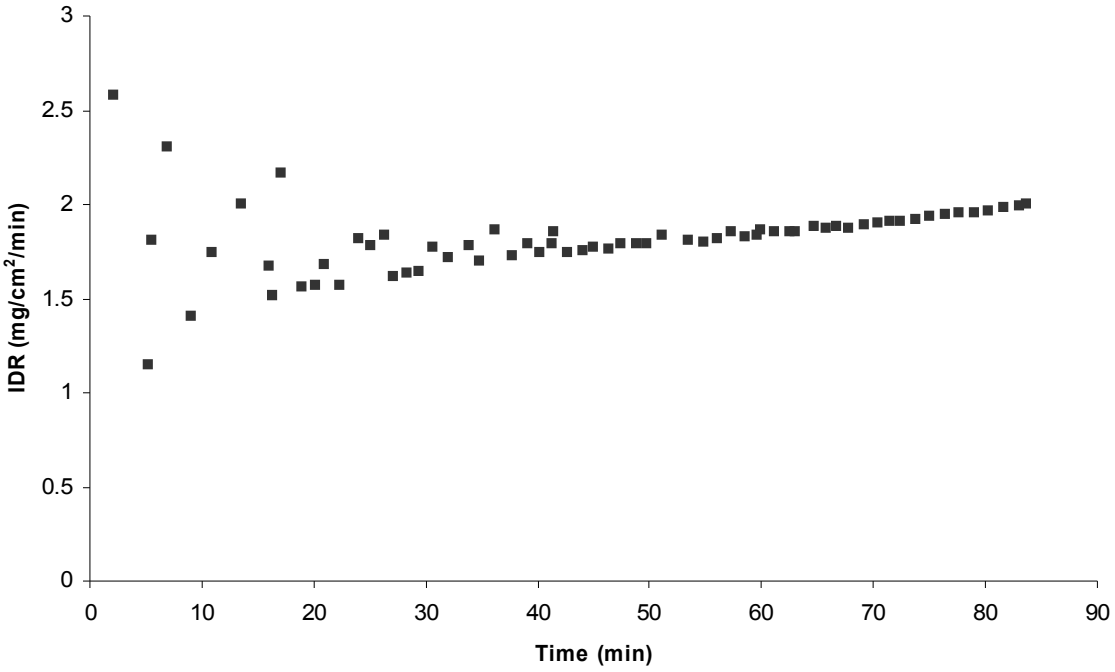

Figure 35. Change in the intrinsic dissolution rate with time of the AD2 experiment.

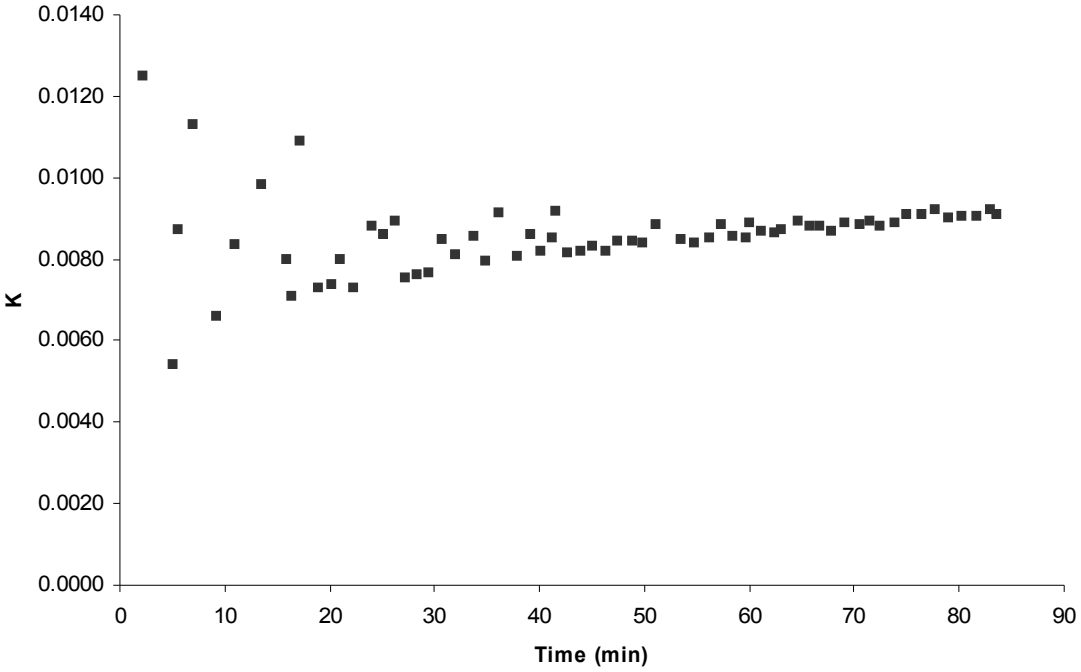

Figure 36. Change in the Hixson-Crowell rate constant, K with time of the AD2 experiment.

16 FUTURE PROSPECTS

The analyzed images in the present study, were collected with an inexpensive digital microscope using manual image processing and public domain image analysis software. Even when using these simple techniques, the acquired dissolution data was practically identical with data from commonly used chemical analysis. It is also inferred that the occasional lower correlations, between some physical and chemical analysis dissolution profiles, can be explained by the inaccuracies of weighing, and of determining the absorbance of dilute samples. Therefore, by using more sophisticated equipment, the results can only get better. It is thus proposed that image analysis can be used, on its own, as a viable analytical technique in single particle dissolution studies.

The possibility of using optical microscopy, without the need for simultaneous chemical analysis, poses many advantages. In contrast to common chemical analysis techniques, no calibration using the investigated substance is needed, therefore decreasing substance consumption. The only primary information required for physical analysis, by optical microscopy, is the initial mass of the studied particle. Additionally there is no sample preparation steps involved, eliminating many possible sources of error. Moreover, the simplicity of the technique and the possibility of rapid information collection, makes studying the dissolution by image analysis highly adaptable to automation and higher throughput screening.

The novel modified Einstein teacup flow-through method, developed in the present study, was successful in creating a collecting flow, keeping the single freely rotating particle in a sufficiently small area to allow continuous image acquisition. It is the first analytical apparatus, with which it is possible to continuously assess the dissolution rate of a freely moving single particle, in a flowing liquid. The rudimentary prototype, consisting of practically two needles and a 96-well plate chamber, is very inexpensive and simple to build, and is therefore easily duplicated for parallel dissolution studies. The flow-through setup also gives an additional advantage, by allowing the use of *in vivo* relevant dissolution conditions. The flow rate can be adjusted to reflect *in vivo* flow rates of 0-7 ml/min (Dressman et al. 1998). The optical method also works with any transparent liquid, which means that biorelevant media, as well as buffered solutions of any pH can be used in the dissolution studies. Additionally the flow-through allows the possibility of dynamic pH gradient runs, for the obtaining of pH-dependent dissolution rates (Okumu et al. 2008).

The developed technique also allowed the obtaining of intrinsic dissolution rates for the substances used, from the data of individual single particle experiments. This means that the solubility of a substance can be predicted from solid dissolving particles, producing much more accurate predictions of thermodynamic solubility, than the data acquired from

kinetic solubility studies of predissolved substance (Yu et al. 2004). Furthermore the intrinsic dissolution rates allow the prediction of the BCS class of a drug substance, from a single dissolving particle, which could be of great value in the early drug development. Because the rotating particle makes it possible to assess the 3D particle shape, it is perceived that by using appropriate shape factors, the modified Einstein teacup apparatus can be used to determine the dissolution rates of single particles of any particle shape. Using this technique, it is therefore possible to acquire quantitative data of physicochemical parameters, which are currently assessed qualitatively with kinetic solubility methods or *in silico* calculations, very early in the drug discovery and development process (Figure 37).

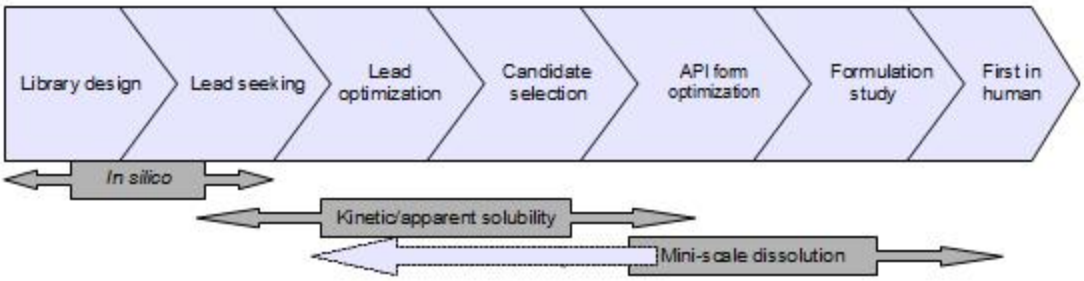

Figure 37. The current state of solubility and dissolution rate assessment in drug discovery and early development (gray boxes), and the possibility of moving mini-scale dissolution testing to earlier stages (pale dotted arrow), with novel mini-scale techniques (modified from Sugano et al. 2007).

The novel apparatus is also very adaptable. If the vortex is produced by a stirrer rather than by the liquid flow of the current prototype, any flow rate could be used. The dissolution could then also be studied under diffusion controlled stagnant conditions, under diffusion and solubility controlled agitated conditions or under solubility and intrinsic dissolution rate controlled sink conditions. If regarded as appropriate, other physical or chemical analysis techniques, including turbidimetry, area imaging, in-line, on-line or off-line techniques as well as *in situ* probes, could be used in the apparatus. Furthermore the possibility of real-time monitoring of solid state properties and transformations by *i.e.* Raman spectroscopy is another interesting possibility (Aaltonen et al. 2006). This would

allow the direct correlation of solid state properties with dissolution rate data (Tong et al. 2009). The technique is also not confined to only single particle experiments, but could additionally be used to study multiparticulate samples.

There is no other current technique that allows the assessment of dissolution of freely moving single particles from 3D morphological data. In addition to real-time assessment of surface specific dissolution rates, the 3D data could be used to construct virtual models of the single particles. This would allow the exact *in silico* investigation of surface topographic dissolution rates, as well as an accurate simulation of particle size dependent dissolution rates. As the development process moves forward, the aim is to maximize the quality of the collected data, by optimizing the apparatus and by using more sophisticated equipment. The aim is also to reduce the size of the studied single particles, and thus also the materials consumption, as well as to study the dissolution of particles of varying shapes. The realistic threshold of around 1 μm for particle size analysis, poses limitations for the optical analytical technique (Allen 1997). However, using particles with the initial diameter of 10 μm, would mean a hundred-fold decrease, from the current setup. This, accordingly, would mean a million-fold reduction in particle volume and mass. The realistic lower limit for single particle dissolution testing by this novel technique is therefore around an unprecedented 1 ng in initial particle weigh, if an accurate assessment of the weight can be made. As this nanogram particle dissolves to the limit of 1 μm, its weight will have been reduced to 1 pg.

17 CONCLUSIONS

Through the work of the present study it can be concluded that:

- Image analysis produces practically identical dissolution profiles with conventional

chemical analysis. Optical microscopy is therefore a viable analytical technique for single particle dissolution testing;

- The possibility of using physical analysis instead of chemical analysis poses many advantages. These include reduced materials consuption, reduced experiment times as well as a reduction in the possible sources of error;
- The main advantage of physical analysis over chemical analysis is, that no prior chemical knowledge about the studied particle is needed. Physical analysis is thus the optimal technique for analyzing new chemical entities;
- The novel modified Einstein teacup flow-through dissolution technique provides the first method, with which it is possible to determine the dissolution rate of freely moving single particles, through continuous physical analysis;
- The possibility of investigating the dissolution from a single, three-dimensional surface, significantly decreases the assumptions involved in dissolution assessments, and allows the extrapolation of the data to any effective surface area;
- Single-particle dissolution is not always accurately modeled by the Hixson-Crowell cube root law. Since this was the theoretically ideal model for the studied spherical pellets, it shows the potential weakness of *in silico* modeling based on theoretical equations;
- By the novel method developed in this study, it is possible to obtain the intrinsic dissolution rate from a single drug particle. Thus, as was shown, it is also possible to predict the BCS classification of a drug subtance, from a single particle;
- The wide adaptability and the relatively simple improvement, of the already very good data, could make this novel dissolution technique an attractive possibility for early qualitative physicochemical screening, in drug discovery and early development. This is especially true, if the theoretical picogram detection limit is achieved.

REFERENCES

Aaltonen J, Heinänen P, Peltonen L, Kortejärvi H, Tanninen VP, Christiansen L, Hirvonen J, Yliruusi J, Rantanen J: In situ measurement of solvent-mediated phase transformations during dissolution testing. J Pharm Sci 95: 2730-2737, 2006

Allen T: Particle size analysis by image analysis. In: Particle Size Measurement Volume 1: Powder sampling and particle size measurement. pp. 112-140, 5. edition. Edit. Scarlett B, Jimbo G. T.J. Press (Padstow) Ltd., Padstow, Cornwall, 1997

Almeida-Prieto S, Blanco-Méndez J, Otero-Espinar FJ: Microscopic image analysis techniques for the morphological characterization of pharmaceutical particles: Influence of process variables. J Pharm Sci 95: 348-357, 2006

Alsenz J, Kansy M: High throughput solubility measurement in drug discovery and development. Adv Drug Deliv Rev 59: 546-567, 2007

Amidon GL, Lennernas H, Shah VP, Crison JR: A theoretical basis for a biopharmaceutic drug classification: The correlation of in vitro drug product dissolution and in vivo bioavailability. Pharm Res 12: 413-420, 1995

Arifin DR, Yeo LY, Friend JR: Microfluidic blood plasma separation via bulk electrohydrodynamic flows. Biomicrofluidics 1: 2007

Avdeef A: Solubility of sparingly-soluble ionizable drugs. Adv Drug Deliv Rev 59: 568-590, 2007

Avdeef A, Tsinman K, Tsinman O, Sun N, Voloboy D: Miniaturization of powder dissolution measurement and estimation of particle size. Chemistry and Biodiversity 6: 1796-1811, 2009

Balbach S, Korn C: Pharmaceutical evaluation of early development candidates "the 100 mg-approach". Int J Pharm 275: 1-12, 2004

Bhattachar SN, Deschenes LA, Wesley JA: Solubility: it's not just for physical chemists. Drug Discov Today 11: 1012-1018, 2006

Brünner E: Reaktionsgeschwindigkeit in heterogenen Systemen. Z Phys Chem 43: 56–102, 1904

Bruner L, Tolloczko S:. Über die Auflösungsgeschwindigkeit fester Körper. Z Phys Chem 35: 283–290, 1900

Börjesson E, Innings F, Trägårdh C, Bergenståhl B, Paulsson M: The dissolution behavior of individual powder particles. Dairy Science and Technology 93: 357-371, 2013

Carlton RA: Image analysis. In: Pharmaceutical Microscopy. pp. 173-192, online edition. Edit. Carlton RA, Springer Science+Business Media, LLC, 2011

Chen X, Antman MD, Gesenberg C, Gudmundsson OS: Discovery pharmaceutics - Challenges and opportunities. AAPS Journal 8: E402-E408, 2006

ChemIDPlus Advanced (online). U.S. National Library of Medicine, Bethesda, USA 2013.Retrieved 1.9.2013, from http://chem.sis.nlm.nih.gov/chemidplus/chemidheavy.jsp

Cohen JL, Hubert BB, Leeson LJ, Rhodes CT, Robinson JR, Roseman TJ, Shefter E: The development of USP dissolution and drug release standards. Pharm Res 7: 983-987, 1990

Costa P, Sousa Lobo JM: Modeling and comparison of dissolution profiles. European Journal of Pharmaceutical Sciences 13: 123-133, 2001

Crank J: The Diffusion Equations. In: Mathematics of Diffusion. pp. 1-10, 2. edition. Clarendon Press, Oxford, 1975

Crist GB: 2009 Trends in small-volume dissolution apparatus for low-dose compounds. Dissolution Technologies 16: 19-22, 2009

Curatolo W: Physical chemical properties of oral drug candidates in the discovery and exploratory development settings. Pharmaceutical Science and Technology Today 1: 387-393, 1998

D'Hollander M: Masters thesis: Development and optimization of a miniaturized extrusion-spheronization process for the formation of pure substance pellets. Ghent University/University of Helsinki, Faculty of Pharmacy, Division of pharmaceutical technology, 2013

Danckwerts PV: Significance of Liquid-Film Coefficients in Gas Absorption. Ind Eng Chem 43: 1460-1467, 1951

De Villiers MM: Influence of agglomeration of cohesive particles on the dissolution behaviour of furosemide powder. Int J Pharm 136: 175-179, 1996

Dokoumetzidis A, Papadopoulou V, Macheras P: Analysis of dissolution data using modified versions of Noyes-Whitney equation and the Weibull function. Pharm Res 23: 256-261, 2006

Dokoumetzidis A, Papadopoulou V, Valsami G, Macheras P: Development of a reaction-limited model of dissolution: Application to official dissolution tests experiments. Int J Pharm 355: 114-125, 2008

Dressman JB, Amidon GL, Reppas C, Shah VP: Dissolution testing as a prognostic tool for oral drug absorption: Immediate release dosage forms. Pharm Res 15: 11-22, 1998

Einstein A: Über die von der molekularkinetischen Theorie der Wärme geforderte Bewegung von in ruhenden Flüssigkeiten suspendierten Teilchen. Ann Phys 17: 549-560, 1905

Einstein A: Die Ursache der Mäanderbildung der Flußläufe und des sogenannten Baerschen Gesetzes. Die Naturwissenschaften 14: 223–4, 1926

Emmanuel S, Marc L, Eric B, Jean-Michel C: Small volume dissolution testing as a powerful method during pharmaceutical development. Pharmaceutics 2: 351-363, 2010

European Pharmacopoeia 7.3 (online) 2013a. Retrieved 4.2.2013, from http://online6.edqm.eu/ep703/

European Pharmacopoeia 7.8 (online) 2013b. Retrieved 1.9.2013, from http://online6.edqm.eu/ep708/

FDA (online). Guidance for industry: Waiver of *in vivo* bioavailability and bioequivalence studies for immediate release solid oral dosage forms based on a biopharmaceutics classification system. U.S. Department of Health and Human Services
Food and Drug Administration, Center for Drug Evaluation and Research (CDER) 2000. Retrieved 1.9.2013, from http://www.fda.gov/downloads/drugs/guidancecomplianceregulatoryinformation/guidances/ucm070246.pdf

Fick A: Über Diffusion. Ann Phys 94: 59–86, 1855

Florence AT, Attwood D: The solubility of Drugs. In: Physicochemical principles of pharmacy. p. 142, 5. edition. Chapman and Hall, New York, 1982

Galia E, Nicolaides E, Hörter D, Löbenberg R, Reppas C, Dressman JB: Evaluation of various dissolution media for predicting In vivo performance of class I and II drugs. Pharm Res 15: 698-705, 1998

Galli C: Experimental determination of the diffusion boundary layer width of micron and submicron particles. Int J Pharm 313: 114-122, 2006

Gardner CR, Walsh CT, Almarsson Ö: Drugs as materials: Valuing physical form in drug discovery. Nature Reviews Drug Discovery 3: 926-934, 2004

Higuchi WI: Diffusional models useful in biopharmaceutics: Drug release rate processes J Pharm Sci 56: p. 315–324, 1967

Higuchi WI, Hiestand EN: Dissolution rates of finely divided drug powders I. Effect of a distribution of particle size in a diffusion-controlled process. J Pharm Sci 52: 67-71, 1963

Hintz RJ, Johnson KC: The effect of particle size distribution on dissolution rate and oral absorption. Int J Pharm 51: 9-17, 1989

Hixson, AW, Crowell, JH: Dependence of Reaction Velocity upon Surface and Agitation I – Theoretical Consideration. Ind Eng Chem 23: 923-931, 1931

Huang L, Tong W: Impact of solid state properties on developability assessment of drug candidates. Adv Drug Deliv Rev 56: 321-334, 2004

Hulse WL, Gray J, Forbes RT: A discriminatory intrinsic dissolution study using UV area imaging analysis to gain additional insights into the dissolution behaviour of active pharmaceutical ingredients. Int J Pharm 434: 133-139, 2012

Hörter D, Dressman JB: Influence of physicochemical properties on dissolution of drugs in the gastrointestinal tract. Adv Drug Deliv Rev 46: 75-87, 2000

Jain N, Yalkowsky SH: Estimation of the aqueous solubility I: Application to organic nonelectrolytes. J Pharm Sci 90: 234-252, 2001

Kerlin P, Zinsmeister A, Phillips S: Relationship of motility to flow of contents in the human small intestine. Gastroenterology 82: 701-706, 1982

Kerns EH: High throughput physicochemical profiling for drug discovery. J Pharm Sci 90: 1838-1858, 2001

Kerns EH, Di L: Physicochemical profiling: Overview of the screens. Drug Discovery Today: Technologies 1: 343-348, 2004

Kerns EH, Di L, Carter GT: In vitro solubility assays in drug discovery. Curr Drug Metab 9: 879-885, 2008

Kubinyi H: Strategies and recent technologies in drug discovery. Pharmazie 50: 647-662, 1995

Lehto P, Aaltonen J, Niemelä P, Rantanen J, Hirvonen J, Tanninen VP, Peltonen L: Simultaneous measurement of liquid-phase and solid-phase transformation kinetics in rotating disc and channel flow cell dissolution devices. Int J Pharm 363: 66-72, 2008

Levich VG: Physicochemical Hydrodynamics. Prentice Hall, Inc. Englewood Cliffs, New Jarsey, 1962

Lindenberg M, Kopp S, Dressman JB: Classification of orally administered drugs on the World Health Organization Model list of Essential Medicines according to the biopharmaceutics classification system. European Journal of Pharmaceutics and Biopharmaceutics 58: 265-278, 2004

Lipinski CA, Lombardo F, Dominy BW, Feeney PJ: Experimental and computational approaches to estimate solubility and permeability in drug discovery and development settings. Adv Drug Deliv Rev 46: 3-26, 2000

Macheras P, Dokoumetzidis A: On the heterogeneity of drug dissolution and release. Pharm Res 17: 108-112, 2000

Marabi A, Mayor G, Burbidge A, Wallach R, Saguy IS: Assessing dissolution kinetics of powders by a single particle approach. Chem Eng J 139: 118-127, 2008

Martin AN, Sinko PJ, Singh Y: Solubility and Distribution Phenomena. In: Martin's physical pharmacy and pharmaceutical sciences. p. 182-196, 6. edition. Edit. Sinko PJ. Lippincott Williams & Wilkins, Baltimore, 2011

McConnell EL, Fadda HM, Basit AW: Gut instincts: Explorations in intestinal physiology and drug delivery. Int J Pharm 364: 213-226, 2008

Mosharraf M, Nyström C: The effect of particle size and shape on the surface specific dissolution rate of microsized practically insoluble drugs. Int J Pharm 122: 35-47, 1995

Nernst W: Theorie der Reaktionsgeschwindigkeit in heterogenen Systemen. Z Phys Chem 47: 52–55, 1904

Nicklasson M, Magnusson AB: Program for evaluating drug dissolution kinetics in preformulation. Pharm Res NO. 6: 262-266, 1985

Nicolaides E, Galia E, Efthymiopoulos C, Dressman JB, Reppas C: Forecasting the in vivo performance of four low solubility drugs from their in vitro dissolution data. Pharm Res 16: 1876-1882, 1999

Niebergall PJ, Milosovich G, Goyan JE: Dissolution Rate Studies II. Dissolution of Particles Under Conditions of Rapid Agitation. J Pharm Sci 52: 236-241, 1963

Noyes AA, Whitney WR: The rate of solution of solid substances in their own solutions. The Journal of the American Chemical Society 19: 930-934, 1897

Okumu A, DiMaso M, Löbenberg R: Dynamic dissolution testing to establish in vitro/in vivo correlations for montelukast sodium, a poorly soluble drug. Pharm Res 25: 2778-2785, 2008

Parrott EL, Wurster DE, Higuchi T: Investigation of Drug Release from Solids I. Some Factors Influencing the Dissolution Rate. J Pharm Sci 44: 269-273, 1955

Peltonen L, Liljeroth P, Heikkilä T, Kontturi K, Hirvonen J: A novel channel flow method in determination of solubility properties and dissolution profiles of theophylline tablets. Journal of Drug Delivery Science and Technology 14: 389-394, 2004

Peltonen L, Liljeroth P, Heikkilä T, Kontturi K, Hirvonen J: Dissolution testing of acetylsalicylic acid by a channel flow method - Correlation to USP basket and intrinsic dissolution methods. European Journal of Pharmaceutical Sciences 19: 395-401, 2003

Prasad KVR, Ristic RI, Sheen DB, Sherwood JN: Dissolution kinetics of paracetamol single crystals. Int J Pharm 238: 29-41, 2002

Pudipeddi M, Serajuddin ATM: Trends in solubility of polymorphs. J Pharm Sci 94: 929-939, 2005

Raghavan SL, Ristic RI, Sheen DB, Sherwood JN: Dissolution kinetics of single crystals of a-lactose monohydrate. J Pharm Sci 91: 2166-2174, 2002

Sandler N: Photometric imaging in particle size measurement and surface visualization. Int J Pharm 417: 227-234, 2011

Stainforth JN, Aulton ME: Particle size analysis. In: Aultons Pharmaceutics: The design and manufacture of medicines, pp. 122-129. 3. edition. Edit. Aulton ME, Churchill Livingstone, Edinburgh, 2007

Stegemann S, Leveiller F, Franchi D, de Jong H, Lindén H: When poor solubility becomes an issue: From early stage to proof of concept. European Journal of Pharmaceutical Sciences 31: 249-261, 2007

Sugano K, Okazaki A, Sugimoto S, Tavornvipas S, Omura A, Mano T: Solubility and dissolution profile assessment in drug discovery. Drug metabolism and pharmacokinetics 22: 225-254, 2007

Takano R, Kataoka M, Yamashita S: Integrating drug permeability with dissolution profile to develop IVIVC. Biopharmaceutics and Drug Disposition 33: 354-365, 2012

Tong C, Lozano R, Mao Y, Mirza T, Ldbenberg R, Nickerson B, Gray V, Wang Q: The value of in Vitro dissolution in drug development: A position paper from the AAPS in Vitro release and dissolution focus group. Pharm Technol 33: 52-64, 2009

Tsinman K, Avdeef A, Tsinman O, Voloboy D: Powder dissolution method for estimating rotating disk intrinsic dissolution rates of low solubility drugs. Pharm Res 26: 2093-2100, 2009

Tsinman K, Avdeef A, Tsinman O, Voloboy D: Powder dissolution method for estimating rotating disk intrinsic dissolution rates of low solubility drugs. Pharm Res 26: 2093-2100, 2009

United States Pharmacopoeia, 25th edition. United States Pharmacopoeial Convention, Rockville, MD, 2001

Venkatesh S, Lipper RA: Role of the development scientist in compound lead selection and optimization. J Pharm Sci 89: 145-154, 2000

Wang J, Flanagan DR: General solution for diffusion-controlled dissolution of spherical particles. 2. Evaluation of experimental data. J Pharm Sci 91: 534-542, 2002

Wang J, Flanagan DR: General solution for diffusion-controlled dissolution of spherical particles. 1. Theory. J Pharm Sci 88: 731-738, 1999

Wurster DE, Taylor PW: Dissolution Rates. J Pharm Sci 54: 169-175, 1965

Yeo LY, Friend JR, Arifin DR: Electric tempest in a teacup: The tea leaf analogy to microfluidic blood plasma separation. Appl Phys Lett 89: 2006

Yu LX: An integrated model for determining causes of poor oral drug absorption. Pharm Res 16: 1883-1887, 1999

Yu LX, Carlin AS, Amidon GL, Hussain AS: Feasibility studies of utilizing disk intrinsic dissolution rate to classify drugs. Int J Pharm 270: 221-227, 2004

Zakeri-Milani P, Barzegar-Jalali M, Azimi M, Valizadeh H: Biopharmaceutical classification of drugs using intrinsic dissolution rate (IDR) and rat intestinal permeability. European Journal of Pharmaceutics and Biopharmaceutics 73: 102-106, 2009

Østergaard J, Ye F, Rantanen J, Yaghmur A, Larsen SW, Larsen C, Jensen H: Monitoring lidocaine single-crystal dissolution by ultraviolet imaging. J Pharm Sci 100: 3405-3410, 2011